Final Report

"Nanostructured Materials for Renewable Alternative Energy"

DOE #08NT0001925

Dept. of Chemical and Biomolecular Engineering, North Carolina State University

Gregory Parsons

Total project period: July 25th, 2008 – July 24th, 2013

Submitted September 27, 2013

Project Overview and Personnel

Overview

This project has been in effect from July 25th, 2008 to July 24th, 2013. It supported 19 graduate students and 6 post-doctoral students and resulted in 23 publications, 7 articles in preparation, 44 presentations, and many other outreach efforts. Two representative recent publications are appended to this report. The project brought in more than $750,000 in cost share from North Carolina State University. The project funds also supported the purchase and installation of approximately $667,000 in equipment supporting solar energy research.

Project highlights, by year, include the following:

Year 1: 7/25/08 to 7/24/09

- Led by Dr. Gregory Parsons, four Principal Investigators (Drs. Dickey, Gorman, Misra, and Velev) and several graduate, undergraduate, and postdoctoral students began working under this effort. Dr. Jesse Jur was hired as Research Assistant Professor on Aug 31, 2008 to manage equipment procurement and set–up and to perform and help direct research tasks.
- A project management plan for the effort was delivered to the DOE on December 18th, 2008.
- The primary activity of Year 1 was to establish the Photovoltaics Process and Analysis Laboratory at NC State, known as the Nanotechnology Energy Laboratory (NEL), and train students on these instruments, demonstrate organic PV processing capability, and begin to examine nanostructure architectures.
- Groups worked to meet their task objectives of inorganic nanostructure development and organic photoactive material formation in preparation of the new instruments and device processing capabilities to be online by the end of the first year.
- Efforts were made to enhance communication among the PIs and advance industrial outreach.

Year 2: 7/25/09 to 7/24/10

- The main efforts of Year 2 were to continue the investigation of new nanostructure fabrication and materials growth, demonstrate organic PV processing capability, and explore new materials systems for photovoltaic manufacturing.
- By April 25, 2010, the acquisition of a modular glovebox from MBraun Corp. was completed.
- Efforts on new photoactive energy systems, specifically photoelectrochemical water splitting, were initiated.

Year 3: 7/25/10 to 7/24/11

- The main efforts of Year 3 were to improve quality and throughput of nano-enabled fabrication techniques for organic, dye sensitized, and gel-based photovoltaic device systems.
- Installation and training for the modular glovebox was completed as of January 29th, 2011, and a standard operating procedure and device fabrication procedure for broad operator use in the NC State Nanofabrication Facility (NNF) was developed.
- Our focus on nanostructured materials for photo electrochemical solar fuels research increased significantly.
- Dr. Jur, the NEL Manager for the project, took a position at the NC State College of Textiles in January 2011. Dr. Christopher Oldham was subsequently hired as the new NEL Manager.

Years 4 & 5: 7/25/11 to 7/24/13

- In the final two years of the project, research efforts continued in the investigation of nano-enabled fabrication techniques for organic, dye sensitized, and gel-based photovoltaic device systems, and devices for photoelectrochemical energy conversion.

Task 1.0 Development Project Management Plan

A project management plan was completed and delivered to DOE on December 18th, 2008.

Task 2.0 Development of Photovoltaics Process and Analysis Laboratory

Task 2.0 highlights, by year, include the following:

Year 1: 7/25/08 to 7/24/09

To inform our tool acquisition decisions, project PIs and students conducted visits to UNC-Chapel Hill and RTI International to meet with other faculty and researchers and discuss their capabilities and tool infrastructure. In addition, vendors visited NC State to showcase potential tools to the project group.

Graduate students from Dr. Misra's group were involved in design and production of photovoltaic devices suitable for DSSC-like and bulk heterojunction solar cells. A suitable apparatus for electrical analysis of the solar cells by solar simulator was constructed. We also designed and fabricated equipment for atomic layer deposition of nanoscale materials, including transparent conducting oxide fibers and nanostructures for integration into PV devices.

During Year 1, installation of the following items was completed:

- AMBiOS Technology Universal SPM
- AMBiOS Technology Q-Scope AFM
- Canon 5D 21 MP digital camera for microscopes
- FEI Phenom benchtop scanning electron microscope
- J. A. Woollam Alpha-SE Spectroscopic Ellipsometer
- LC Technologies stainless steel 2-port glove box
- Olympus SZ61 reflected and transmitted stereo microscope

- Olympus BX51 reflected and transmitted microscope with BF/DF/DIC capabilities
- Olympus BX60 reflected and transmitted microscope with BF/DF/DIC capabilities
- Veeco Dektak D150 with advanced automation package for 3D profiling
- Newport Oriel 91160 300 Watt Solar Simulator (with AM1.5 filter)
- Diener Plasma Cleaner
- Veeco Dimension 3000 AFM CPU and software upgrade
- Thermo Scientific Evolution 300 UV-Vis Spectrometer
- Thermo Scientific Nicolet 6700 Fourier Transform Infrared Spectrometer

In addition to the tool installation, we conducted student education and training on the tool capabilities. We also demonstrated a photovoltaic testing platform (device and measurement apparatus) that can be used to examine bulk heterojunction and hybrid-type photovoltaics.

Year 2: 7/25/09 to 7/24/10

By April 25, 2010, the acquisition of a modular glovebox from MBraun Corp. was completed. Figure 1 shows a schematic of the glovebox, which includes an integrated spincoater and thermal evaporation system, allowing for a full photovoltaic (PV) device production within the confines of glovebox. The laboratory space in the NNF was upfitted to meet the safety requirements of NC State Environmental Health and Safety, which included the installation of N2 and exhaust lines for use with this system.

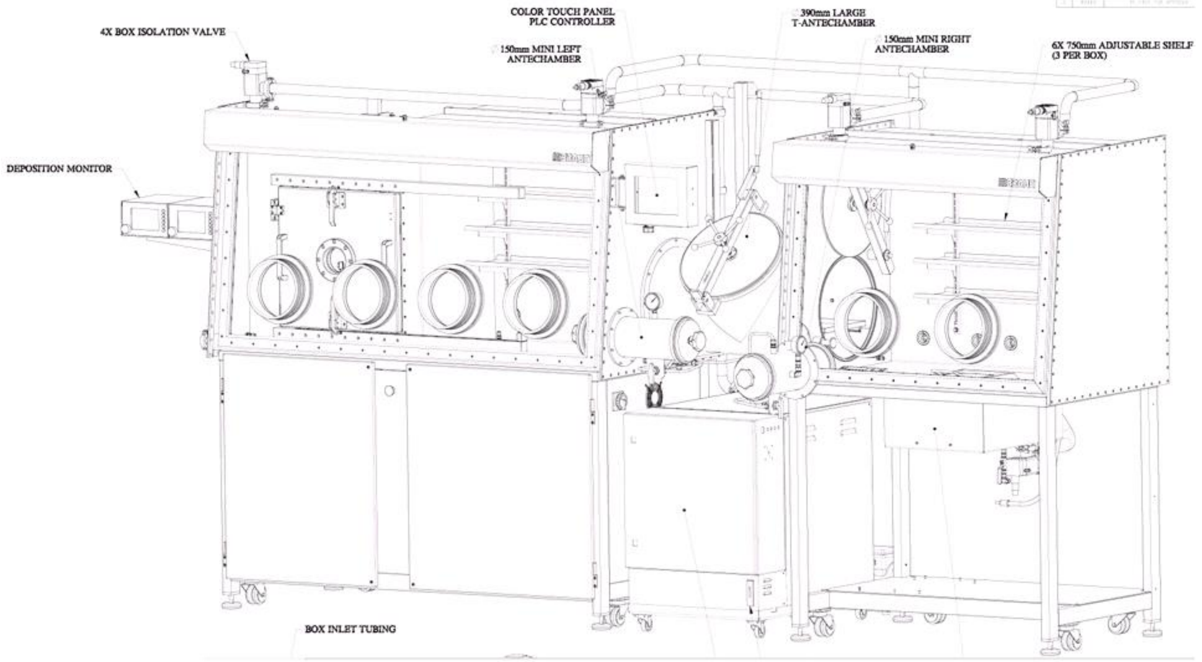

Figure 1. Drawing of the glovebox system that is being purchased and installed by the NC State Nanotechnology Energy Laboratory. The system is comprised of an integrated spincoater and thermal deposition system in the right and left chambers, respectively.

Year 3: 7/25/10 to 7/24/11

Installation and training for the modular glovebox from MBraun Corporation that was acquired in project year 2 was completed as of January 29th, 2011. Installation was completed onsite by an MBraun service engineer and was assisted by Henry Taylor and Marcio Cerullo of the NNF. The NNF added the glovebox onto their login control system so access is granted only to specific users that have received training for operating the glovebox, including faculty at NC State and the local industrial community.

We also purchased a NIST-reference solar cell for calibration of our light source that is primarily used with the organic photovoltaic and dye-sensitized solar cell testing. An additional light source was purchased from Newport Oriel that serves as a dedicated system for the photoelectrochemical solar fuels research. Finally, we evaluated different models of a QE/IPCE instrument.

With the installation completed, a standard operating procedure and device fabrication procedure for broad operator use in the NNF was developed. Teaming with faculty from the NC State Mechanical and Aerospace Engineering (MAE) and Electrical and Computer Engineering (ECE) Departments, we created a common practice and obtained the materials necessary for organic solar cell fabrication. This effort was directed by Dr. Jur, Nicole Hedges, and Marcio Cerullo. This subtask was completed at the end of Year 3, July 25, 2011.

Task 3.0 Inorganic Nanostructures for Photovoltaics

Subtask 3.1 Atomic Layer Deposition Fabrication and Modification of Nanostructures *(Parsons)*

Q1:

Three new atomic layer deposition (ALD) systems under construction will allow for highly specialized processing of metal oxide layers, metals, and metal-organic complexes in complex nanostructure frameworks. Approximately 90% of the parts for the equipment fabrication have been secured. To support highly specialized metal oxide film development through ALD processing, an ozone generator (with proper deconstruct

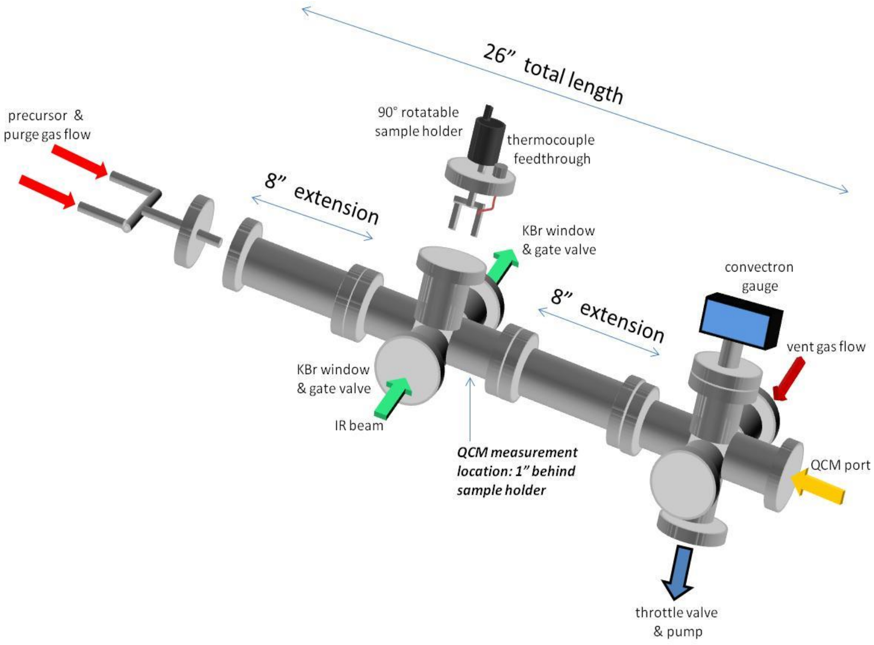

Figure 2. Simplified design for an in situ FT-IR ALD reactor.

and ozone sensors) has been acquired. Two undergraduate students in Chemical and Biomolecular Engineering assisted in the design and formation of the electronic control units for the ALD systems.

In addition to these three new systems for ALD growth of nanostructures, an ALD system incorporating *in–situ* FT-IR analysis capabilities is in design. Based on a simplified design, as shown in Figure 2, this ALD system will allow for unique characterization of the ALD process and be able to couple this analysis with substrate dependencies.

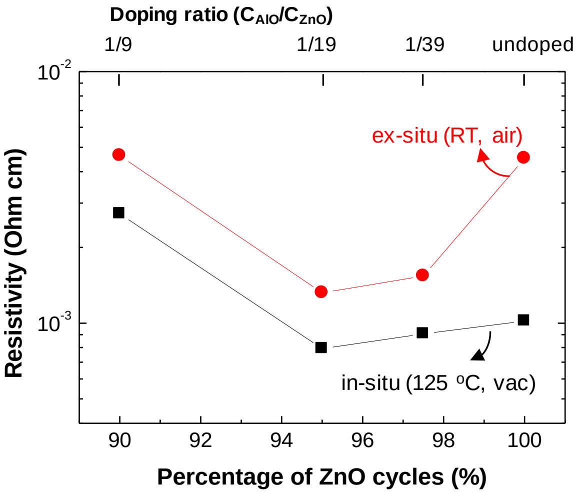

Figure 3. Resistivity measurements of Al-doped ZnO conducted in- situ and ex-situ for varying precursor cycle ratios of ZnO and Al_2O_3 deposition.

Q2:

Al-doped ZnO growth by atomic layer deposition (ALD) is being investigated as a means to form a transparent electrode comparable in performance to ITO. The controlled extrinsic doping of ZnO film with an aluminum impurity was performed using ALD at a temperature of 125 °C for 240 cycles. Figure 3 shows that the *in-situ* and *ex-situ* resistivity of Al-doped ZnO films can be controlled by changing the precursor cycle ratio. A minimum resistivity value of 8×10^{-4} Ω cm was achieved at a 1/19:Al_2O_3/ZnO cycle ratio (ZnO concentration of 95%). For comparison, ITO typically has a resistivity of ≈1×10^{-4} Ω cm. Methods to decrease the resistivity of the Al-doped ZnO films further by ALD process modification are underway. This data does show that the Al-doped ZnO films deposited by ALD could be utilized as a transparent electrode in the organic-associated photovoltaic devices.

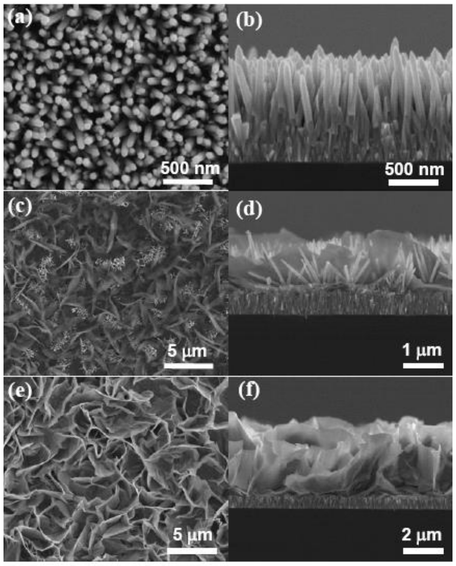

Figure 4. SEM images (top and cross-sectional views) of samples with morphology evolution from ZnO 1D NRs to 2D NWs after the 2nd hydrothermal growth. Here the growth conditions are the same except the 2nd ALD coating layer consisting of (a)-(b) ZnO (100 cycles), (c)-(d) Al_2O_3/ZnO (20/100 cycles), and (e)-(f) Al_2O_3/ZnO (100/100 cycles).

Three new atomic layer deposition (ALD) systems to facilitate core-shell nanostructure investigation are near completion. These system will allow for deposition of TiO_2, $TiO_2(N)$, Al_2O_3, ZnO, and Al_2O_3:ZnO. In addition, an ALD system incorporating *in-situ* FT-IR analysis capabilities has been constructed and is in preliminary characterization.

Q3:

High surface area nanostructures are being investigated by the use of ALD processing. ZnO nanostructures has been shown by combining atomic layer deposition of Al_2O_3/ZnO and hydrothermal growth of ZnO. First, 1D nanorods of ZnO were synthesized by performing a hydrothermal growth of ZnO on a Si substrate coated with ZnO using ALD. A thin ALD coating of ZnO or Al_2O_3/ZnO was applied to these nanorods, followed by another hydrothermal growth of ZnO. Examples of the growth properties are shown in Figure 4. It is observed that the vertical alignment of ZnO nanorods is influenced by the presence of Al_2O_3 layer. In particular, a transformation from a ZnO nanorod to a nanowalls structure is observed Al_2O_3 into the ALD processing. This is due to the inherent polar interface of the ZnO becoming less polar with addition of Al_2O_3 to the surface. The controlled growth technique of the different ZnO morphologies is to be explored in the development of hybrid photovoltaic devices in Q4. In addition, work has begun on ALD processing of conductive oxides which could influence charge transport properties in organic photovoltaics.

Q4:

High surface area nanostructures are being investigated by the use of atomic layer deposition (ALD) processing. Previous work has shown the formation and tuning of ZnO nanostructures by the combined use of hydrothermal growth of ZnO and atomic layer deposition of Al_2O_3 and ZnO. These nanostructures can either be implemented directly on the ITO structure or as an inexpensive replacement of ITO as the transparent conductive oxide in organic photovoltaics. Electrical results of the Al-doped ZnO (AZO) have shown that the films are conductive, although not as conductive as commercial-grade ITO. Understanding of the mechanism for doping and conductivity enhancement is needed to develop the use of the ALD for formation of AZO. Research has been conducted on *in situ* conductivity measurements combined with mass uptake measurements by the use of a quartz crystal microbalance in order to investigate the characteristic doping mechanism by the use of a sequential Al_2O_3-ZnO depositions. From this work it was observed that 1) the precursor exposure procedure ($Al_2O_3 \rightarrow$ ZnO vs. ZnO $\rightarrow Al_2O_3$) is pivotal in proper film growth, and 2) conductivity enhancement of the Al presence only occurs once the Al is sufficiently covered by the ZnO. The doping profile was also investigated by secondary ion mass spectroscopy. This research was presented by Jeong Seok Na at the 2009 ALD/AVS Conference in Monterey, CA July 20th-22nd. Jeong Seok Na also recently completed his PhD thesis defense and has accepted a position at Novellus Corp. in San Jose, CA.

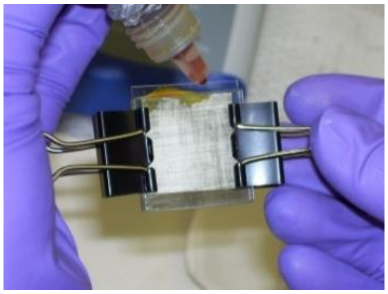

Figure 5. Dye sensitized solar cell developed in Nanotechnology Energy Laboratory.

Work has also been conducted on the formation of tungsten oxide (WO_3) by atomic layer deposition to use as an electron blocking layer on transparent conductive oxides. The method being studied for WO_3 growth consists of W ALD growth and subsequent oxidation. In general, the nucleation of tungsten is very difficult and varies between substrates. Therefore, a process for tungsten thin film growth using WF_6 and Si_2H_6 as the ALD A/B half reactions is being investigated by quartz crystal microbalance coated with various materials. Once the nucleation behavior of the tungsten has been analyzed, implementation of an oxidizing reactant will be studied.

A system for the deposition of TiO_2 by ALD has been created and is in the initial stages of testing. The system is a hot-walled reactor and will initially use titanium isopropoxide and water for the ALD A/B half reactions. Combination of ALD TiO_2 and hydrothermal TiO_2, similar to the previous reports on ALD ZnO and hydrothermal ZnO, will be examined for the formation of high surface area nanostructures useful for dye sensitized solar cells (DSSCs).

Parallel to this work, the protocol for DSSCs formation (device shown in Figure 5) is being developed with the assistance of two undergraduate students from the department of Chemical and Biomolecular Engineering.

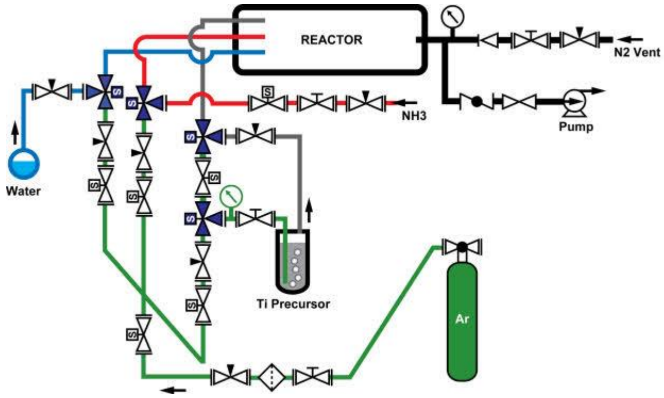

Figure 6. Schematic of the atomic layer deposition for TiO_2 growth.

Q5:

A new system for the atomic layer deposition (ALD) of TiO_2 was fabricated and initial testing has been completed. A diagram of the ALD system is shown in Figure 6. The ALD process for TiO_2 growth incorporates the reaction between Titanium Isopropoxide (TiP) and water. The TiP is delivered by the use of bubbler apparatus with flowing argon gas. The growth rate has been determined to be 0.38 nm/cycle, which corresponds with reports in literature for the same system. In the coming quarter, we will begin to investigate the use of TiO_2 for the modification of hydrothermal growth processes to form unique nanostructures. This is similar to work on ZnO nanostructure growth and modification by the combined use of ALD and hydrothermal growth, which was previously reported on in Q2-Q4. It is believed that the use of these nanostructures will be useful for enhanced exciton separation in organic, hybrid inorganic-organic, dye-sensitized, and photoelectrochemical systems. During Q5, our work has also been focused on the examining the photo-activity of nonwoven fabrics with coatings of ZnO by ALD. ZnO is a direct band gap material (3.4 eV) that is transparent to the infrared and visible light, but undergoes a large photoresponse in the UV. Typically, there are two stages with the photoresponse of ZnO. The first is a rapid exciton formation and the second is a slow chemisorptions and photodesportion of oxygen on the ZnO surface. To investigate these processes on a fibrous system, ALD of ZnO was performed on a nonwoven polypropylene mat. The conductance of the ZnO was determined with the

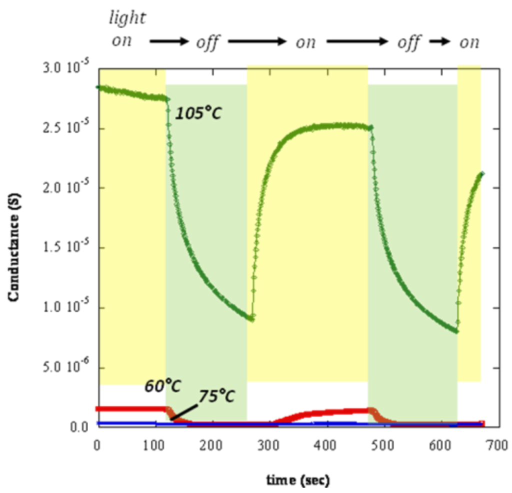

Figure 7. Conductance under illumination and dark conditions of the polypropylene fiber mat with 500 cycle of ZnO deposited at temperatures of 60, 75 and 105 °C.

use of a large area 4-point probe electrical measurement. Figure 7 shows the conductance of polypropylene with 500 ALD cycles of ZnO at various deposition temperatures. Conductance under illumination (1 sun, Am1.5 spectrum) and dark conditions is shown. It is observed that the photoresponsive nature of the ZnO is enhanced at higher ALD processing temperatures. Work is underway to improve the ZnO photoresponse and overall conductivity.

Q6:

Research activities in Q6 have focused on characterizing an atomic layer deposition (ALD) process for titanium dioxide (TiO_2) growth, and investigating new opportunities for ALD TiO_2 film growth for photoactive nanostructures. The TiO_2 ALD reactor is based on a hot walled, flow through design in which the Ti precursor, titanium isopropoxide, is delivered to the system by a bubbler unit. The system has been successfully characterized to yield ALD TiO_2 thin film growth on Si with growth rate per cycle (GPC) of 0.3-0.4 Å/cycle (Figure 8). Comparison between the GPC data in this work and the GPC determined in literature for a similar system is also provided in Figure 8.

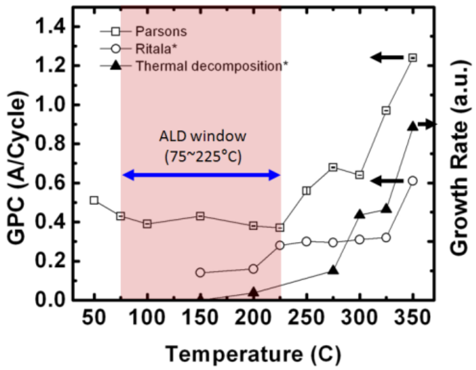

* M. Ritala et al, *Chem. Vap. Deposition*, 2002, 8,21

Figure 8. ALD window for TiO_2 film growth.

The operating temperature window for ALD growth is has been determined to be between 75 °C and 225 °C. The upper limit in temperature defines the processing point at which thermal decomposition of the Ti precursor begins to thermally decompose (also shown in Figure 8). The low processing temperature determined in this work allows for TiO2 deposition on thermally sensitive substrates such as polymers.

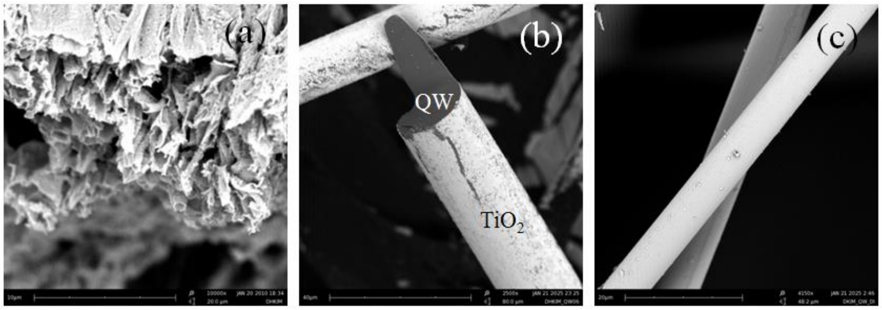

Figure 9. SEM images of ALD TiO_2 (a) on polypropylene fiber after the polymer has been burned out, (b) quartz wool, and (c) quartz wool that has been treated by silane.

Atomic layer deposition of TiO_2 has been investigated on nonwoven polypropylene (PP) fiber mat and quartz wool. Figure 9(a) provides an SEM image of a 140 Å TiO_2 film deposited at 100 °C on PP and subsequently annealed to remove the PP, resulting in the porous, tube structure shown. Figure 9(b) provides an SEM image of quartz wool with an ALD TiO_2 coating. The rough surface is due to surface contamination which can be reduced by a silane treatment. Figure 9(c) shows an SEM image of TiO_2 growth on silane treated quartz wool. The quartz wool represents a high-surface area host structure that is ideal for investigating the TiO_2

properties after high temperature annealing, which is typically required to make an anatase phase. Our future work will investigate the crystal structure and photoactivity of the coated TiO_2 films on polypropylene and quartz wool for fabrication of novel energy devices. In addition we will investigate doping effects that are allowed through ALd processing or post-deposition annealing.

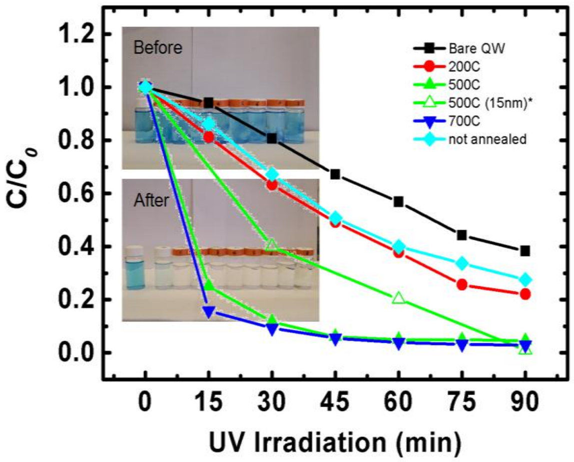

Figure 10. Methylene Blue concentration change under UV-irradiation depending on annealing temperatures.

Q7:

We have studied the use of atomic layer deposition TiO_2 on quartz fibers for use in dye sensitized solar cells. As-deposited TiO_2 film on quartz fiber is amorphous, but annealing results in the formation of anatase-phase TiO_2 and subsequent transformation to rutile phase at annealing temperatures of 500 °C. The rutile phase is known to be photoresponsive in visible light. To this effect, we have examined the photocatalytic activities using the common methylene blue (MB) test for samples at various conditions, as shown in Figure 10. Significant photocatalytic activity is observed for the sample annealed above 500 °C. We have fabricated dye sensitized solar cells (DSSCs) using TiO_2 coated quartz filter as a photoanode. Overall conversion efficiency of our first DSSCs test was measured to ~2.5%. In comparison, an examination of a conventional dye sensitized solar cell with a TiO_2 nanoparticle photoanode with an approximate thickness of <5 micrometers exhibited a1.1% conversion efficiency.

Work has also begun on the use of atomic layer deposition as a means to produce an electrode passivation for use in photoelectrochemical water splitting semiconductor devices. We will first investigate the corrosion of crystalline silicon semiconductors under solar illumination in aqueous solution. The electrodes will oxidize or reduce depending on the type of doping. Electrochemical techniques, such as cyclic voltammetry, will be performed to degrade the electrode surface, which will subsequently be characterized in order to assess the degree of degradation. Once surface damage has been confirmed, atomic layer deposition (ALD) will be used to deposit thin films of TiO_2 on the electrodes. The effectiveness of this passivation layer in inhibiting surface corrosion will be tested using electrochemical techniques.

Q8:

We have demonstrated a dye sensitized solar cell (DSSC) using TiO_2 coated quartz fibers to enhance light scattering in the photoanode. Quartz fibers (~10 μm in diameter) were coated with a conformal TiO_2 layer with 50 nm thickness by atomic layer deposition (ALD). The quartz fibers were then embedded into a TiO_2 nanoparticle photoanod. The entangled structure of quartz fiber allows for Rayleigh scattering inside the photoanode which in return increases the photon adsorption. In addition, TiO_2 on quartz fibers provides additional absorption sites for dyes resulting in more photocurrent generation. We observed that the reflectance was increased by a factor of ~5.6 compared to a planar substrate and the dye adsorption was dramatically enhanced by a factor of ~8.2 in comparison to bare quartz fibers. A comparison of a conventional DSSC with a 12 µm TiO2 nanoparticle layer and ALD TiO_2 coated quartz fiber DSSC framework is provided in Figure 11. The photoconversion efficiency of the quartz fiber-based DSSC is determined to be 4.0% while the conventional DSSC shows an efficiency of 3.1%.

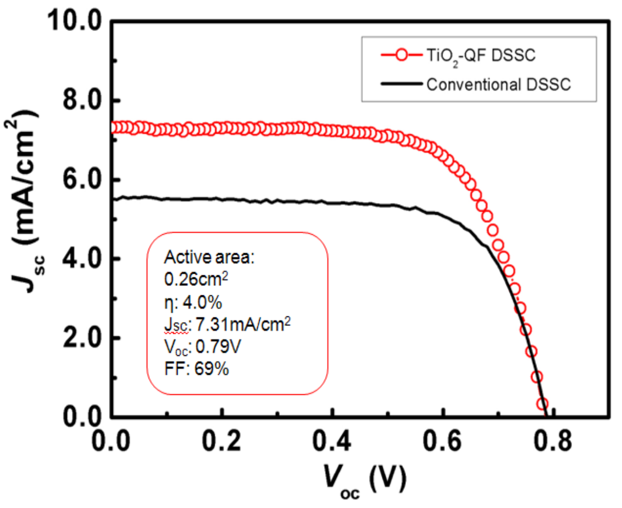

Figure 11. Photocurrent and voltage curve (I-V curve) of conventional and TiO_2-QF DSSCs where the conversion efficiency was increased by 23%.

Q9:

In this subtask, we have prveiously have report the use of TiO_2 coated quartz fibers in a dye sensitized solar cell (DSSC) to improve light scattering and adsorption. In this quarter, we have investigated the temperature-dependent phase transformation of TiO_2 (thickness = 50 nm) deposited by atomic layer deposition on quartz fibers. The X-ray diffraction pattern (Figure 12) shows the phase evolution from the as-deposited film to an anneal temperature of 1050 C. The initial amorphous phase TiO_2 is transformed into anatase at an anneal temperature of 450°C and remains stable after annealing at 1050°C. Based on known literature reports, it is believed that Si from the quartz fiber diffuses into TiO_2 and impedes the rutile formation. We have also observed that its stability was maintained for TiO_2 film with a thickness increase to ~230 nm. For application in electronic devices, such as the dye-sensitized solar cells investigated in this work, a stable anatase can be useful to engineer its band gap energy by doping with nitrogen, carbon, and boron. This allows for enhanced light adsorption in the visible range as the anatase phase has faster electron transport property than rutile phase. Most doping techniques require a high temperature anneal process in which a rutile phase transformation is

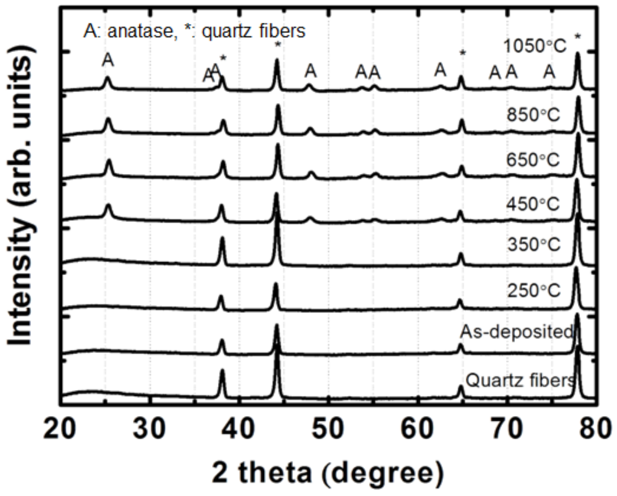

Figure 12. X-ray diffraction pattern of TiO_2-coated quartz fiber at various anneal temperatures.

thermodynamically unavoidable. In the upcoming quarter we have a plan to synthesize doped TiO_2 coated quartz fibers using stable anatase on quartz fibers with lower band gap energy.

We have also previously reported our initial process development and verification of a photoelectrochemical solar fuel research testing platform. In this quarter, the investigation of new materials for solar water splitting was initiated. A number of working electrodes, based on fluorine-doped tin oxide glass substrates, were constructed and tested in various electrolytes and pH conditions. Light absorbing materials, such as TiO_2 and α-Fe_2O_3, were deposited on this conductive substrate. The electrodes were further functionalized by a layer of water oxidation catalysts such as Co and Pt deposited using solution-based or electrochemical methods. Cyclic voltammogram (CV) from each electrode allowed the evaluation of oxidation and reduction overpotentials for each material-catalyst combination (Figure 13, top). Electrode degradation was observed particularly in acidic pH conditions and under reducing potentials (Figure 13, bottom). In the next quarter, the stability of the electrodes will be improved by employing a conformal TiO_2 passivation layer via atomic layer deposition (ALD). Furthermore, a dye-sensitized solar cell (DSC) will be integrated into the back of each working electrode in order to construct a tandem water splitting device.

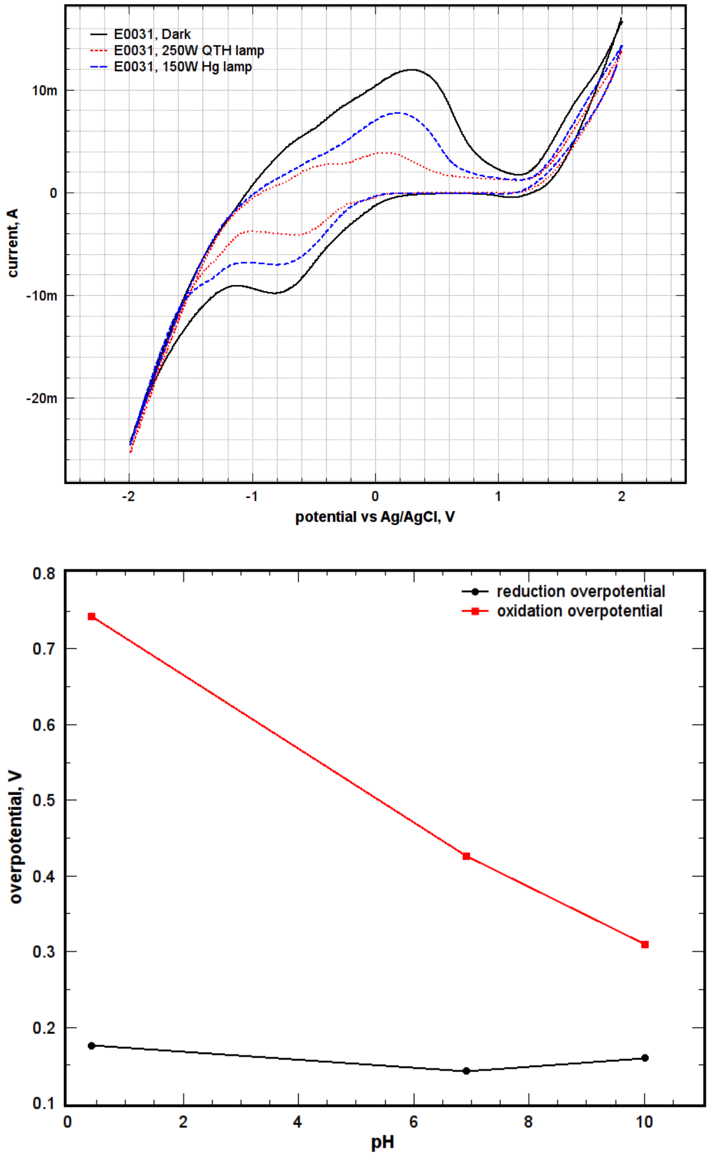

Figure 13. (top) C-V measurement of a FTO + Fe_2O_3 electrode (phosphate solution, pH 7.12). (bottom) Overpotential as a function of pH for a solution-deposited Pt

Q10:

In this quarter, efforts related to this subtask have been to characterize dye-sensitized solar cells (DSSC) using TiO_2-quartz fibers (QF) with three kinds of photoanodes: 1) conventional nanostructured TiO_2, 2) a TiO_2 modified quartz fiber (QF), and bare QF. As reported earlier, the QF-based photoanodes are integrated in a TiO_2 nanoparticle layer for testing. A comparison of the incident photon to conversion efficiency (IPCE) and absorbed photon to conversion efficiency (APCE) for each photoanode is shown in Figure 14 (a) and (b), respectively. The IPCE data indicates that the bare and TiO_2-QF caused a significant light scattering effect at wavelengths between 400-550 and 600-700 nm, while conventional DSC exhibited no such light scattering effect. This observation is consistent to the diffuse reflectance results previously reported. Moreover, additional dye absorption on TiO_2-QF leaded an enhanced peak around 535 nm where N719 dye has the highest absorbance compared to bare QF. The APCE data (Figure 14(b)) shows a larger difference between TiO_2-QF and bare QF at a wavelength of ~535 nm as compared to the data shown in the IPCE (Figure 14(a)). We believe that this is an indication that the ALD TiO_2 film on QF allows for a direct pathway for electron transport from the TiO_2 coated QF to the TiO_2 nanoparticle layer.

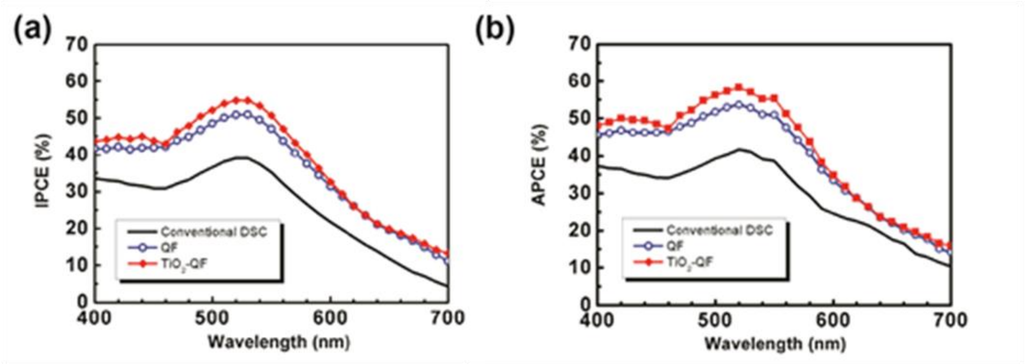

Figure 14. (a) IPCE and (b) APCE data comparison of photoanodes made by conventional methods as well as with bare and modified quartz fiber scattering layers.

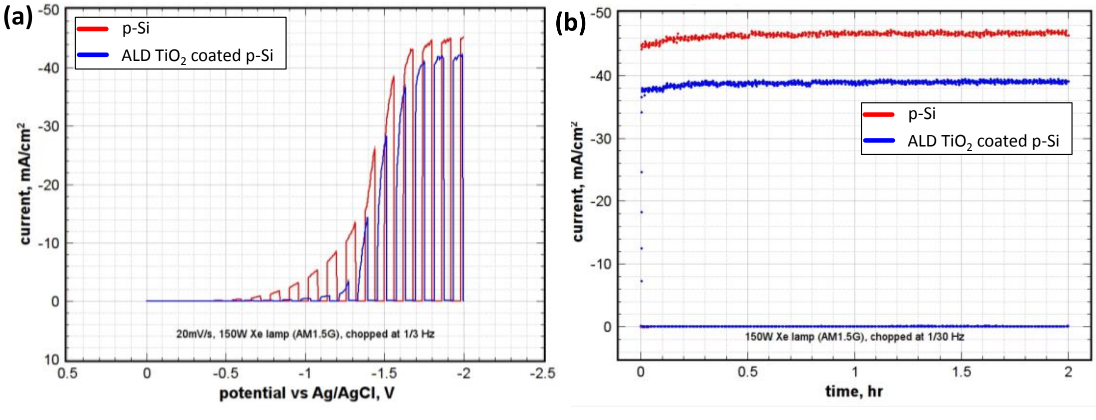

Figure 15. (a) Voltammogram showing the photoresponse of uncoated and TiO_2 passivated (1 nm) p-Si samples in a 0.5 M H_2SO_4 solution. (b) Stability of the same electrodes under a -1.5 V bias in a 0.5 M H_2SO_4 solution

In addition to the DSSC research, we are continuing to examine the use of ALD to modify photoelectrochemical cell structures. In this quarter, we examined the electrode stability of p-type [111] silicon samples mounted on fluorine-doped tin oxide (FTO) glass substrates. In addition, we examined the effects of a TiO2 passivation layer grown by ALD on the p-type Si surface (Figure 15(a)). As shown in Figure 15(b), these electrodes were found to be stable under solar illumination for at least two hours, with and without a passivation layer. Similar electrodes consisting of p-Si and FTO glass were coupled with commercial amorphous solar cells to construct tandem water splitting devices (Figure 16). One such device was tested in aqueous KCl under natural sunlight. With only the energy supplied by the sun, the electrode was observed to bubble continuously at each electrode, suggesting that unassisted water splitting took place. The current measured across the device indicated that the solar-to-hydrogen (STH) efficiency was approximately 0.1%. The same device was also constructed with in conjunction with a (DSSC), however the solar cell could not supply enough voltage to drive unassisted water splitting. In the next quarter the stability of n-type and p-type silicon samples will be investigated as a function of passivation layer thickness, silicon crystal type, and silicon conductivity.

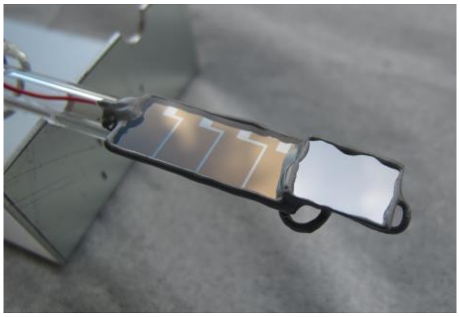

Figure 16. A tandem photovoltaic-photoelectrochemical electrode constructed from an amorphous solar cell (left) and a p-type silicon photoelectrode (right).

Q11:

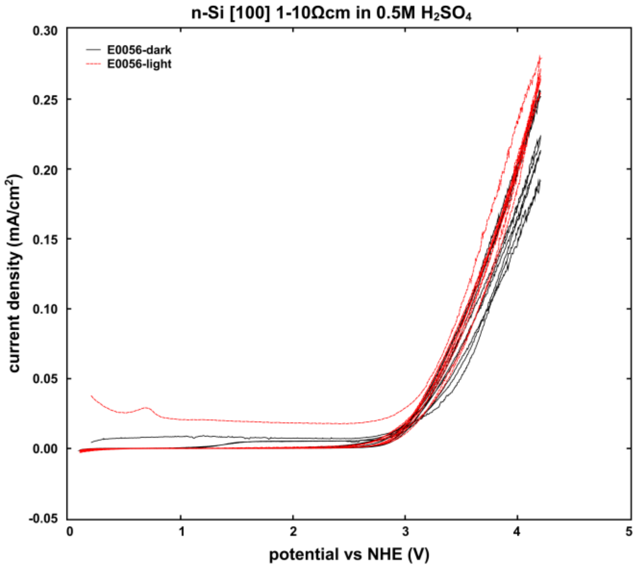

Figure 17. Cyclic voltammogram for n-Si electrode without passivation layer. Scan taken at 20 mV/s in 0.5 M sulfuric acid. One of five cycles is shown. Black traces represent dark measurements and red traces are measured under solar illumination. Over the course of five cycles surface oxide thickness increases from 8 to 35

We are continuing to examine the use of ALD to modify photoelectrochemical cell structures.   In this quarter we investigated the effectiveness of atomic layer deposition (ALD) processed metal oxides as passivation layers on unstable photoelectrodes. We deposited various thicknesses of Al_2O_3, ZnO, and TiO_2 on n-type [100] Si etched with hydrofluoric acid. The thin films ranged in thickness from 1 to 10 nm. To test the electrodes, we placed coated and uncoated samples of n-Si on FTO glass, sealed around the cleaved face with epoxy, and placed the completed device in a sulfuric acid solution. After each electrochemical test we measured the thickness of the silicon oxide layer using spectroscopic ellipsometery. We determined that metal oxide passivation films with thicknesses <50 Å impeded the growth of silicon oxide on n-Si photoanodes without degrading the electrochemical performance of the electrode. Thicker films resulted in loss of current density, while still functioning as effective passivation layers. With thin TiO_2 films we observed a tenfold increase in current, both in dark and under solar illumination, which indicates that titanium dioxide may facilitate hole transport into solution. We will further investigate metal oxide passivation films, with and without catalysts, and evaluate the long-term stability of n-Si electrodes with passivation.

Q12:

Research this quarter produced new results regarding metal oxide passivation films for long term stability of n-Si electrodes in photoelectrochemical cells. To establish a baseline for n-Si decomposition, we first recorded cyclic volt-ammograms in dark and then under illumination. The decay in current density (both in dark and with light) and any changes in water oxidation overpotential were interpreted as a sign of electrode decomposition by etching or formation of an insulating SiO_2. N-type silicon electrodes were measured at 20 mV/s scanning from 0 to 4.2 V vs. NHE in 0.5M H_2SO_4. There is no significant activity in dark, but under illumination, water oxidation starts at around 1.8 V in the first sweep, but shifts to higher potentials with each successive cycling, consistent with surface oxidation. Likewise, current density drops to 60% of its original value after the first sweep, and continues to decay with successive passes. Figure 18 shows current plotted against time to display the decay in current density. Each sharp peak corresponds to the current density measured at the far vertex of the CV sweep (4.2 V vs NHE).

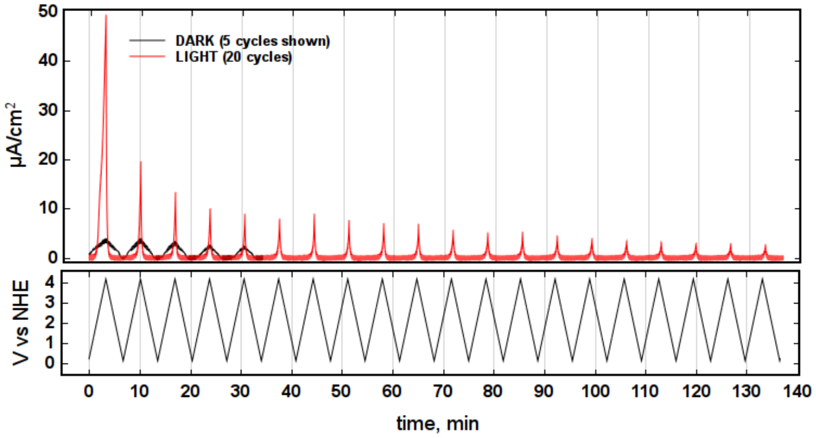

Figure 18: CV data from a bare n-Si (100) electrode plotted against time.

To evaluate surface passivation, three types of metal oxide films were deposited by ALD on n-Si substrates at thicknesses less than 15 nm and their stability under CV testing was evaluated. The best performing coating was generally TiO_2, and the performance versus ALD layer thickness is plotted in Figure 19. Work will continue in this area, including integrating catalyst layers.

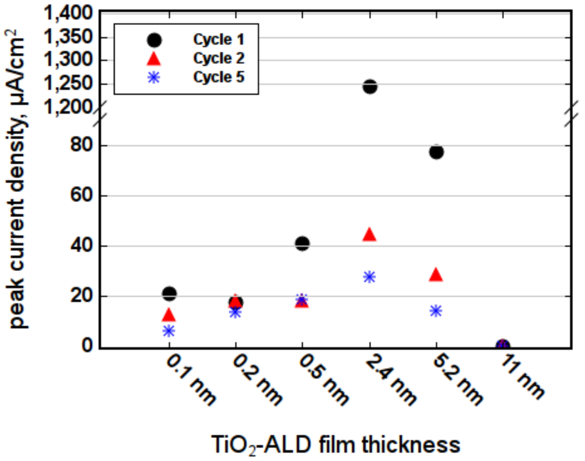

Figure 19: Passivation data for TiO_2-coated n-Si samples as a function of film thickness. Symbols show the peak current density for each sample at the vertex (4.2 V vs NHE) of voltammetry cycles 1, 2, and 5. The films that are 5nm thick show the best performance to date.

This project has enabled us to build significant interactions with the Research Triangle Solar Fuels Institute housed at Research Triangle Institute. The Solar Fuels Institute is a joint venture between NC State, Duke University, UNC-Chapel Hill and RTI, and our efforts on ALD coatings for stabilization are adding value to this activity.

Q13-15:

Our research in photoelectrochemical cells (PEC) devices focuses on utilizing atomic layer deposition (ALD) as a means to engineer the semiconductor-liquid interface of photoelectrodes. ALD modification can both impart chemical stability and tune the electronic band structure at the semiconductor's surface. P-type silicon photocathodes are a model PEC system capable of high photocurrents (>10 mA/cm^2) in aqueous electrolytes under AM 1.5 illumination. We are working to improve the reproducibility of silicon photocathode fabrication and to use TiO_2 ALD coatings for band engineering that permits planar catalyst integration. During this period, we examined silicon photocathodes fabricated from p-type Si (100) wafers with ~1 cm^2 functional area. Electrodes were tested in a three-electrode electrochemical cell containing sulfuric acid electrolyte (0.5M, pH ~0), a Pt mesh (>5 cm^2) counter electrode, and a Ag/AgCl reference electrode. To ensure similar dopant profiles, experiments were run using a range of silicon samples from the same wafer. We find a large and distinct effect on both the photocurrent saturation value and the photocurrent onset potential with the size and composition of this back contact. Through contact optimization, series resistance of the back contact can be reduced by 5x, as measured by impedance spectroscopy. This work allows us to reproducibly prepare electrodes for reliable surface engineering studies using ALD TiO_2. Deposition of a coalesced Pt thin film catalyst layer directly on p-type silicon is well known to form an ohmic contact that pins the silicon's Fermi level in a nearly flat band state. We find that without the internal bias caused by surface carrier depletion, photoelectrode activity is eliminated. However, by inserting an interfacial TiO_2 layer with sub-nanometer thickness control, a p-n junction can be formed which generates the necessary electric field for photoelectrode operation. ALD layers are capable of providing the necessary electronic band engineering to form completely planar p-Si/TiO2/Pt structures with photocurrents exceeding 10 mA/cm^2 with no applied bias.

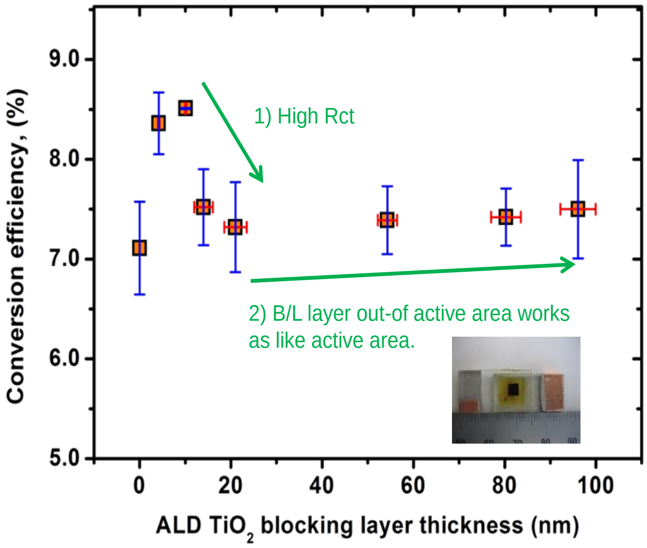

Figure 20.

In addition to PEC cells, we continue to investigate surface engineering in dye sensitized solar cells. In dye-sensitized solar cells, one of major recombination routes occurs at the interface of fluorine-doped tin oxide (FTO) glass and electrolyte solution. To reduce electron loss, a thin and compact blocking layer

(B/L) is typically deposited on the FTO-glass before mesoporous TiO_2 layer integration. Optimal thickness that suppresses the recombination on the interface of FTO glass and electrolyte, is typically 25 to 450 nm, depending on deposition methods and conditions. Compared to other methods, atomic layer deposition (ALD) with TiO_2 is not well established and investigated for blocking layers even though it is a valuable process in making pin-hole, crack-free, and dense TiO_2 films.

During this period, we studied ALD TiO_2 on FTO-glass with titanium isopropoxide and H_2O as precursors to form blocking layers with thickness from 5 to 100 nm. Cells without mesoporous titania but with ALD TiO2 B/L were also constructed. We find a blocking layer of 10 nm significantly reduces recombination, resulting in an average overall efficiency of 8.5% , compared to 7.1% for similar cells without the blocking layer present. We also find that a blocking layer of 4.3 nm effectively prevents electrons of FTO surface from recombining with I^{3-} in the electrolyte. On the other hand, a thick ALD TiO_2 blocking layer in excess of 10 nm tended to reduce the overall efficiency because the thick ALD TiO_2 film increases the charge transfer resistance and hinders the electron transport to FTO-glass. Results of overall cell efficiency versus ALD blocking layer thickness are presented in Figure 20. This work contributes to understand effective blocking layer from TiO_2 ALD process for DSSCs and other high-performance electrical devices.

Q16-17:

We have continued research in the area of photoelectrochemical cells (PECs) for solar water splitting and sustainable hydrogen fuel generation. P-type silicon is currently being investigated because of its high performance (> 10 mA/cm^2 of photocurrent) and substantial terrestrial abundance. We have continued with our optimization of the electrode fabrication and the use of atomic layer deposition (ALD) to modify the electronic band structure of planar silicon photocathodes. During the past 6 months we have also begun developing a synthesis route for creating silicon micro-pillars with controlled dimensions. We expect to use these silicon micro-pillars to understand how structure affects light absorption, charge collection, and bubble release.

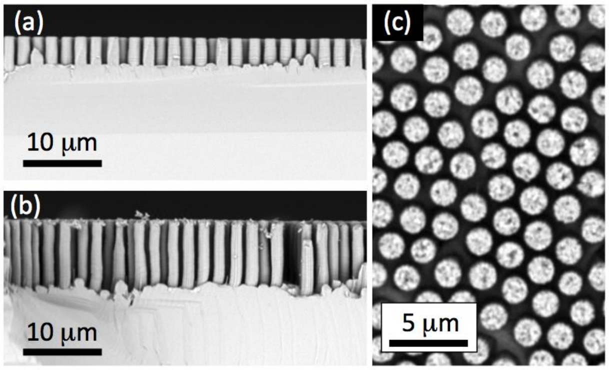

Fig. 21: *SEM micrographs of silicon micro-pillars being investigated for solar water splitting. Cross-sectional images for (a) 10 min of etching and (b) 40 min of etching. (c) top-down image.*

Fig. 21 shows SEM micrographs of the silicon micro-pillars that we are fabricating. These have been synthesized using a combination of colloidal sphere lithography and metal-assisted etching. A monolayer of PMMA spheres is spun-cast onto the silicon surface and used as a mask during silver deposition. The subsequent silver pattern is used for metal-assisted etching of the silicon in a HF-H_2O_2 solution mixture to create the silicon pillars shown here. Micro-pillar length can be varied based on

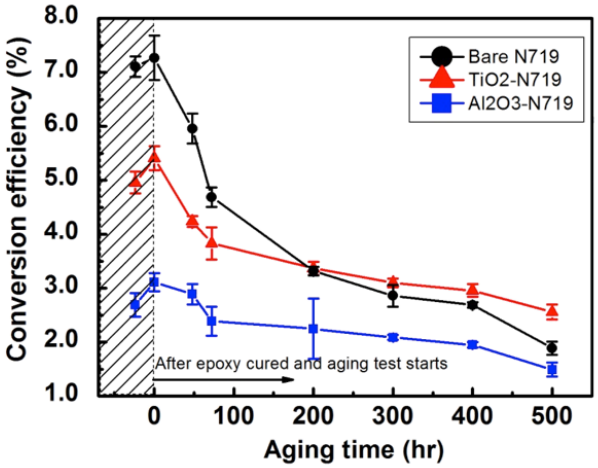

Fig. 22: *Long-term stability evaluation of DSSC conducted at 80 °C with and without ALD coatings.*

etching times (Fig. 21a and 21b). Pillar diameter can be adjusted depending on PMMA sphere size following a partial oxygen plasma etch. This process is still being optimized. Based on our prior work with silicon photocathode fabrication, we can reproducibly add back-side electrodes to these structures and confidently compare photocathode performance of each structure. Initial measurements of PEC performance show variation in saturation current with micro-pillar length.

Besides PECs, we also continue to investigate ALD modifications to dye sensitized solar cells (DSSCs). Over the past 6 months, we have started evaluating ALD coatings post-dye attachment as a means to increase long-term stability of DSSCs. Dye detachment and ligand exchange due to ambient conditions (e.g. humidity) is well-known to degrade DSSC performance. We hypothesize that sub-nanometer coatings applied via ALD may assist in chemically binding dye-sensitizers to the conductive scaffold and improve long-term stability. We have examined DSSCs treated with both a TiO_2 and Al_2O_3 coating (both less than 0.5 nm thick). Fig. 22 shows a standard 80 °C accelerated aging experiment for these DSSCs. While these coatings diminish the initial solar cell efficiency, the ALD treated DSSCs exhibit much slower degradation with time. Untreated DSSCs show an efficiency loss of 73% over 3 weeks' time while TiO_2 coated DSSCs lose 45% over the same period. *In-situ* infrared spectroscopy reveals that the ALD treatment is increasing the bridging linkages of the carboxylate groups of the dye molecule, which is presumably responsible for the improved stability.

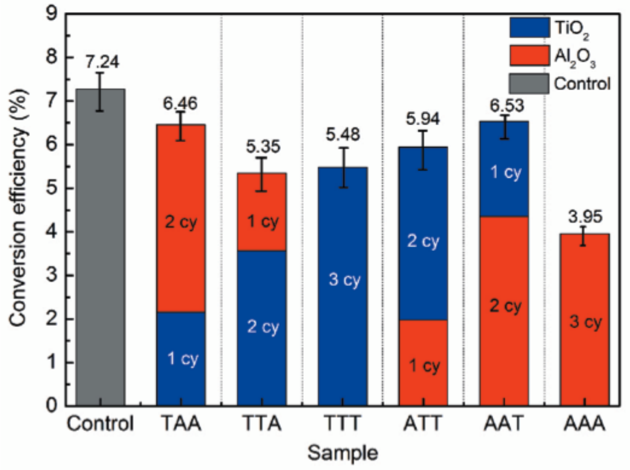

Fig. 23: *DSSC efficiency after coating with 3 ALD cycles of varying composition. A = Al_2O_3 ALD cycle, T = TiO_2 ALD cycle. (e.g., TAA = 1 TiO_2 ALD cycle followed by 2 Al_2O_3 ALD cycles).*

Q18-20:

During this project period, we have worked to better understand the use of atomic layer deposition (ALD) to improve the attachment of molecular dyes used in devices like dye-sensitized solar cells (DSSCs). In particular, we have focused on the stabilization of N719 functionalized mesoporous TiO_2 DSSCs when aged at elevated temperatures. Using in-situ FTIR analysis during ALD deposition, we have been able to identify reaction pathways between the ALD precursors and N719's carboxylate groups that lead to stronger binding to the mesoporous scaffold. In addition, we have found that ALD layers of mixed Al_2O_3 / TiO_2 chemistry show better DSSC efficiencies than either pure component. Previously, we found that while these sub-nanometer ALD layers improved device lifetime, overall performance was significantly degraded (25% to 45% worse than control DSSCs). However, these mixed ALD layers provide performance that is within 10% of control DSSC devices.

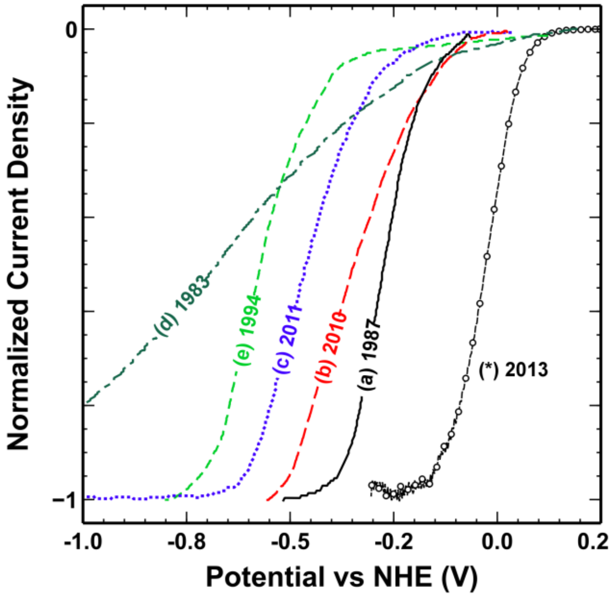

Fig. 24: *Representative polarization curves for p-Si photocathodes from the literature. From right to left, the curves were replotted from (a) J. Electroanal. Chem. 228 1987, (b) Electrochem. Commun. 12 2010, (c) Energy Environ. Sci. 4 2011, (d) Appl. Phys. Lett. 42 1983, (e) Appl. Surf. Sci. 75 1994, and (*) this research project.*

We have also continued to work in the area of photoelectrochemical cells (PECs) for solar water splitting. During this period, we have finalized our investigation of standardizing the fabrication of high-performance silicon photocathodes. A number of researchers are interested in applying nanostructures or electronic band engineering to silicon photocathodes to improve photocathode performance. However, as Fig. 24 illustrates, the unmodified control silicon photocathodes produced by researchers in different labs can vary considerably. Our research has established straightforward protocols for reproducible, high-performance silicon photocathodes, which can then be used as a starting point for further modification. For instance, we are now examining the addition of TiO_2 ALD layers as a strategy for modifying the electronic band structure at the cathode / electrolyte interface.

Finally, during this project period, we have also constructed an additional ALD reactor to further support the ongoing work to stabilized molecularly sensitized systems (see Fig. 25). We suspect that hold steps may be important to the infiltration of vapor phase precursors into the nanostructured electrodes of interest for these applications. For this reason, we have constructed an ALD system with an advanced hold system design to permit more detailed investigations of this process.

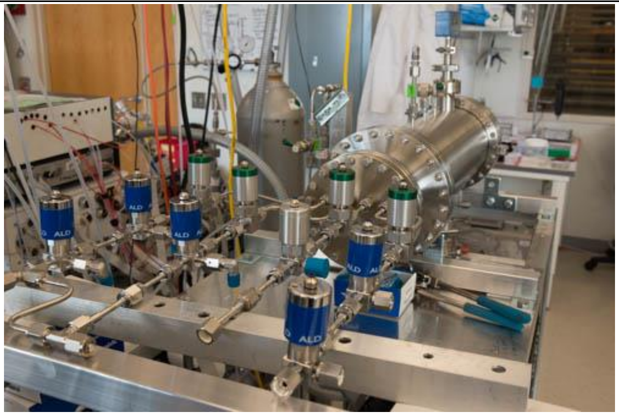

Fig. 25: *Photograph of new ALD reactor.*

Subtask 3.2 Enhanced Photon Absorption with Nanostructures *(Dickey)*

Q1:

Initial efforts have begun on the investigating high surface area electrodes for high-efficiency solar cells. A commercial e-beam evaporator (Kurt J Lesker) that has been used in the laboratory previously is in process of being refurbished for this purpose. This system will be used for investigation of metal film buckling phenomena and shadow evaporation into nano-scale templates as high surface area electrodes for high-efficiency solar cells. Effort has been spent on setting up a new laboratory for not only for thin film evaporation, but also for the in-house chemical synthesis of the poly-3-hexylthiophene (P3HT). P3HT is a conjugated polymer that is commonly used in organic electronic devices, including transistors and solar cells. We are presently characterizing the material chemically (NMR, GPC) and electrically. We plan to incorporate this material into the nanostructured solar device.

Q2:

Nanostructured substrates have been successfully fabricates as a first step towards the goal of producing high surface area electrodes for high-efficiency solar cells. Characterization of the fabricated substrates is underway with the new tools that have completed installation (Task 2.0). We are also studying methods to deposit indium doped tin oxide--a transparent conductive oxide used in solar cells--onto these nanostructured surfaces. The installation of a thin film deposition system (e-beam evaporator) continues to be a priority.

Q3: Full efforts are underway on investigating high surface area electrodes for high-efficiency solar cells. This project requires deposition of thin-films of metal and metal-oxides. We have refurbished and installed a commercial e-beam evaporator (Kurt J. Lesker) in the laboratory. This system is operational and being used to study a spontaneous metal film buckling phenomena. We have also been working with a colleague, Prof. JP Maria, on thin-film deposition techniques, such as sputtering. Dr. Maria has committed a student to help us deposit Indium Tin Oxide (ITO) films, which is a transparent conductive oxide. We are currently exploring a matrix of processing conditions (pressure, temperature, power) to better understand the key variables in the deposition process and have found some surprising results that disagree with the literature. Figure 26 is an AFM

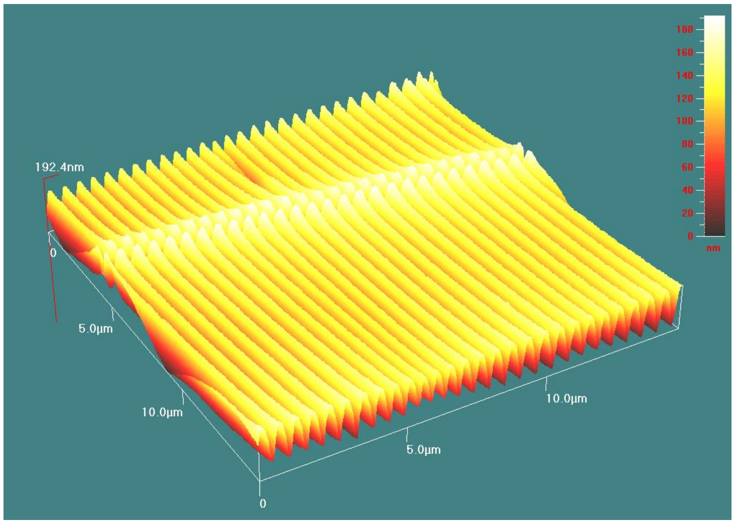

Figure 26. Atomic force micrograph of a buckled substrate with a Indium Tin Oxide coating.

image of ITO buckles. The graduate student working on this project, Ms. Ying Liu, has completed her first academic year and successfully passed her "proposition" course in which she wrote and defended an independent proposal that expanded on this work. These efforts have provided her with an excellent background in the field and she will be fully engaged in research this summer. We have also hired an undergraduate research assistant, Mr. Jackson Menius, who has been advancing this project by studying the optical properties of buckled substrates using UV-Vis measurements. His work suggests that the buckles improve the light absorption of conformal thin-films coated on the buckles, which is critical for improving solar cell efficiency.

Q4:

Efforts continue on investigating high surface area electrodes for high-efficiency solar cells. A hierarchically-structure consisting of buckles (i.e., superimposed wrinkles of indium tin oxide with wavelengths ranging from nm to mm) of has been developed through collaborative work with Prof. J.-P. Maria (Materials Science and Engineering) and Prof. Jan Genzer (Chemical and Biomolecular Engineering). Such a structure would improve the light harvesting efficiency of organic photovoltaic (OPVs) and be compatible with goal of a flexible substrates. The optical properties of the ITO are being investigated as a function of deposition parameters and optimization is underway for the useful implementation into the buckled nanostructured device. With the use of an integrating sphere accessory on a spectrometer it has been demonstrated that the buckled structures absorb light more efficiently than planar structures. In parallel, development of the laboratory techniques for bulk heterojunction solar cell is underway, with the guidance of the Misra group.

Q5:

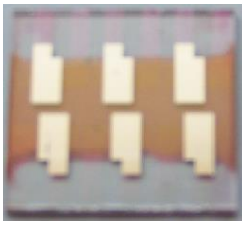

Figure 27. Photograph of a prototype photovoltaic device fabricated using our new facilities.

Our top priority is to illustrate the benefits of nanostructuring a thin film photovoltaic device by comparing the performance of a nanostructured organic photovoltaic (OPV) with a conventional planar OPV. The appeal of our approach is the simplicity by which we can create light harvesting structures in a thin film OPV device. We produce the nanostructures by harnessing a thin film instability known as buckling. We have successfully created our first working OPV structure on a flat piece of glass. The device is composed of indium tin oxide (ITO, a transparent conductive electrode), PEDOT:PSS, P3HT:PCBM (the bulk heterojunction polymer blend), and Al (as the top electrode). Figure 27 is a photograph of a representative substrate, which has six devices on a single glass substrate. This standard structure is our benchmark to which we will compare our results. Without optimization, we have achieved two percent conversion efficiency in this device. Our next step is to create a buckled solar cell and compare the performance with that of the benchmark. The benchmark solar cell is fabricated on commercial ITO on a glass substrate. In contrast, the buckled solar cell requires the deposition of our own ITO. ITO is a challenging material to deposit effectively to achieve high transparency and low resistivity. We are currently collaborating with the Maria group in Materials Science (NC State) to optimize this process.

We are characterizing these substrates to understand differences between our as-deposited devices and those purchased commercially. For example, we are studying the roughness of the surface by atomic force microscopy, the crystallinity by x-ray reflectivity, and the hydrophobicity of the surface by contact angle measurements. We are systematically varying the processing parameters to determine the important aspects of the process. Prof. Maria has committed a student to help us deposit the ITO films. Concurrently to this work, we have prepared a series of samples with different buckling patterns (of polymer thin films) and are evaluating the optical properties of these surfaces through the use of an integrating sphere and a UV-Vis spectrometer. The first step is to characterize these substrates carefully using atomic force microscopy. Figure 28 is an atomic force microscopy of a representative surface.

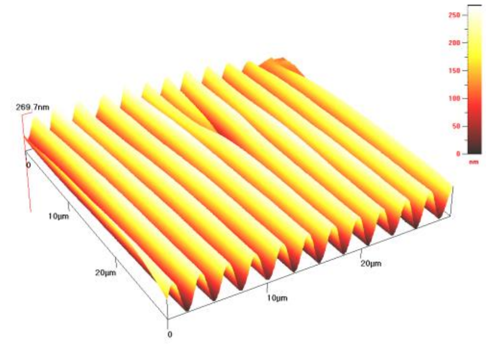

Figure 28. Atomic force micrograph of a buckled substrate with a thin film coating.

Q6:

The goal of this subtask is to improve the efficiency of organic photovoltaics (OPVs) through the use of topography. We produce hierarchical topography (superimposed corrugations with wavelengths ranging from nm to mm) by harnessing a thin film instability known as buckling. We have made significant progress toward the goal of comparing a conventional (i.e., planar) OPV with one featuring topography. Figure 29 is a current-voltage (I-V) trace from a typical OPV fabricated in our laboratory. We are optimizing the process used to fabricate these devices since it is the benchmark to which we will compare the OPV featuring topography. Fabrication of the buckled OPV requires the deposition of indium tin oxide (ITO), which is a notoriously challenging material to deposit effectively. We have shown that our as-deposited ITO is less crystalline and more resistive (by ~10x) than commercial ITO, but has similar transparency as measured by UV-Vis spectroscopy

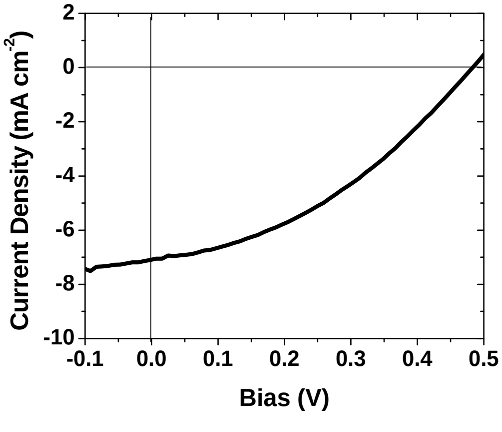

Figure 29. I-V trace of a organic photovoltaics fabricated in our laboratory. The PCE is 1.3% and fill factor is 0.38.

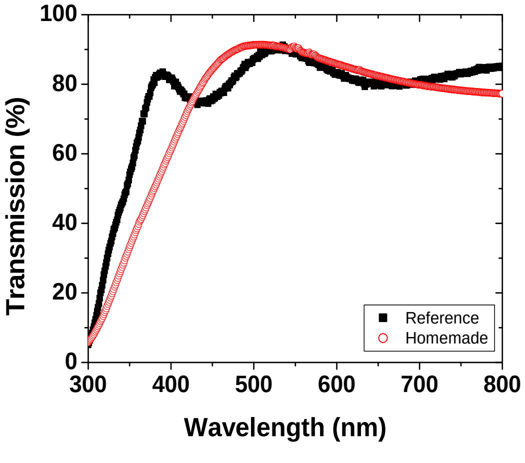

Figure 30. UV-Vis transmission spectra of commercial ITO ("reference") versus ITO deposited in our lab ("homemade").

(Figure 30) We are optimizing the deposition process of ITO and evaluating the extent to which the ITO properties affect our solar devices. We have also optimized the processing parameters for one of the organic layers in our device (PEDOT:PSS). We have varied the thickness, annealing conditions, and filtration steps and identified the best conditions for the OPV. We are working currently to build on this knowledge to fabricate a buckled OPV. Perhaps the most promising result is we have shown that the buckled topography increases absorption by ~30% relative to a planar geometry.

Q7:

Our ultimate goal in this subtask is to compare a conventional (i.e., planar) organic photovoltaic (OPV) with one featuring topography (formed by thin-film buckling) to improve light harvesting. We are doing several tasks in parallel toward this goal. We are optimizing the processes used to fabricate the planar OPV, which involves many steps that are poorly understood in the literature. Our devices are just below 2% efficient, which is approaching the best reported results for the materials we are using. Establishing a reliable planar process is important as a basis for comparison with buckled surfaces. We are also developing new methods to form the buckles with processes that are more compatible with OPV processing. Figure 31 is an optical micrograph of representative buckles formed by depositing indium tin oxide (ITO) on a polymer film supported by a glass substrate. The buckles form due to thermally induced stresses. To maximize light harvesting, we have been optimizing the processing conditions to maximize the aspect ratio (height to wavelength) of the buckles. For example, the first three columns in Figure 32 illustrate the way in which the aspect ratio depends on surface treatment (as predicted, more rigid films give higher aspect ratios). We are also developing a rapid prototyping technique for replicating the buckles using curable pre-polymers. Figure 32 shows how well the aspect ratio is replicated into various polymers (NOA 81, NOA 63, and Epofix). This rapid prototyping technique will expedite the rate in which we can produce samples in the future.

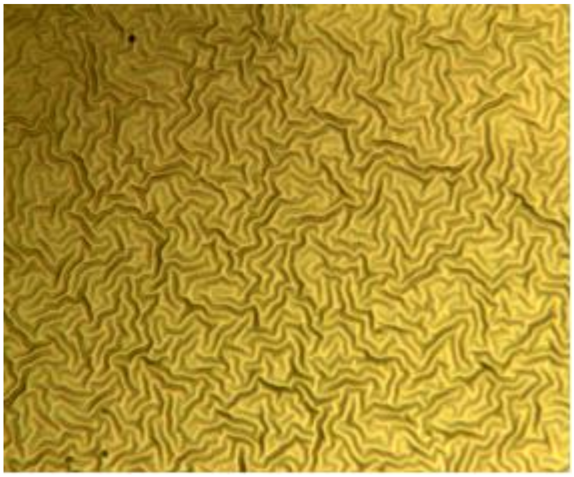

Figure 31. An optical micrograph of thermally induced buckles of an ITO films on a polystyrene film supported by a glass substrate. The buckle period is ~1μm.

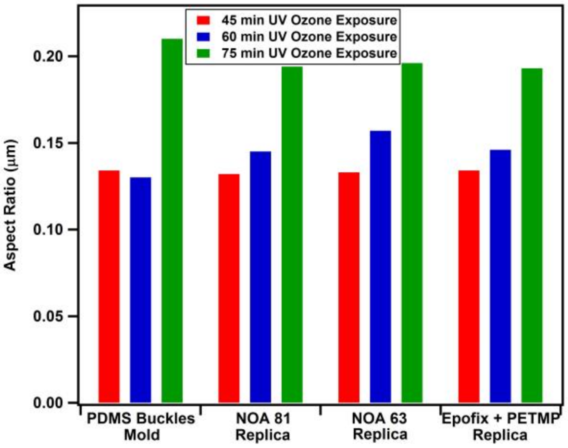

Figure 32. The aspect ratio of the buckles depends on the processing conditions (red, blue, green) and can be replicated into various polymers (NOA 81, 63, and Epofix).

Q8:

We are progressing toward our goal of improving the light harvesting of organic photovoltaics (OPVs) by introducing topography (formed by thin-film buckling) in a cost effective and scalable manner. We have identified a standard process to fabricate the OPV devices (this process involves ~30 steps, so it was a major undertaking to optimize the process). We fabricated our first buckled OPV device, shown in Figure 33. The device consists of larger buckles with smaller buckles superimposed. The first batch of devices have a low yield, so we are currently studying ways to improve reliability. We have also collected significant amounts of optical data to show how the topography of the substrate improves light harvesting. Figure 34 is a plot of absorbance versus wavelength that compares a flat OPV versus an OPV featuring topography. Although these results are promising in the sense that they suggest improved light absorption by substrates featuring topography (which is the premise of the project), we are currently re-evaluating these results because of some complexities arising from integrating sphere measurements used to capture the data.

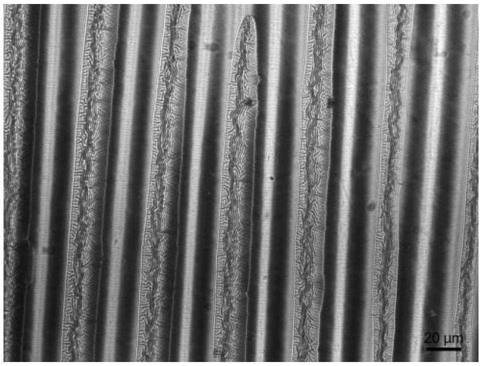

Figure 33. An optical micrograph of an OPV. device on a hierarchically buckled substrate.

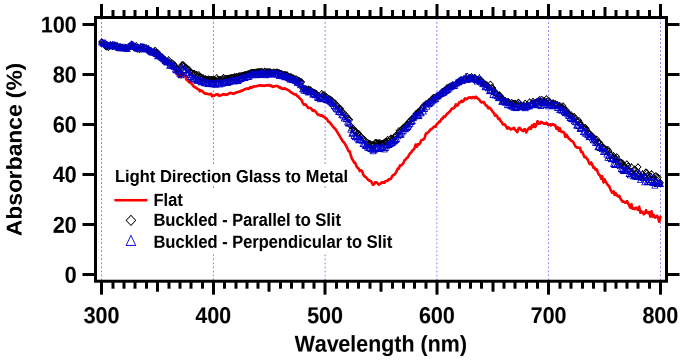

Figure 34. UV-vis absorbance spectra that show improved absorbance with substrates featuring topography.

Q9:

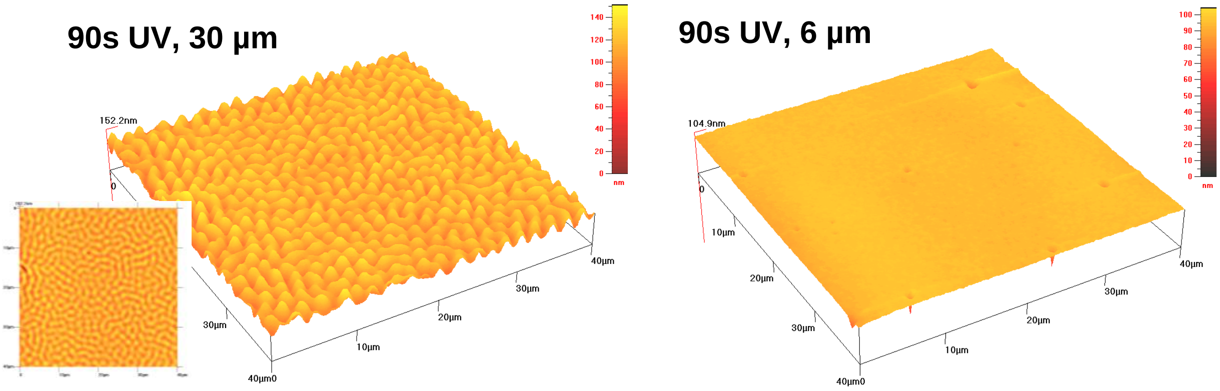

Figure 35. Atomic force micrographs of ITO films on epoxy substrates.

In prior quarterly reports, we outlines our progress toward our goal of improving the light harvesting of organic photovoltaics (OPVs) by introducing topography (formed by thin-film buckling) in a cost effective and scalable manner. We are pleased to report that we have repeatably measured a 40-60% increase in electrical current for organic photovoltaics (OPVs) featuring topography versus OPVs that are planar (i.e., conventional devices). The improvement in current may correspond with improved light absorption, which is a primary goal of this subtask. We are currently working toward improving the reliability of the OPV devices and improving the fill factor. The fill factor is relatively low, which we believe to be due to the interface of the indium tin oxide (ITO) used to fabricate the OPVs. In parallel, we continue to measure the optical properties (e.g., absorbance) of topographical substrates versus planar substrates. We have measured some improvement in optical absorption of light using the topographical substrates, although these measurements have been complicated by the limitations of integrating spheres. Finally, the topography we use for the OPVs is built on top of a transparent polymer substrate. We have been optimizing the processing parameters to ensure that the OPV devices do not crack during processing (e.g., due to poor interfacial adhesion or thermal stresses). Figure 35 shows two atomic force micrographs of ITO on epoxy with different topographies that results from different processing conditions of the underlying polymer film (in this case, different thickness, although we have varied many different parameters). This result is useful because we can tune the topography (or lackthereof) by simple, controllable processing conditions.

Q10:

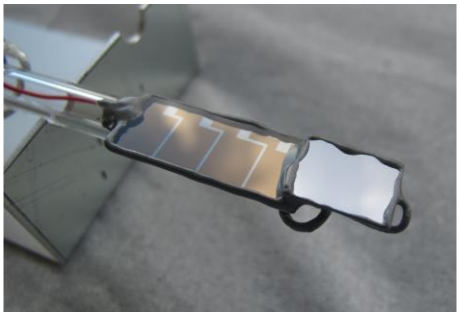

Figure 36. A tandem photovoltaic-photoelectrochemical electrode constructed from an amorphous solar cell (left) and a p-type silicon photoelectrode (right).

Last quarter, we reported measuring a 40-60% increase in electrical current for organic photovoltaics (OPVs) featuring topography versus OPVs that are planar (i.e., conventional devices) and we repeated these results three times (although we have also had many failed devices). This encouraging result was the primary goal for this project, but we are still trying to elucidate the mechanisms and improve reliability. We have been working this past quarter on improving the fill factor (an important metric that affects efficiency) by coming up with new ways to fabricate the devices. One of the primary issues that we identified was poor film quality of PEDOT (a conducting polymer) on ITO electrodes supported by a polymeric substrates. Modifying the surface energy of the polymer substrates proved to be a simple method to improve film quality. Figure 37 shows a picture of a 1”x1” substrate featuring six devices. The buckled topography is

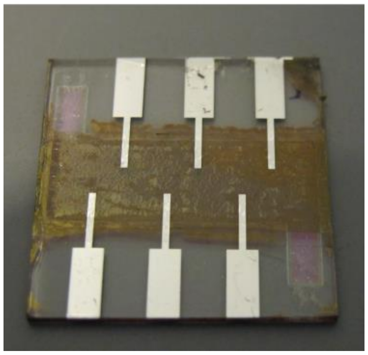

Figure 37. Optical micrograph of an OPV featuring topography.

apparent from the rough surface. We have been developing models in COMSOL and a ray tracing software to understand the role of the topography for improving light absorption. The goal of the modeling is to elucidate the mechanisms responsible for improved OPV performance. We have also been evaluating simple methods to increase the aspect ratio (i.e., height to width) of the topography to increase the light harvesting further. For example, we have shown that electric fields can amplify the surface features resulting in an increased aspect ratio.

Q11:

We have two primary accomplishments this quarter. First, we have nearly completed a first draft of a manuscript describing the use of topography to capture light more effectively for organic photovoltaics. Second, we have begun exploring an unconventional approach to make topography for light harvesting. Our original goal (and the focus of the manuscript) was to use nano- and microscale buckles to harvest light more efficiently in OPVs. The appeal of our approach is that we could build the OPVs using planar processing and then use stresses in the film stack to create the topography. We now report an alternative approach that is equally compelling. In this approach, we use flat, pre-stressed polymer films as substrates (which can be used to build solar cells, such as organic photovoltaics). These substrates are inexpensive, transparent, and readily available (e.g., heat shrink films). Onto these substrates, we pattern light absorbing lines and upon irradiation with an unfocused, inexpensive light bulb, these two-dimensional sheets fold within seconds. The heat generated by the lamp causes the stress to relax and therefore hinge. The appeal of our approach is that it harnesses the capabilities of common 2D patterning techniques (e.g., lithography, roll-to-roll, inkjet printing) to create 3D structures. These self-folding substrates are simple and inexpensive and may be useful for packaging and actuation, in addition to light harvesting. Examples of the strcutures capable by this process are shown in Figure 38. We have completed a manuscript on this work and plan to submit it within the week.

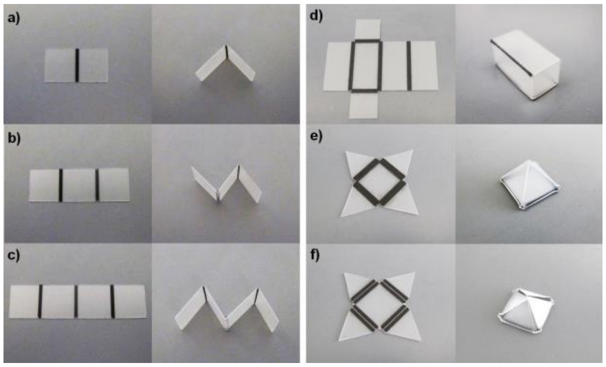

Figure 38. Photographs of self-folded structures that convert. 2D patterns into 3D shapes.

Q12:

In this quarter we continued our efforts to construct pre-stressed polymer films as substrates for inexpensive construction of organic photovoltaics. This work was motivated by the spirit of subtask 3.2, which is to demonstrate simple method of creating light harvesting patterned topograhy. These patterned regions become ‘hinges’ that allow the sheet to fold into useful structures upon exposure to light (the hinges absorb the light and get hot, which triggers the folding). We reported on the details of the mechanism in the previous report. The “V-shaped” structures we create could be useful for optical funneling of light. We have begun drafting a follow up manuscript that goes into more details of the mechanisms, including the heat transfer mechansim (Figure 39) Our second major accomplishment is that we have developed a collaboration with Prof. Ert Cubukcu (U. Penn) to help us with the optical modeling of our buckled solar cells. This model is the only missing piece that we need to publish our work. The initial modeling shows a significant increase in light absorption by using a buckled topography relative to a planar topography. We are currently working with the Cubukcu group to ensure that the model is physically realisitic. We have drafted the experimental portion of the manuscript and are only awaiting these modeling results to complete it.

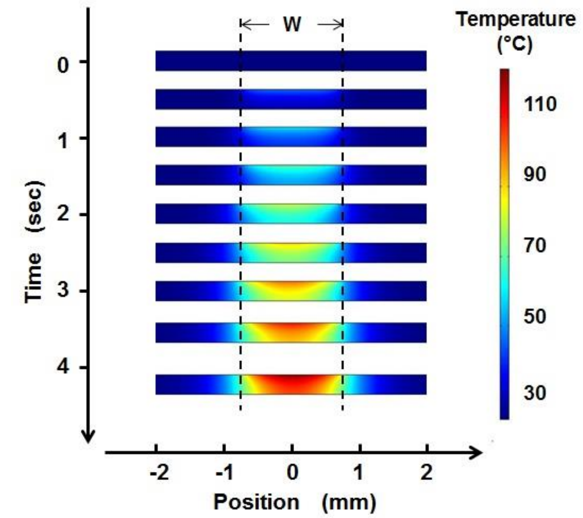

Figure 39. A cross-sectional view of the temperature profile in a self-folding sheet exposed to light as a function of time. The hinged region is of width, *W*. The model shows that the top surface of the film gets hotter, which is critical for creating the folded topography.

Q13-15:

We continue to focus on methods to convert planar surfaces into surfaces featuring topography, which has implications for light harvesting. Recently, we published our first paper on this topic in Soft Matter in which we converted 2-D patterns into 3-D structures via 'self-folding'. In that work, hinges patterned by an inkjet printer absorb light, which causes local heating of the hinges and thereby induces folding. During the current reporting period, we have been studying many aspects of this process. For example, we have demonstrated sequential folding by varying the light absorptivity of the hinges. We have explored the use of laser 'writing' to directly deliver heat locally, which eliminates the need for pre-patterened hinges (Figure 40). We have also been working to elucidate the temporal-temperature-mechanics relationships and the role of the hinge geometry. To that end, we have been measuring the thermo-mechanical properties of the polymer and have worked in collaboration with Prof. Yong Zhu (MAE, NC State) to model the mechanics. The concept is to convert information about the temperature profile in the hinge (reported last period) into mechanical response. We are aso using the "V-shaped" structures we create to improve absorption of light for solar cells. The idea is to create substrates that fold toward the direction of the sun and thereby create an optical funnel geometry. We are currently drafting two papers; one on understanding the fundamentals of self-folding and another on the influence of topography on light absorption.

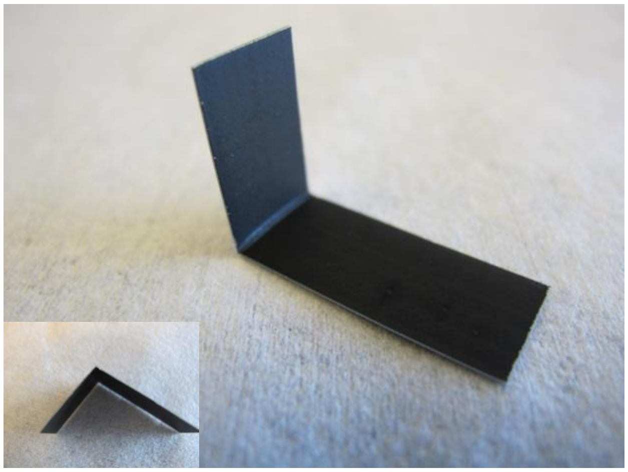

Figure 40. A photograph of a polymer sheet (~1 cm wide) that self-folds in response to a rastered laser beam. We are using

Q16-17:

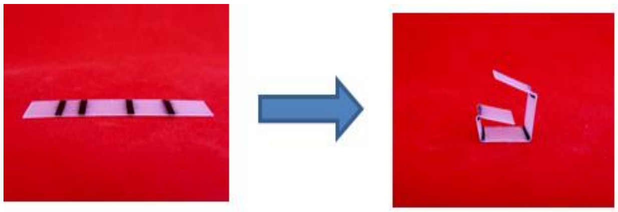

Figure 41. A photograph of a polymer sheet (~1 cm wide) that self-folds sequentially in response to different wavelengths of light. The ability to control the sequence of folding is important for making more complex structures. The appeal of this approach is it converts 2D patterns into 3D shapes.

We continue to focus on methods to convert planar surfaces into surfaces featuring topography, which has implications for light harvesting. During the current reporting period, we have been working on sequential folding (i.e., controlling folding temporally and spatially). We have used two approaches. In the first approach, we have been using inks with selective light absorption so that we can use the light from light emitting diodes (LEDs) to induce the folding. With this approach, the hinges can be activated depending on the wavelength of light utilized (Figure 41). In the second approach, we are using an IR laser to initiate folding. The laser can be rastered across a surface and anywhere it strikes the substrate, it generates sufficient heat to induce folding in pre-stress polymer sheets. The advantage of this approach is that it requires no pre-processing or patterning of the sheets and it is compatible with high throughput processing. We have begun drafting a manuscript for this work. Finally, we have nearly completed a manuscript describing the thermo-mechanical behavior of self-folding polymer sheets. We have used two approaches to our modeling including thermal-mechanical measurements and finite element modeling.

This subtask was completed at the end of Q17, October 24, 2012.

Subtask 3.3 Nanostructures for Organic Photovoltaics *(Misra)*

Q1:

Research has focused on extracting the electronic and photoactive properties of porphyrin molecules in novel nanostructure-based photovoltaic devices. Porphyrins have very strong absorption coefficient and, similar to most organic polymers, they have small diffusion length of the primary excitons generated during absorption of photon. Porphyrin is being incorporated in novel nanostructured devices, shown in Figure 42, that consists of ordered pillars of electron acceptors (such as fullerenes or TiO_2) such that every exciton formed in the electron donor polymer layer is within a diffusion length of the electron acceptor in the device. We have investigated the carrier transfer mechanisms of these porphyrin polymers interfaced with semiconductors, dielectrics and metals. Traditional cyclic voltammetric measurements indicate that these polymers are incorporated with 1×10^{15} charges/cm^2 and when this polymer is deposited on silicon, these redox states are able to communicate with the valence band of Si. The nanostructure design is in process of being investigated by the use of a Deep UV 193nm scanner (ASML 5500/950B) and novel fabrication routes such as e-beam lithography to achieve a dense pitch between the anode and cathode lines.

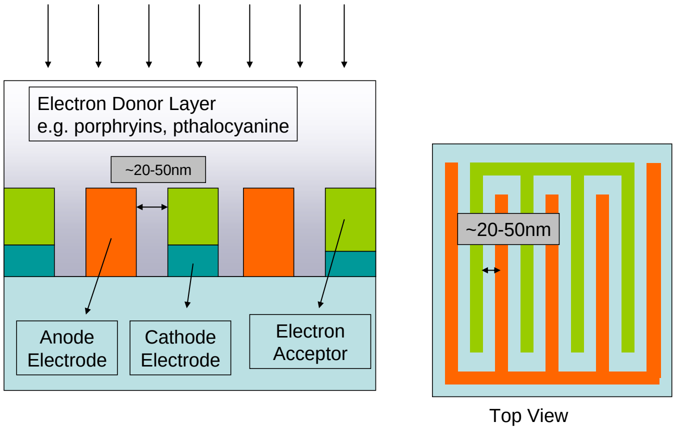

Figure 42. Nano-pillared structures proposed for novel solar cell designs based on porphyrin polymers.

Q2:

Methods to fabricate our previously proposed nanopatterned solar cell devices are underway with the goal of incorporation of these nanopatterned structures with the organic photovoltaic materials detailed in *Subtask 4.2*.

Q3:

The impetus to fabricate nanostructured organic solar cells stems from the fact that most organic molecules, which constitute the active components, have small exciton diffusion lengths. The immediate nanostructuring goal for this project is to create an array of nanopillars 300nm in width and height. While there are many possible

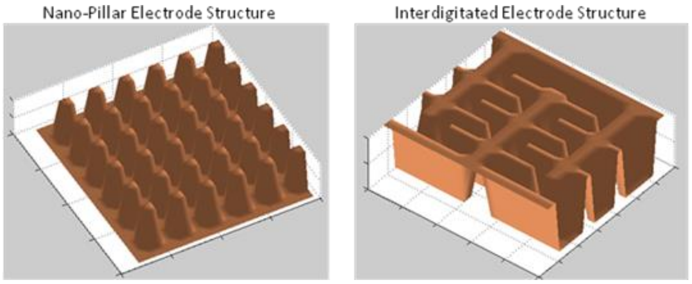
Nano-Pillar Electrode Structure

Interdigitated Electrode Structure

Figure 43. Schematics of features in the nanostructured solar

techniques for fabricating nanostructures, using a patterned mold structure with a nano-imprint tool in particular is being investigated because of its low fabrication cost. Recently, a test run using E-Beam Lithography has been undertaken to create a small pattern in a 2 inch Silicon wafer that could be used as a nano-imprint mold. The write time for this method was very long, and other options are being considered for higher throughput. As an alternative that is more suitable for large area molds, fabrication using a 193nm scanner is currently being planned. Once a suitable sized mold is created, application with the nano-imprint tool will be performed. PMMA may be spin-coated on top of existing solar cell substrates then patterned using the nano-imprint tool. The PMMA and ITO can then be directionally etched in a controlled manner; optimization of these etch recipes is being currently explored. In this way the array of 300nm pillars on the ITO substrate of the solar cell can be realized. Future goals for similar processes include creating designs of more complex electrode structures. Of particular interest is the realization of opposing electrodes in an interdigitated network, as shown in Figure 43.

Q4:

The use of nanostructures is investigated as a method to overcome the small exciton diffusion lengths that most organic molecules used in organic photovoltaics. Nanoimprinting is used in this work as a low cost technique to achieve nanostructured devices with enhanced performance. We have used the NC STATE ASML193nm deep UV lithography tool to fabricated nanoscale molds of varying sizes and densities by varying exposure energies (Figure 44, top: 120nm holes). Following lithography, the patterned photoresist was etched into the underlying SiO_2 so it may be used as a mold for imprinting. Reactive Ion Etching (RIE) is currently being explored to accomplish this and this is currently under development to optimize size, aspect ratio. While this process is still under development, the pattern has been successfully etched into the silicon wafer using this method as shown in Figure 44 (bottom).

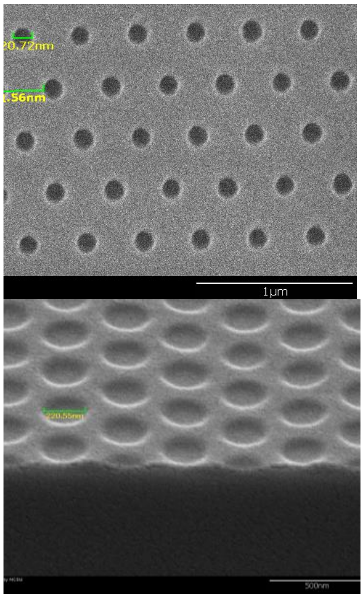

Figure 44. Nanoscale mold formation: 120 nm holes patterned by deep UV lithography (top), and etched hole in underlying Si substrate (bottom).

While development of an optimized mold structure is underway, initial tests of the nanoimprinting process have also been done on solar cells. We have used a nanoscale mold to imprint into PMMA for solar cell applications. Difficulties in the imprinting process that were encountered included optimization of the PMMA thickness, and overcoming wafer sticking which can damage the imprinting pattern. Furthermore, use of a simple anti-stick monolayer is also being investigated to prevent any further issues with wafer sticking.

Q5:

In order to overcome the weak absorbance of photoactive layer, we are incorporating metal nanostructures between the ITO substrate and the active layer. When the frequency of the incident light is in resonance with the surface plasmon of the metallic nanoparticles, a strong scattering of the incident light is exhibited. As a result, absorption of the active layer is enhanced due to the high electro-magnetic field strength in the vicinity of the excited surface plasmons. In this regard, we are depositing gold nanoparticles (Au np) on the ITO substrate.

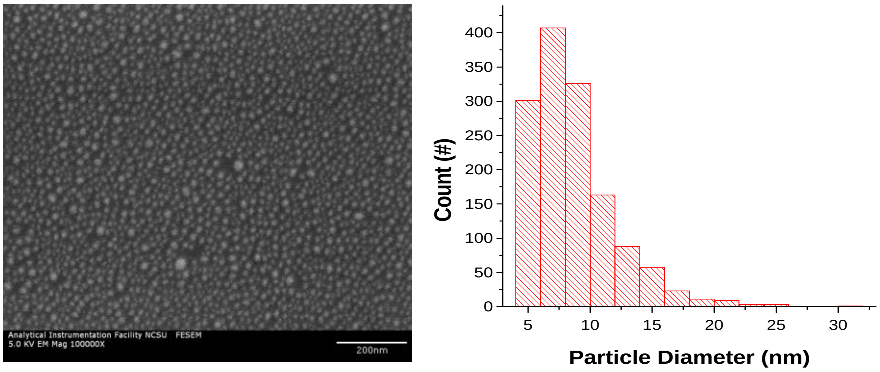

Figure 45. SEM of Au nanoparticles formed on 37 Å SiO_2/Si substrate and the particle distribution for these nanoparticles.

In our initial approach, we assembled citrate stabilized Au nanoparticles on the surface using a layer by layer approach. A positively charged layer of poly-l-lysine was formed on the surface and negatively charged citrate stabilized Au nps electrostatically interacted with this layer to form quantum dot/poly-l-lysine aggregate. However, the loading density of gold did not increase considerably with subsequent layer formation. Therefore, we used another route for the formation of gold nanoparticles. A thin film of Au is deposited using E-beam evaporation followed by a rapid thermal annealing for a minute at 600°C yielded a high density of nanoparticles as shown in Figure 45. We are currently assembling the Au np on the patterned ITO substrate and our future efforts include studying the SERS effect for these nanostructured substrates for solar cell application.

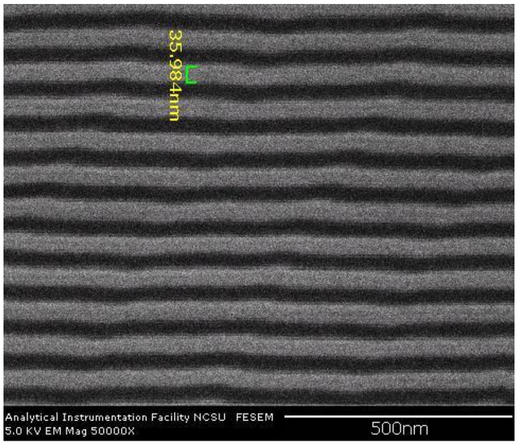

Figure 46. SEM of sub-40 nm mold that will be used to transfer patterns into the ITO/P3HT BHJ devices.

In addition to the above, new imprinting designs are being explored for use in nano-structured solar cells. A new mold (Figure 46) is being used to replicate nano-structures with smaller features than any attempted so far. A structure such as this may be used to realize long term goals of a double electrode solar cell structure. With a pattern similar to the one shown above, oxide sidewall spacers can be formed on the sides of the first pre-patterned metal lines. The second metal electrode can then be filled in the gaps between the first metal lines, forming the double electrode structure. Once this is done, the oxide spacers can be removed, and the organic light absorbing polymer layer can be deposited everywhere, finishing the process.

Q6:

Recent progress in achieving an interdigitated two-electrode structure has been accomplished by utilizing E-Beam Lithography (EBL). Schematic representation of the structure has been shown in Figure 47. This method of lithography is used to pattern an array of gold nano-wires on a non-conductive substrate, followed by patterning an identical array of aluminum nano-wires placed in between the gold wires. The organic polymer would be spun on top of the nano-structured interdigitated electrode with light coming from the top end of the structure.

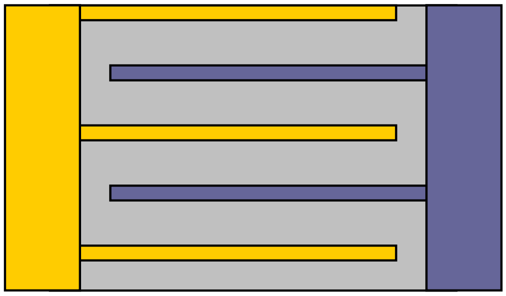

Figure 47. Schematic representation of the interdigitated two-electrode structure

The device patterns were written using two separate aligned layers of EBL. For the first layer of EBL, electrons were accelerated at 50 Kev at a beam current of 50 pA to create nanowires with a designed thickness of 50 nm on a silicon wafer with 80 nm thick thermal oxide. After patterning nanowires, the samples were subjected to brief oxygen plasma to remove residual photoresist. This was followed by deposition of Au layer by e-beam evaporation and lift-off. Prior to Au deposition, a 7 nm of Ti layer was deposited for better adhesion of gold. An identical procedure was followed for patterning another set of nanowires that were spaced in between the gold nanowires using EBL. After a descum process using oxygen etch, and a 150 nm aluminum evaporation was done using e-beam evaporation and followed by liftoff with acetone.

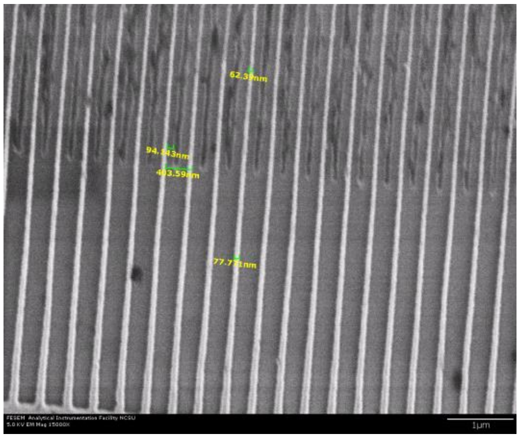

Figure 48. SEM micrograph of the interdigitated metal lines. Gold lines can be seen with lighter coloring coming the bottom

SEM image for one of the nanostructured device is shown in Figure 48. The thickness of the gold layer, aluminum layer and the spacing between the two layers are 150 nm, 150 nm, and 150 nm, respectively. The lines have presently been patterned over a field 300 um x 300 um, and placed connecting to respective contact pads to the left and right of the device. Our current efforts involve (i) improving the fabrication techniques such as liftoff and exposure to improve resolution of nanostructures on the surface (ii) increasing the spacing between the two metal layers, and (iii) deposit bulk heterojunction polymer layer top of the nanostructured surface to test the photovoltaic response.

Q7:

Organic solar cells have the potential of becoming ubiquitous sources of renewable energy however; they undergo rapid degradation upon exposure to oxygen and water. Therefore, adequate encapsulation from ambient oxygen and water is an essential requirement. In our recent effort, we have utilized ultrathin Al_2O_3 layers deposited by atomic layer deposition (ALD) as the primary barrier layer for protecting OPVs from ambient moisture or oxygen without the requirement of UV-curable epoxy resin film as an additional sealant. This work shows that encapsulation characteristics of a barrier layer, deposited using ALD, can be accentuated by replacing H_2O with O_3 as the ALD oxidant. Al_2O_3 layers deposited using O_3 offered superior device encapsulation compared to the films deposited using H_2O. The organic solar cell efficiency has been studied as a function of Al_2O_3 thickness and effective encapsulation has been monitored for two different ALD temperatures. Amongst the various Al_2O_3 thicknesses monitored, 210 cycles of O_3-Al_2O_3 offered the best device encapsulation and the OPV retained 80% of its initial efficiency over a period of 500 hours. The barrier layer thickness of 18 nm, utilized in the present work, is one of the thinnest encapsulating layers reported in literature providing excellent protection of organic solar cell from ambient water and oxygen. The O_3-Al_2O_3 films demonstrated excellent encapsulation characteristics for a much lower effective oxide thickness compared to the H_2O-Al_2O_3 films.

Q8:

There is no new data to report in this quarter.

Q9:

In this subtask we have previously reports a novel interdigitated Double-Electrode (DE) structure that aims to reduce device losses from carrier recombination by allowing long optical path, such that all photons may be absorbed and that enables short diffusion path for carriers to reach the electrode. Numerical simulations were performed to understand effects of the double-electrode structure and were compared with the conventional planar cells. The simulated J-V characteristics (following Koster, Phys Rev B. 2005) for planar cells were in good agreement with the experimental data. When the active area thickness was varied from 50nm, 100nm, 150nm, and 200nm, J_{SC} showed strong thickness dependence (Figure 49, top) that can be related to the number of photo-generated

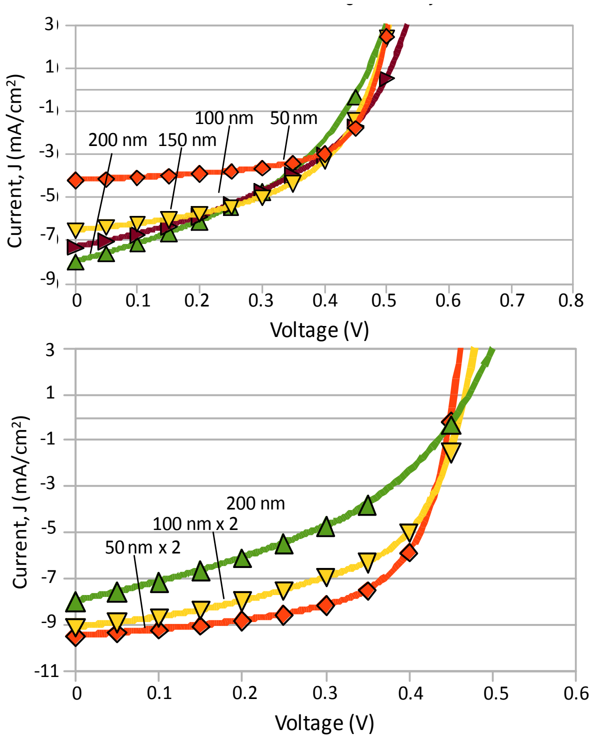

Figure 49. (top) J-V characteristics simulation of devices with varying thickness. (bottom) J-V characteristic of structured and unstructured 200 nm thick cells.

Table 1. Performance of 200 nm thick structured cells and unstructured cell.

Thickness	Jsc	Voc	Max Power	Efficiency	FF
50 x 4	-9.52	0.46	4.38	2.64	0.6
100 x 2	-9.14	0.46	4.2	2.22	0.53
200	-8.01	0.45	3.6	1.43	0.4

carriers with slight variation in V_{OC}. This is because thin films cannot completely absorb incident light while thicker film absorb more photons and demonstrate larger J_{SC}. Simulations were also performed for a stack of four 50nm thick cells reaching a total 200nm thickness, a double-stacked 100nm cell and these were compared with the traditional planar 200nm cell. The J-V characteristics for the three cells are shown in Figure 49 (bottom) and Table 1 lists the cell performance. The 50nm width cell showed a ~85% improvement over a 200nm spaced cell. This performance gain is believed to be due to a reduced carrier recombination inside the cell, resulting in an improved in fill factor. Considering the above simulation, the double-structured electrode is a very interesting device structure as it has the potential to explicitly demonstrate the effects of electrical losses within the organic solar cell.

Q10:

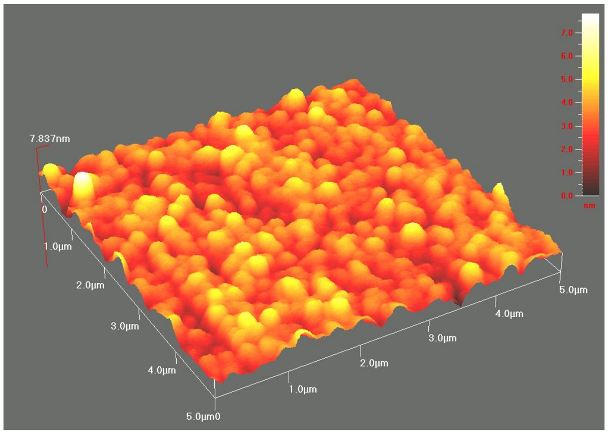

Figure 50. Atomic force microscopy of a graphene oxide layer on glass by spincasting (4000 RPM).

In the present work, we have utilized graphene oxide to replace PEDOT:PSS as the hole blocking layer in a bulk heterojunction (BHJ) solar cell design. Graphene oxide (GO) is a graphene sheet functionalized with oxygen groups in the form of epoxy and hydroxyl groups on the basal plane and edges. The PEDOT layer is typically deposited from highly acidic solutions and known to corrode ITO electrodes at high temperatures. The GO layer, on the other hand, can be deposited from neutral solutions. In this work, a 2 mg/mL GO solution was spuncast on to an ITO substrate at 3000 rpm. These substrates were then taken inside the glovebox and spuncast with a P3HT:PCBM to form the bulk heterojunction. The samples were then taken outside the glovebox for thermal evaporation of Al. After the deposition of top electrode the samples were subjected to post deposition anneal at 150 °C for 20 minutes in controlled environment. The devices were tested outside the glovebox. An atomic force microscopy (AFM) image of the GO layer deposited on glass slide at 4000 rpm is shown in Figure 50. The thickness of the layer is determined to be ~4 nm. A representative J-V measurement of the BHJ solar cell utilizing GO as a hole blocking layer is provided in Figure 51(a). The solar cell shows an open circuit potential of 0.64 V, a fill factor of 50% and an efficiency of 1.65%. Efforts are being made to make the GO layer thinner which should result in an increased current density and overall devices efficiency. Furthermore,

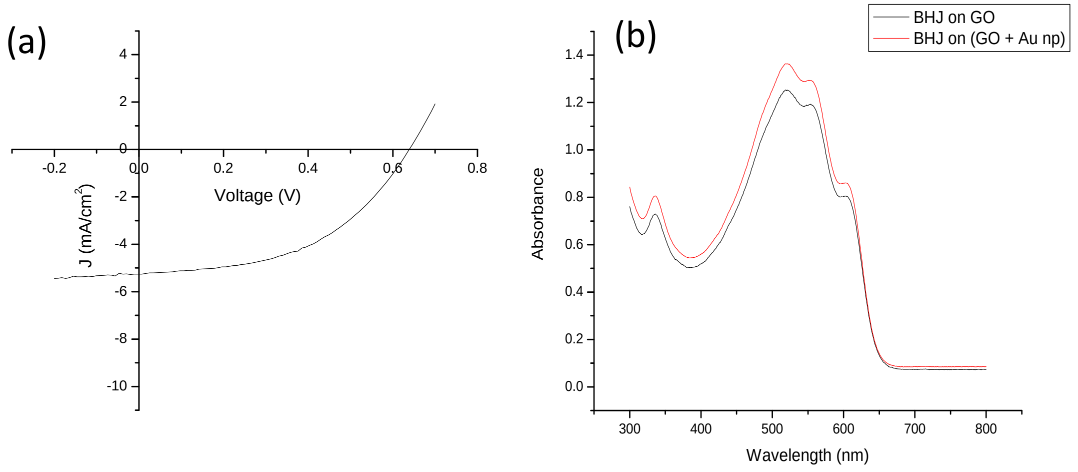

Figure 51. (a) J-V characteristic of graphene oxide-based bulk heterojunction solar cell, and (b) visible spectroscopy analysis of the bulk heterojunction layer on glass slide modified with graphene oxide (black) and graphene oxide layer embedded with gold nanoparticles (red).

we have explored embedding 2 nm Au nanoparticles in the graphene oxide layer to take advantage of the SERS effect of the nanoparticles on the polymer layer which would increase the optical absorbance. In this regard, we have mixed citrate stabilized Au nanoparticles with the GO solution (10% vol/vol) and spuncast the solution on a glass substrate. Figure 51(b) shows that the overall polymer layer exhibits a small enhancement in the UV-absorption measurement with the incorporation of gold nanoparticles. We are currently working towards increasing the loading density of nanoparticles in the GO layer in order to observe a more substantial SERS effect.

Q11: Plasmonic solar cells are emerging as promising candidates amongst many solar energy technologies in order to improve device performance. When the frequency of the incident light is in resonance with the surface plasmon of the metallic nanoparticles, a strong scattering of the incident light is exhibited. As a result, absorption of the active layer is enhanced due to the high electromagnetic field strength in the vicinity of the excited surface plasmons. Noble metals are ideal for this purpose as they do not have many interband transitions and hence, do not absorb much light. In this regard, we are incorporating silver nanostructures within the device stacks owing to its lower cost compared to gold. The nanostructures are formed by depositing thin film of silver by e-beam on the ITO substrate followed by rapid thermal anneal for 30s at 550 °C. The SEM in Figure 52 shows the formation of silver

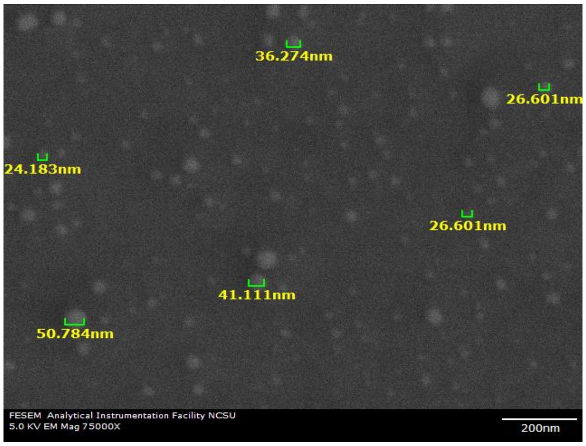

Figure 52. SEM of an ITO substrate coated with 15 Å of silver followed by a rapid thermal anneal at 550°C for 30 s.

nanostructures on ITO substrate for a sample where 15Å of silver was deposited and annealed for 30 s at 550°C. Figure 53 shows the J-V characteristic of an organic solar cell, where nanostructures were formed by depositing 7 Å of silver film on ITO followed by a subsequent anneal. We obtained an efficiency of 2.45 % for this cell and this is lower than that observed for a control cell without the incorporation of metal nanoparticle (2.8 %). We believe that device efficiency would improve with increase in loading density of the nanoparticle in the OPV cell. This can be achieved by increasing the thickness of the silver film. Our current efforts are directed in systematically changing the metal film thickness and form nanostructures with different size and loading density on the ITO surface.

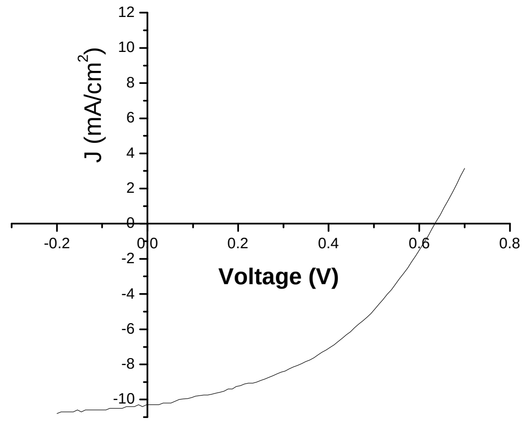

Figure 53. J-V characteristics for an OPV cell incorporating nanostructures formed by depositing 7 Å of silver followed by 30s of RTA at 550°C.

Q12:

This subtask was completed at the end of Q12, July 25, 2011.

Task 4.0 Photoactive Nano-materials

Subtask 4.1 Gel-based Photovoltaic Materials (Velev)

Q1:

Experimentation is under way of a new concept for how the matrix and the rectifying junctions of organic solar cells can be reconstructed based on the use of simple and inexpensive gels. Previous work has shown that a new type of ionic rectifying junction can be formed at the interface of two water-based gels doped with polyelectrolytes of opposite charge (JACS, 2007, 129, 10801). Preliminary prototypes of photovoltaic cells have been constructed by forming a fixed ionic junction between agarose gels doped with photosensitive organic molecules, DAS- Na+ as an electron donor and $[Ru(bpy)_3]_2+(Cl^-)_2$ as an electron acceptor. Nearly all prototypes of various gel/dopant configurations demonstrated photovoltaic generation. Results have shown an open circuit voltage as high as 0.6 V while current density is comparable to polymer photovoltaics.

Q2:

Research continues with the investigations of the mechanism of operation and means of optimizing the water-based solar cell technology that they have developed. The effect of the aqueous gel composition on the photovoltaic performance of the cells has been investigated. The results confirm that the gel composition can be improved by adding polyelectrolytes to increase the ionic conductivity. Inexpensive copper electrodes with carbon coating were tested as a substitute for the platinum counter electrodes. The copper electrodes showed comparable photocurrent, solving the problem with high cost of the originally used platinum electrodes. Further studies are under way to characterize the effect of the surface area of the working electrode, which may drastically increase the efficiency of these organic devices.

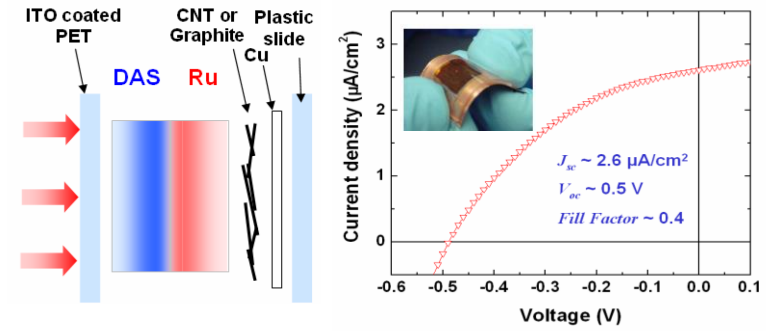

Figure 54. Performance data, schematic and photograph of a test prototype of new flexible gel-based photovoltaic device using an inexpensive Cu/Carbon electrode (Velev group, NCSU).

Q3:

We continued the characterization and optimization of the prototypes of photovoltaic cells formed by a fixed ionic junction between two oppositely charged polyelectrolyte gels containing photosensitive organic molecules. The prototypes were tested in terms of voltage output, photocurrent generation under various loads, I-V cycle characteristics with and without illumination, speed of response and physical stability. We performed a cycle of studies directed at replacing the platinum with an inexpensive metal. This turned out to be a nontrivial task, as the electrochemical potentials of Al and Cu were too high for the generation of a large voltage. We found an efficient solution by coating the Cu surface with a layer of carbon nanotubes or graphite. The modified Cu/C surfaces had a performance comparable to the Pt electrodes and allowed us to construct a prototype of a flexible and inexpensive cell (Figure 54). These devices are made by a benchtop process, which involves mostly preparation of water-based agar gels and is much simpler compared to the oxygen-less, ultra-clean environment that is needed to fabricate polymer solar cells. Recently, we also tested water gel devices made on the basis of biological photoactive molecules – Chlorophyll and Photosystem II. We proved that both bio-complexes generated photocurrent and voltage, where the performance of the Chlorophyll was significantly better.

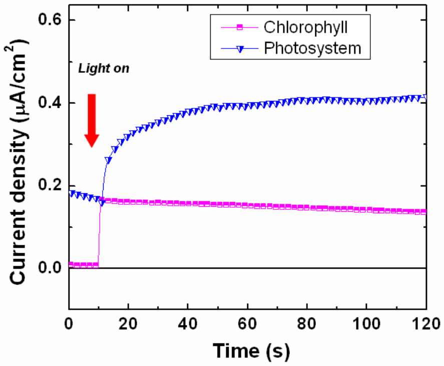

Figure 55. Photocurrent performance of gel-based cells operating on biological photosynthesizing complexes.

Q4:

We continued our investigation of photovoltaic cells formed by a fixed ionic junction between two oppositely charged polyelectrolyte gels containing photosensitive organic molecules. In previous reports it has been shown that prototypes devices were tested in terms of voltage output, photocurrent generation under various loads, I-V cycle characteristics with and without illumination, speed of response and physical stability. It was observed that the Pt electrode could be efficiently replaced with a Cu surface coated with carbon nanotubes or graphite. The modified Cu/C surfaces had a performance comparable to the Pt electrodes and allowed us to construct a prototype of a flexible and inexpensive cell. While much of this work has focused on photosensitive synthetic dyes, it would be preferable to use environmentally benign components that are efficient in aqueous systems. Therefore, a goal of our research is to replace the original photoexcitable molecules with light harvesting complexes of biological origin, Chlorophyll and Photosystem II (provided by collaborators in the RX Bio Program at AFRL). Figure 55 shows that both bio-complexes generated photocurrent and voltage, where the performance of the Chlorophyll was significantly better. Future work will be based on the assembly of nano-complexes composed of natural photosystems (PS) and phycobiliproteins (PB) (from plants and bacteria) and optically-active metal or semiconductor nanoparticles (NPs). In addition, we will investigate the immobilization of the photosensitive molecules in the gel matrix in order to prevent performance deterioration due to their diffusion across the gap.

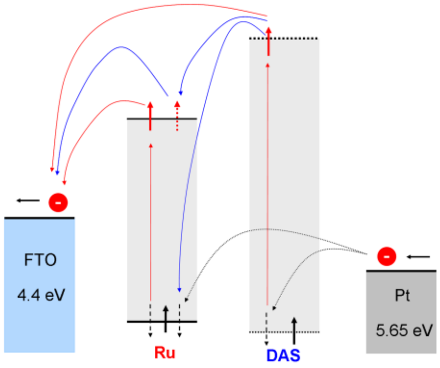

Figure 56. Provisional mechanism for new hydrogel-based photovoltaic cells (Velev group, NCSU).

Q5:

We have optimized and characterized the prototypes of hydrogel-based photovoltaic devices, formed by ionic junction between gels containing two oppositely charged photosensitive molecules. To understand the working mechanism of the photosensitive molecules in the devices, we investigated the effect of the dye location in the gel by inserting dye-infused dry gel into the interfaces between FTO glass/gel or Pt electrode/gel. A series of experiments showed that Ru dye is predominantly photoactive at the FTO glass surface while DAS dye generates photocurrent not only on FTO surface but also in the bulk of the hydrogel. Based on the result about the effective location of each dye, we suggested the provisional mechanism shown in Figure 56. The energy levels of two dyes are qualitatively estimated based on UV-vis absorption data. Both DAS and Ru dyes can generate the photocurrent by absorbing light and directly injecting the excited electrons to the FTO side. Moreover, the DAS dye in the bulk of the gel probably contributes to the regeneration of the oxidized dye molecules by providing the excited electrons. The lower LUMO level of the Ru dye than the DAS dye may also facilitate the electron injection from the DAS dye. Thus, the two dyes are likely to have cooperative functionalities. The device with both DAS and Ru dyes showed photocurrent density nearly five times higher than those with either of the dyes (Figure 57), which supports the hypothesis of synergetic effect of the dyes.

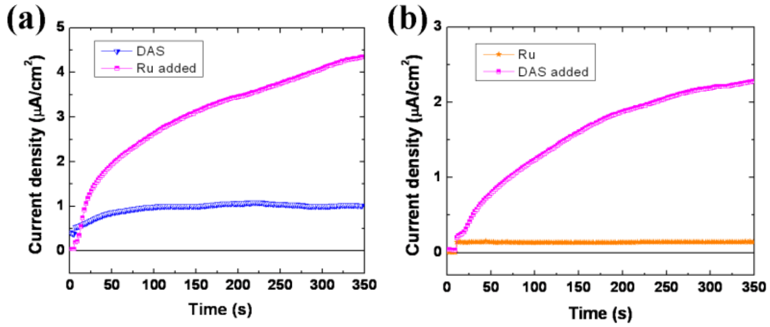

Figure 57. Photocurrent densities as a function of time. (a) DAS was added to the device first, followed by Ru addition. (b) Ru was added to the device first, followed by DAS addition. Both cases show the large increase of photocurrent densities when the other dye was introduced.

Q6:

Previously, we have reported the photoactive dyes in our system work not only on the surface of electrodes but also in the bulk of the hydro-gel. Due to the contribution of the dye ions in the bulk, the hydro-gel photovoltaics (HGPV) cells have time-dependent current response to the illumination. We have further investigated transient ionic characteristics of HGPVs by comparing the photocurrent responses of HGPV cells with that of standard dye-sensitized solar cells (DSSCs). Since all of the dyes in DSSCs are adsorbed on electrodes, they exchange current with

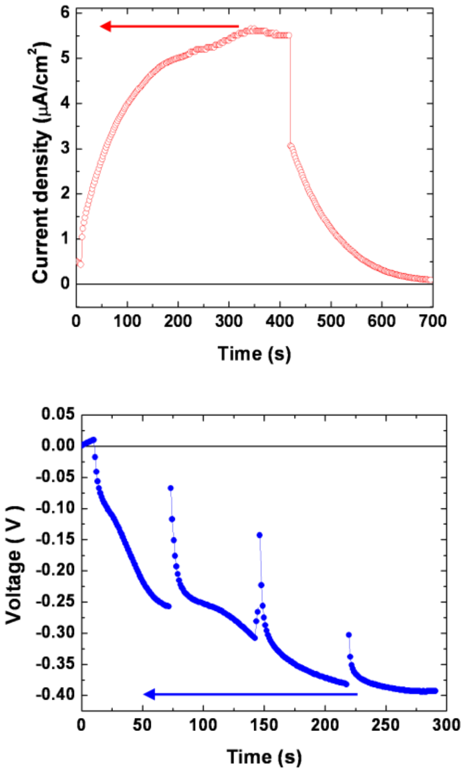

Figure 58. The intrinsic (saturated) photovoltaic properties of HGPVs: photocurrent density at V = 0 V (top) and photovoltage at I = 0 A (bottom). The photovoltage was measured four times under continuous illumination, which results in the discrete curve.

the electrode directly, not through the bulk. When the light is turned on, the DSSCs exhibited an immediate response to the light, while the photocurrent in the HGPV cells gradually increased after an initial current leap. These different time-dependent responses of two systems were also displayed when the light is off. The transient current response of the HGPV cells probably results from the contribution of the DAS ions in the bulk to the current. It takes time for the excited DAS ions in the bulk to affect the photovoltaic properties by performing either or both functions of “photocurrent generating” and “photoreducing” agent based on our model mechanism reported previously.

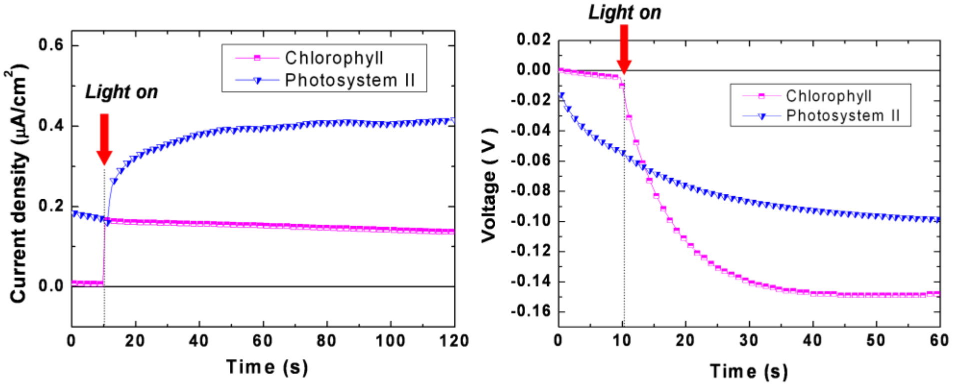

Figure 59. Photocurrent densities and photovoltage of gel-based cells operating on biological photosynthesizing complexes. The red arrows indicate the time when the light turned on.

To examine the intrinsic photovoltaic properties, J_{sc} and V_{oc} of HGPVs were measured under continuous illumination until the values are saturated. As shown in Figure 58, J_{sc} and V_{oc} stabilized at 5.6 μA/cm^2 and 0.4 V after 300~400 seconds. These saturated values are 30~40% higher compared to the performance by the bias sweep method (J_{sc}: ~4 μA/cm^2 and V_{oc}: ~0.31 V). The sweep rate of 17.5 mV/s is too rapid for the stabilization of the dye ions, which may be the reason for the under-estimation by the bias sweep method.

We also fabricated hydro-gel photovoltaic devices made on the basis of Chlorophyll and Photosystem II to replace the original dye molecules with biological photoactive molecules, which operate in an aqueous environment. Both biomolecules generated comparable photocurrents of 0.2 μA/cm^2, while the voltage developed by the Chlorophyll (0.16 V) was better than the one of Photosystem II (0.07 V) (Figure 59). Even though the photovoltaic performance of these prototype devices was not high enough yet, the performance could be improved further because the amount of the biomolecules used was very small (7.6×10^{-10} mol of Chlorophyll and 3.6×10^{-9} mol of Photosystem II) and the devices tested were only the first prototype. We believe that such biomolecule-based devices will be key components in biomimetic, environmentally benign photovoltaics and water based HGPVs.

Q7:

The degradation of photoactive molecules in dye-based photovoltaic systems, including common DSSCs and our newly developed HGPV cells, is a critical problem, which decreases the long-term performance of photovoltaic cells. Continuous slow replenishing the photo-damaged dye molecules can solve the regeneration problem in a biomimetic fashion. Microfluidic channels embedded in the hydrogel of plant

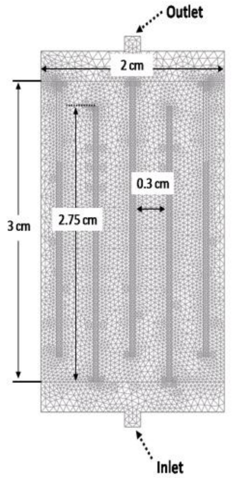

Figure 60. A top-view illustration of the pattern of the meshed simulated microfluidic solar cell. The channel length was varied from 1.5 cm to 2.95 cm.

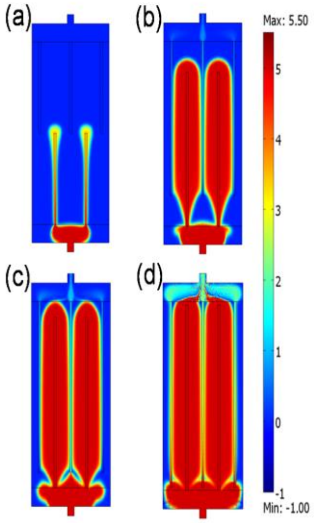

Figure 61. Simulation results for the effect of the channel length on dye supply and distribution at 500 seconds. Channel length: (a) 1.5 cm, (b) 2.5 cm, (c) 2.75 cm, and (d) 2.95 cm.

leaves through which reagents are provided for photosynthesis. We developed modeling tools in order to investigate how rapidly and efficiently the dye could be supplied and distributed in microfluidic channel networks of various designs embedded in hydrogel cells. 2D numerical modeling of the dye distribution in hydrogel devices with interdigitated microfluidic channels was performed by using COMSOL multiphysics simulation package. An example of the dimensions and structure of a simulated microfluidic design is shown in Figure 60. The computational model takes into account two physical phenomena: the fluid transport in the porous hydrogel media and the convection and diffusion of the dye solute. The simulated results of dye distribution in the hydrogel microfluidic devices with different channel length are shown in Figure 61. The images represent the dye distribution at time t = 500 seconds after dye injection. Qualitatively, the area covered with dye increases as the relative length of the linear interdigitated channels increases, which means that the longer microfluidic channels provide a higher influx of the dye. As the flow resistance of this pattern is lower, under an identical pressure, the flow rate becomes higher as the channel length increases. When the channel length is too long, however, the supply of the dye becomes less efficient because a larger amount of incoming dye flows out through the exit port (for example, in a 2.95-cm channel design, relatively large amount of the dye flows out of the device compared to the designs with shorter channel lengths). We are presently performing and in-depth quantitative evaluation of the rate of dye supply and the efficiency of various channel designs.

Q8:

We continued the fundamental research on the gel-microvascular networks that will serve for efficient replenishment of the degraded dye in organic photovoltaic cells. Such microfluidic networks can act as the capillary network in live green leaves and can solve the problem of photomolecule degradation in dye based photovoltaic systems. A two-dimensional numerical model of the dye distribution in hydrogel devices with interdigitated microfluidic channels was developed by using a COMSOL multiphysics simulation package. In the previous quarter, an in-depth parametric study was conducted to quantitatively evaluate and compare the efficiency of the different shapes of the microfluidic design based on simulation results. Three basic shapes of the channels have been compared; “linear”, “T-shaped” and “fractal” structures as shown in Figure 62. The efficiency in dye replenishment was determined on the basis of the required time and the amounts of supplied and lost reagent for specific coverage of the dye in the gel media. The efficiency of dye distribution in three different channel geometries is compared in Figure 63. Even though the fractal structure has fastest inflow rate of the dyes into the channel, it has the lowest efficiency because of the higher amount of dye loss as shown in Figure 62 (c). According to our parametric study, the T-shaped channel structure would be the preferable geometry for the fast and efficient replenishment of dyes in dye-based photovoltaic systems. Experiments to observe the dye transport through the gel-microvascular networks are underway to evaluate the validity of the time profiles and the computational optimization of the channel design.

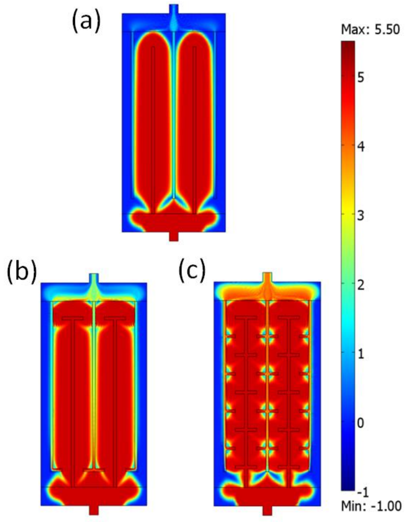

Figure 62. Simulation results for the dye distribution in gel-microvascular networks with three different shapes at 500 seconds. (a) linear, (b) T-shaped and (c) fractal design.

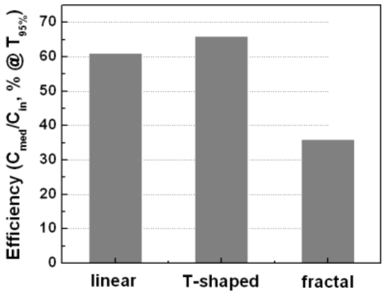

Figure 63. Effect of the channel shapes on the dye-replenishment efficiency.

Q9:

The solute transport through the gel-microvascular networks for regenerative dye-based photovoltaic cell was investigated by using COMSOL simulation program in previous quarterly report. To evaluate the validity of the simulation results, we also fabricated a prototype of the gel-microfluidic device, as shown in Figure 64, and observed the dye transport through the channel-gel network. Microfluidic channels with fractal design were embedded in the hydrogel by a replica molding method. The microfluidic gel is sandwiched between two glass substrates.

The PDMS spacer supports the microfluidic hydrogel and also prevents from the leakage of the dye solution out of the gel. Dye solution was injected at a constant flow rate by a syringe pump. The time-dependent penetration of water-soluble dye solution was followed by optical imaging. The dye distribution profiles at 5, 10, 20 and 30 minutes after the dye injection were compared to the simulation results as shown in Figure 65. The

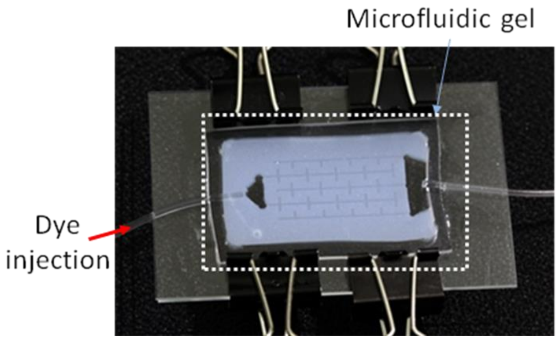

Figure 64. A prototype device from hydrogel with microvascular networks. Microvascular channels with fractal structure are embedded in hydrogel, mimicking the vascular structure of live leaves.

temporal distribution of the dye of the experimental data is in excellent agreement with that of the simulation, which proves that the dye transport through the gel-microvascular networks can be reasonably predicted by the simulation procedure that we have developed. We believe the microfluidic gel device could become a platform for the regenerative photovoltaic systems by effectively replenishing degraded dye with fresh one. Experiment is underway to demonstrate a prototype device of such new photovoltaic structure that will be regenerated.

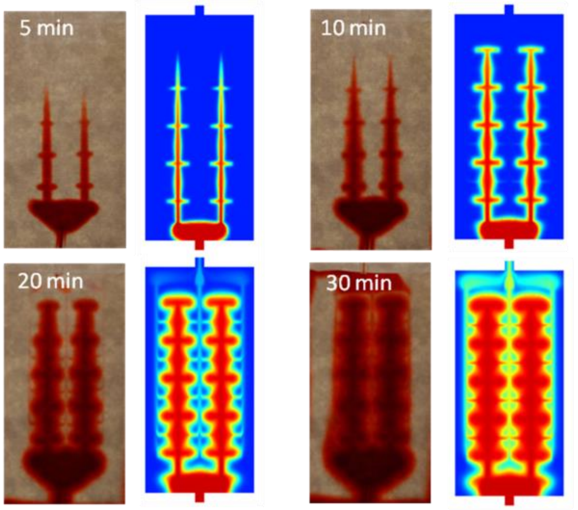

Figure 65. Experiment and simulation results of the transport of the dye through the gel-vascular networks.

Q10:

We have continued our work on the development of new generation of solar cells with regeneration capabilities. We have included the new gel structure with embedded microvascular channels reported in the earlier quarter into a dye-based photovoltaic cell to demonstrate our new concept inspired by the venation network of natural leaves. Figure 66 shows the structure of the prototype photovoltaic device based on the hydrogel with embedded channels. The microvascular network in the gel was formed by a replica molding method. The channel-embedded gel layer was sandwiched between two FTO glass electrodes, with pre-deposited layer of a TiO_2 nanoporous film or Pt catalyst. The channels in the gel layer face the TiO_2 film, where dyes adsorb for the photovoltaic operation.

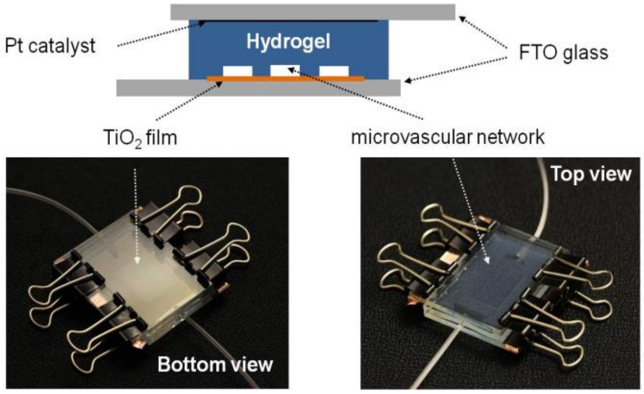

Figure 66. A prototype of a conceptually new photovoltaic device combining DSSC and a microvascular network of channels embedded in the hydrogel.

We have measured the photovoltaic performance of the device before and after the dye supply. The I-V curves of the device under the illumination are shown in Figure 67. The photocurrent starts to increase as more dye is supplied till 30 min, when we stopped injecting the dye. Compared to the photocurrent of ~0.2 mA before the dye injection, the photocurrent increases about 6 times after the dye has been supplied for 30 mins. The photocurrent density and conversion efficiency after the dye injection are 0.4 mA/cm^2 and 0.12%, respectively. The active area of the device was 3 cm^2, which is relatively large compared to other prototype photovoltaic devices reported in literature. Moreover, an inexpensive organic dye (Eosin Y) and water-based electrolyte were used for the device. Overall, we believe the performance of such a prototype device is more than adequate and promising for continuing the research by investigating processes for using the channel network for dye replenishing and device regeneration. Experiments are underway to control the adsorption and desorption of the dyes on the surface of the TiO_2 film as means for achieving efficient dye replenishment.

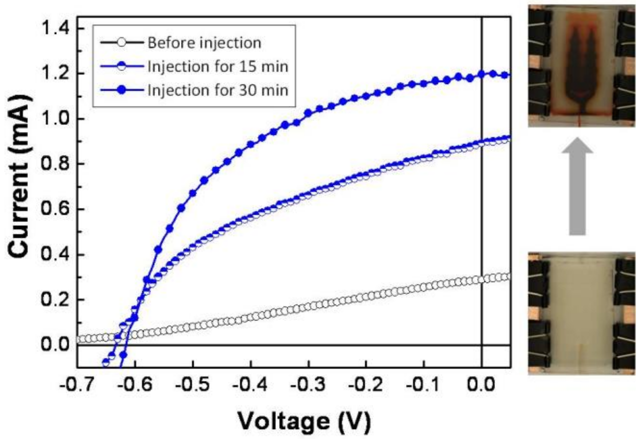

Figure 67. I-V curves of the prototype device and its top view images before and after dye injection in the channel network.

Q11:

No new developments this quarter.

Q12:

In the previous quarterly reports, we have shown efficient supply and removal of a dye in the prototype device of the microfluidic gel based solar cells, but the dye replenishing process to demonstrate self-regeneration functionality of the device was inefficient. In this reporting period, we continued the development of a reliable process of the dye replenishment. Since the isoelectric point of TiO_2 is ~6.2, the TiO_2 films have negatively charged surfaces in basic pH environment. Eosin Y, the dye we use for this project, also has negative charges on it. We hypothesized that the electrostatic repulsion between the dye and the TiO_2 films hinders the re-adsorption of the dye after dye removal step with a NaOH aqueous solution (pH ~12). We have compared the amount of dye on the TiO_2 films after the adsorption, desorption and re-adsorption steps by UV-vis spectroscopy (Figure 68). The amount of the dye on the films after the re-adsorption step is less than 50% compared to that after the first adsorption step. To change the polarity of the TiO_2 film surface, we soaked the films in an HCl acid solution (pH ~3.5) for 30 min. After the acid treatment, the amount of the re-adsorbed dye is even higher than that after the first adsorption step.

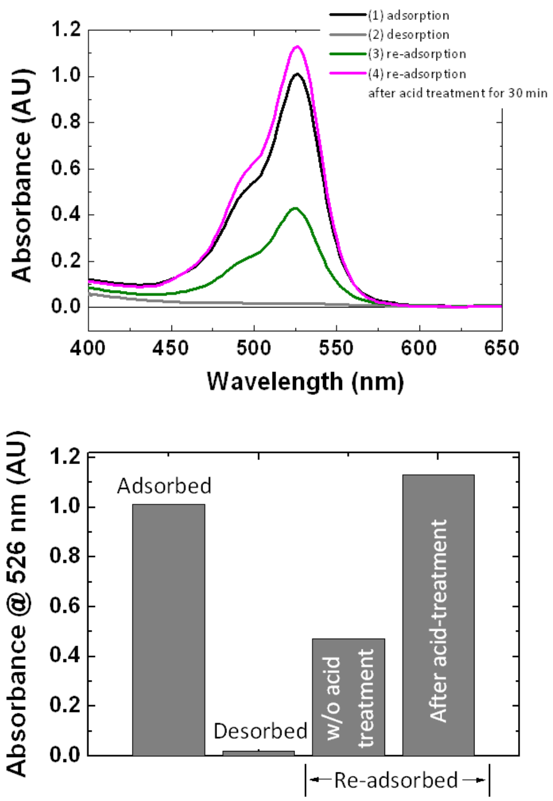

Figure 68. (Top) UV-vis absorption spectra of the TiO_2 films after adsorption, desorption and re-adsorption process of the dye. (Bottom) Comparison of the absorption peak intensities of the spectra.

We performed preliminary experiment to confirm the effect of the increase of the re-adsorbed dye amount by the acid treatment on the regeneration of the photovoltaic performance. Figure 69 shows the I-V curves of the device after the adsorption and re-adsorption steps. The device structure of normal DSSCs was used for the preliminary experiment (see inset in Figure 69). Contrary to the inefficient current recovery (< 50%) of the device after the dye re-adsorption without the acid treatment (curve (2)), the photocurrent was ~80% recovered after the re-adsorption step with the acid treatment (curve (3)). Thus, the modification of the TiO_2 surface charge by the acid treatment could enable the efficient replenishment of the fresh dye in the microfluidic gel based solar cells. Further experiment is now underway to demonstrate the reliable replenishment of the dye and the efficient recovery of the photovoltaic performance of the microfluidic gel based solar cells.

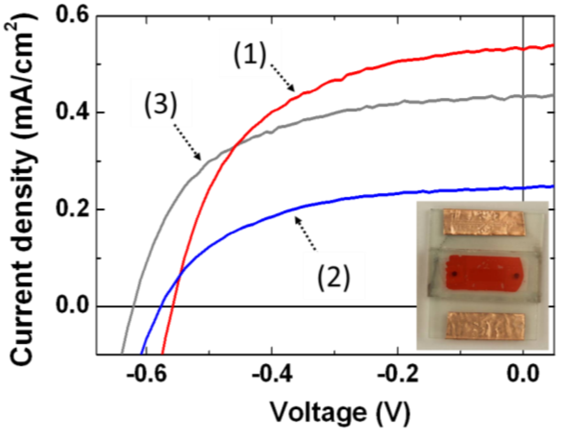

Figure 69. Preliminary result of the effect of the acid-treatment on I-V performance of the dye-replenished solar cells.
(1) After dye adsorption on a fresh TiO_2 film.
(2) After dye replenishment without acid treatment.
(3) After dye replenishment with acid treatment.
(Inset) Photo of the device structure for the preliminary experiment.

Q13-15:

In the studies described in the previous reports, we investigated the effect of pH of the cell medium on the adsorption/desorption of photoactive dye on the TiO_2 anode surface. We established that the dye molecules form a strong adhesion to the surface under low pH conditions, while they are desorbed from the surface under high pH conditions. Based on these results, we have now developed a robust procedure for replacement of the degraded photomolecules with fresh dyes on the anode electrode in the microfluidic-gel based solar cells. The procedure is shown in Figure 70. First, the fresh dyes and the electrolyte are supplied to the device with the pristine TiO_2 anode, where the dyes reaching the vicinity of the electrode via the microfluidic supply network are adsorbed. When the photoactive molecules are degraded after long term operation

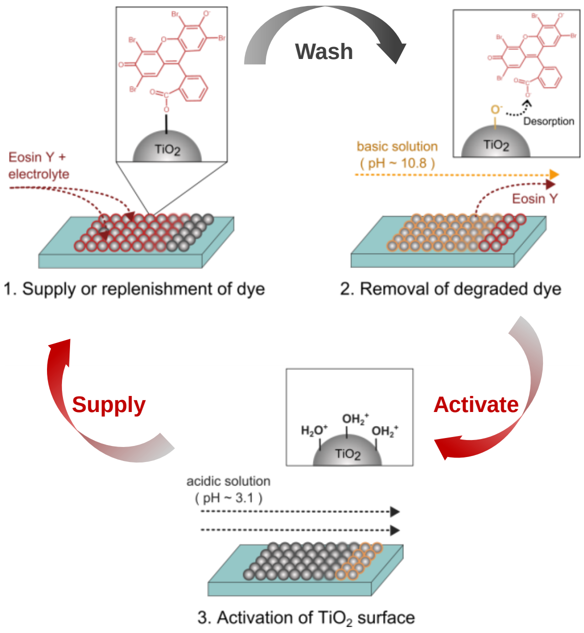

Figure 70. Procedure of the dye replenishment in the microfluidic DSSC solar cells based on hydrogels.

(which will be simulated in our cells by intense UV illumination), the adsorbed dyes are removed by washing with basic solution. The dye-free TiO_2 anode is then treated with acidic solution, which "activates" the TiO_2 surface by inverting the surface charge suitable for the dye adhesion. Finally, fresh dyes from solution are re-supplied and are adsorbed onto the activated anode surface. All the solutions are delivered uniformly, rapidly and efficiently via the microfluidic channels embedded in hydrogels the designing of which is described in the previous reports. Thus, we could realize the biomimetic functionality of regeneration in the microfluidic-gel based solar cells by utilizing the adsorption/desorption kinetics of the photoactive dye molecules on the TiO_2 anode.

We performed experiments with a prototype device to demonstrate the efficient replenishment of the dyes in the microfluidic-gel photovoltaics. We measured the photocurrent generation of the device during three cycles of the regeneration process as shown in Figure 71. The recovery of the original photocurrent supports the hypothesis that the microfluidic-gel solar cells could be efficiently and repeatedly regenerated by the procedure suggested in Figure 70. In this experiment, we started to replace the adsorbed dyes one hour after they supplied. Since we could not detect any significant dye degradation within an hour, further experiment is in progress to confirm the regeneration procedure is effective for the replacement of the degraded dyes with the fresh ones. The data, however, prove that our innovative concept of hydrogel-based solar cell with regeneration capability is workable.

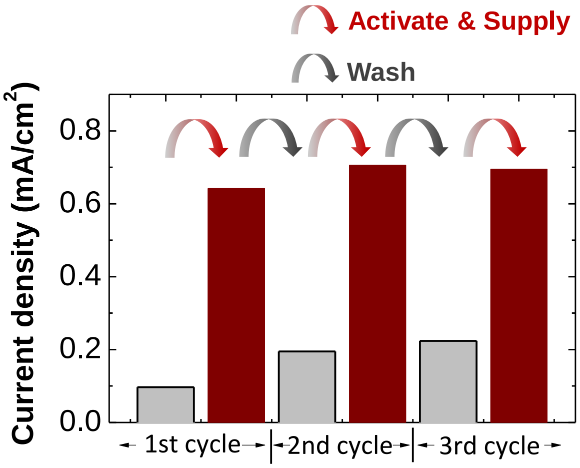

Figure 71. Change in the photocurrent density exhibited by the microfluidic-gel solar cells during three subsequent cycles of the dye replenishment. The grey and brown color bars represent after the washing and the replenishing steps, respectively.

Q16-17:

This subtask was completed at the end of Q17, October 24, 2012.

Subtask 4.2 Photoactive Organic Materials (Gorman/Misra)

Q1:

Novel polymer materials (Gorman) and Porphyrinic materials and devices (Misra):

A series of low band gap polymers and oligomers are being examined that are considered good candidates for the solar cell test bed which is in development (Gorman et al.) These are designed to organize well in the solid state which should lead to acceptable carrier mobilities. They are also designed to be air stable. Currently we are exploring two opportunities that these molecules potentially afford us. First, we are looking at how conductance might increase as the result of acid-doping. Second, we are looking at how precursors to these molecules can be photopatterned, using a photoacid generator. Both of these questions are being directed at how to generate an optimal charge separation and/or charge transport layer in a photovoltaic device.

Q2:

Novel polymer materials (Gorman) and Porphyrinic materials and devices (Misra):

Since the last quarterly report, we have synthesized the polymer with potential for use in the PV devices. We are continuing to optimize conditions to increase the molecular weight of the polymer and are characterizing the material using various characterization methods. The material is ready for spin coating into the PV test bed when it has been optimized by other members of the team.

In a separate research effort, we have been exploring mixtures of porphyrins and P3HT+PCBM for improved absorption of the solar spectrum. Recent UV-vis studies have shown that incorporation of Zn-porphyrin polymers in P3HT can increase absorption in the range of 400 to 500nm which can lead to improved solar cell efficiencies. Another potential advantage of these mixtures is the possibility that porphyrins have more efficient exciton generation while the P3HT may provide faster hole transport. XRD studies of these composite materials indicate small changes in the microstructure and this is currently being investigated in solar cell devices.

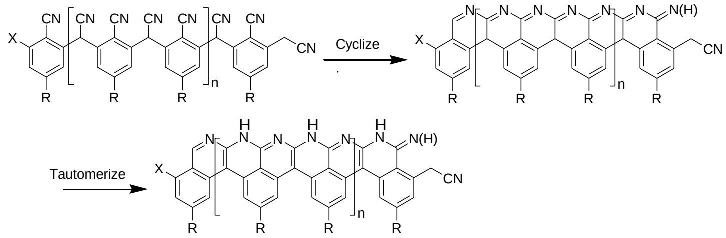

Figure 72. Cyclization schematic for conductive polymer investigated.

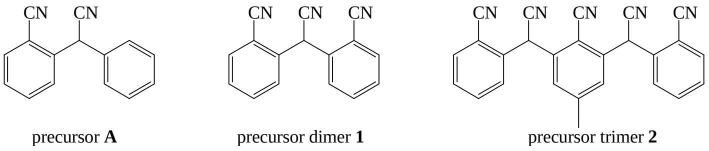

Figure 73. Structures of molecules explored for cyclization/aromatization

Q3:

Novel polymer materials (Gorman):

In this quarter, we have been working on optimization of the synthetic conditions for production of the precursor to the aromatic ladder polymer shown in Figure 72. Specifically, we are iterating to find conditions to maximize the molecular weight. We have been characterizing our novel material with gel permeation chromatography and end group analysis, while obtaining UV/Vis spectra to help determine materials properties. Table 2 provides a summary of the data to date. In the next quarter, we hope to incorporate the aromatized material into a photovoltaic device.

Table 2. Summary of process conditions for maximizing the molecular weight of the aromatic ladder polymer.

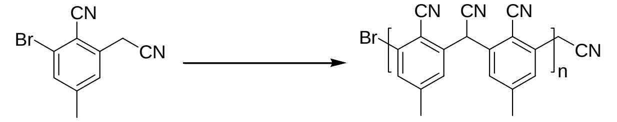

	Solvent[a]	Catalyst	Ligand	Cat/Lig[b]	Time (min)	Conc (M)[c]	Temp (°C)	$\overline{n}$ [d]
No catalyst								
1	DMF	None	None	--	10	1.5	100	1
2	THF	None	None	--	5 days	0.2	RT	1
Variation of solvent								
3	o-DCB	Pd(OAc)$_2$	P(*t*Bu)$_3$	0.1/0.2	5	1.5	140	1.2
4	THF	Pd(OAc)$_2$	P(*t*Bu)$_3$	0.1/0.2	5	1.5	140	8
Variation of catalyst loading								
5	THF	Pd(OAc)$_2$	P(*t*Bu)$_3$	0.01/0.02	65	1.5	100	1
6	DMF	Pd(OAc)$_2$	P(*t*Bu)$_3$	0.02/0.04	5	1.5	150	10
7	THF	Pd(OAc)$_2$	P(*t*Bu)$_3$	0.1/0.2	5	1.5	140	13
Variation of catalyst								
8	THF	Pd$_2$dba$_3$	P(*t*Bu)$_3$	0.1/0.2	7	0.5	120	1
9	THF	Pd$_2$dba$_3$	BINAP	0.1/0.2	8	1	130	1

[a] DMF = dimethyl formamide, THF = tetrahydrofuran, o-DCB = *ortho-*

Another major focus has been the cyclization/aromatization chemistry for dimer and trimer precursors shown in Figure 73. Attempts employing bases such as KO^{t}Bu, K$_2$CO$_3$ and the weak base KCN as a potential cyclization catalyst either showed no reaction or decomposition. Acidic cyclization conditions using catalysts such as HBr/HOAc resulted in efficient chemistry to from the desired products. The cyclized products have been fully characterized by ^{1}H NMR, ^{13}C NMR high resolution MS and IR. In addition, electronic absorption and emission spectra of these cyclized/aromatized products that support the increased conjugation as the result of these reactions.

Porphyrinic materials and devices (Misra):

The properties of porphyrins molecules in organic solar cells are also being investigated. Porphyrins are active components in the photosynthetic machinery, which is the most efficient solar cell known in nature. Currently, most organic solar cells utilize P3HT and PCBM as the active components. Incorporation of porphyrins (porphyrin polymer, *Por-P*) with P3HT and PCBM resulted in substantial broadening of the absorption profile of the active layer, as shown in Figure 74.

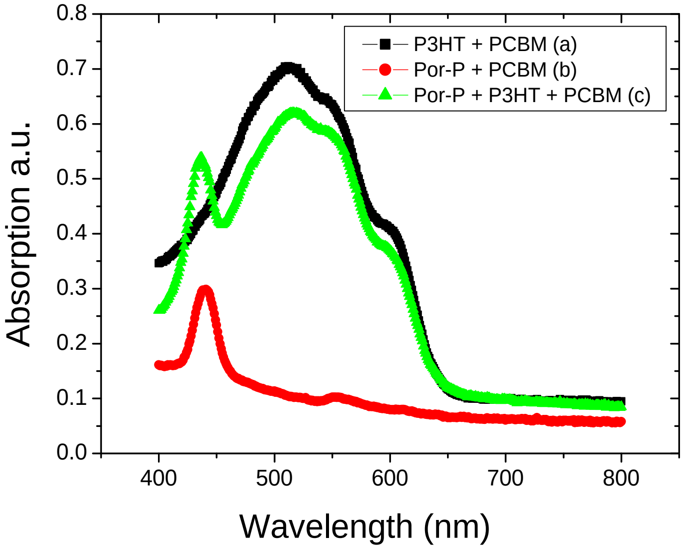

Figure 74. Absorption profile of P3HT-PCBM, Por-P-PCBM, and P3HT-Por-P-PCBM films.

All the initial processing steps, including mixing of active components, spinning of active material on substrate, and annealing of films are performed inside a glovebox. However, metal evaporation is performed outside under ambient conditions. Solar cell electrical characterization has also been performed outside in open environment. The active components of organic solar cells such as P3HT, PCBM, and porphyrin polymers undergo substantial degradation in the presence of moisture and oxygen, which is well documented in literature. Hence, prior to our discussion on the efficiencies of solar cells, it should be noted that these solar cells may possibly be compensated with exposure to ambient conditions. This efficiency may be significantly improved if all components of the fabrication step and characterization are accomplished in controlled environment. Finally, we are also looking into encapsulating these organic solar cells in order to minimize exposure to oxygen and water.

Table 3. Summary of device performance for various PV devices in the work.

	Voc (V)	J_{SC} (mA/cm^2)	Max Power (mW/cm^2)	Peak Power (mW/cm^2)	Fill Factor	Efficiency (%)
P3HT:PCBM	0.39	7.51	2.82	1.06	0.37	1.06
197:PCBM	0.44	0.53	0.23	0.06	0.28	0.06
P3HT:197:PCBM	0.33	2.5	0.84	0.25	0.30	0.25

Table 3 provides a summary of device performance for solar cells incorporating P3HT-PCBM, *Por-P*-PCBM, and P3HT-*Por-P*-PCBM in the active layer. Figure 75 shows the I-V characteristics obtained for the solar cell with P3HT-PCBM as the active layer. The efficiency of P3HT-PCBM solar cell is lower than the reported value and we believe this can be attributed to the factors discussed above. No significant change in the P3HT structures can be observed by X-ray diffraction upon incorporation of PCBM. However, upon incorporation of *Por-P* into the active layer of P3HT-PCBM, the efficiency of the cell significantly reduces. We attribute this lowering in efficiency to many factors including, probable disorientation of the P3HT assembly caused by the presence of porphyrin polymers.

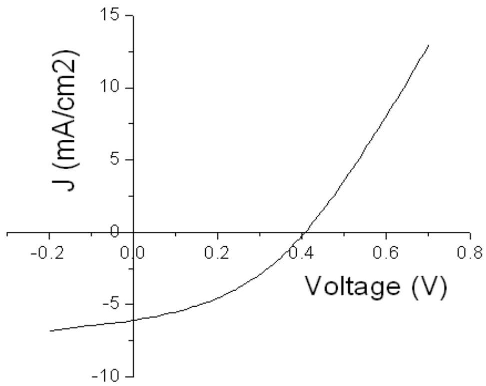

Figure 75. *J–V* characteristics under illumination for device comprising P3HT-PCBM as the active layer.

Currently, we are performing a detailed XRD characterization in establishing the extent of disorientation caused by *Por-P* assemblies. The main reason behind the selection of *Por-P* is that *Por-P* is among the more robust molecular system that we have used in our work. Since the active components in the solar cells get exposed to moisture and oxygen, we decided on using a more robust porphyrin-based polymer (*Por-P*) for the present work. We plan on utilizing other porphyrinic moieties for incorporation into solar cells. We also plan to utilize ultraviolet photoelectron spectroscopy (UPS) to establish the HOMO-LUMO levels for the ternary system.

Q4:

Novel polymer materials (Gorman):

In this quarter, we have been working on optimization of the synthetic conditions for production of the precursor to the aromatic ladder polymer shown in Figure 76. Specifically, we are iterating to find conditions to maximize the molecular weight. We have been characterizing our novel material with gel permeation chromatography and end group analysis, while obtaining UV/Vis spectra to help determine materials properties. Future work will measure the figures of merit of these new oligomers in photovoltaic test beds.

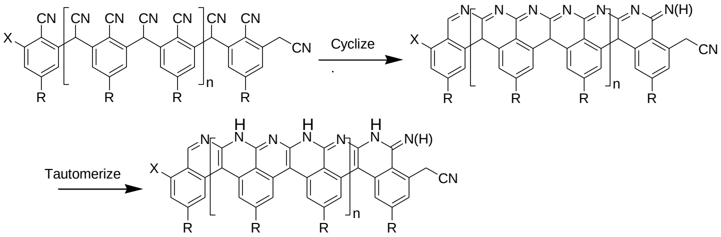

Figure 76. Cyclization schematic for conductive polymer investigated.

Porphyrinic materials and devices (Misra):

In order to increase the absorption profile of the solar cell, porphrins were incorporated in the active layer. Although the absorption spectrum of the active layer broadened considerably, the efficiency was compensated in the presence of Por-polymers. However, while the control samples (with P3HT and PCBM) showed an efficiency of 1.3% with V_{oc} of 0.4 V and a fill factor of 0.4 V, the samples with porphyrins resulted in lowered efficiencies. We attribute this lowering in efficiency to many factors including, probable disorientation of the P3HT assembly caused by the presence of porphyrin polymers. We are looking into other porphyrin derivatives in order to increase efficiency and minimize structural disorganization. In addition, further increases in efficiency may be possible by i) depositing metals under ambient conditions and ii) performing electrical characterization in a controlled environment. We believe these two factors degrade the active layer material, which severely limits the performance of solar cell. Future work will investigate the (i) possibility of performing the entire fabrication in controlled environment and (ii) encapsulation of these cells for minimal exposure to moisture and oxygen during measurements.

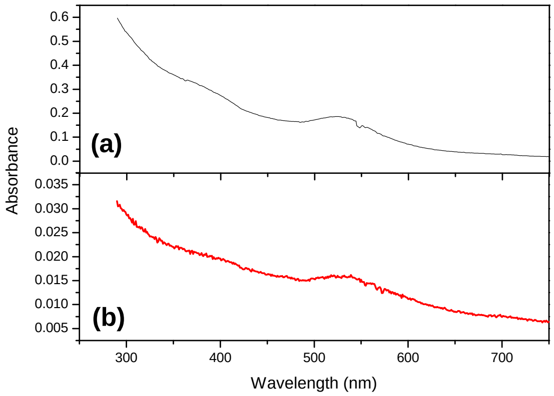

Figure 77. Absorbance spectrum of (a) citrate stabilized Au np in water and (b) upon modification of substrate complexes.

In another effort to overcome the weak absorbance of photoactive layer, we are incorporating metal nanostructures between the ITO substrate and the active layer. When the frequency of the incident light is in resonance with the surface plasmon of the metallic nanoparticles, a strong scattering of the incident light is exhibited. As a result, absorption of the active layer may get enhanced due to the high electromagnetic field strength in the vicinity of the excited surface plasmons. In this regard, we have are depositing gold nanoparticles (Au np) on the ITO substrate. Figure 77a shows the absorbance spectrum of citrate stabilized Au np in water and the corresponding spectrum after deposition of Au np on the substrate is shown Figure 77b. Our current efforts in this project include increasing the loading density of Au np on the substrate, study the morphology of Au np on these substrates, and study the effect of temperature on the Au.

Q5:

Novel polymer materials, (Gorman):

Table 4. Failed attempts to affect the cascading cyclization under single nucleophile conditions in acid.

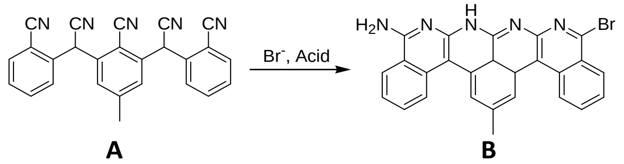

Entry	Br$^-$ Source	Acid	Temp (^{o}C)	Time
1	(n-Bu)$_4$NBr	CCl$_2$HCOOH	90	12
2	(n-Bu)$_4$NBr	CCl$_2$HCOOH/H$_2$SO$_4$	0	4
3	(n-Bu)$_4$NBr	CCl$_2$HCOOH/H$_2$SO$_4$	0	3
4	(Et)$_4$NBr	CCl$_2$HCOOH/H$_2$SO$_4$	0	3
5	(Et)$_4$NBr	TFA/TF$_2$O/H$_2$SO$_4$	0	2

[a]Analyzed by ESI mass spectrometry

We have investigated the conversion of poly-cyano polymers to fused photoactive aromatic ladder materials through a cascading pathway. Ideally, this system requires only single nucleophilic attack at an aryl cyanide followed by a kinetically favorable cascading cyclization. However, prior work has shown incomplete cyclization. Ring closings employing single equivalents of nucleophile under acidic conditions were explored. A bromide anion nucleophile is needed in addition to a strong acid to promote cyclization. Therefore, the efficacy of a single equivalent of nucleophile to close molecule **A** was tested with various Br- sources and strong acids. Attempts to convert molecule **A** to molecule **A** using acetic acid derivatives in H$_2$SO$_4$ at 90 ^{o}C resulted in uncharacterized alternative products. However, molecule **A** was re-isolated when not heated. This behavior suggests two problems with these approaches. First an acid similar to or stronger than HBr is needed. Sulfuric acid is 6 pKa units less acidic than HBr but appears to be unacceptable. It is reckoned that only hydroiodic acid (HI) with a pKa of -10 compared to the pKa of -9 for HBr is strong enough and has a nucleophilic, conjugate base to be a viable alternative. In addition to this first concern, it is unclear whether addition of only one equivalent of bromide anion is acceptable. It may be necessary to use excess bromide anion

Scheme 1.

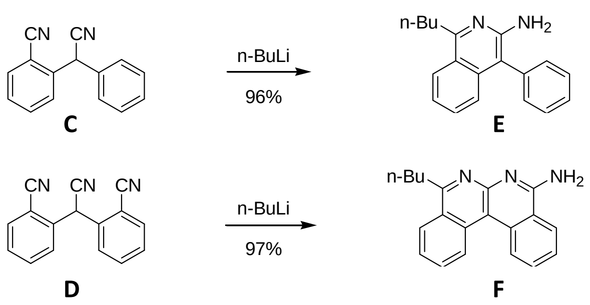

nucleophile to obtain the product. It is concluded that use of an acidic medium to cyclize larger poly cyano containing oligomers and polymers is not attractive.

Our current efforts involve use of a nucleophile rather than an activating acid to effect these cyclizations. The ring closing of molecules **y** employing n-BuLi as the nucleophilic partner was attempted under similar conditions. Treatment of molecules **C** and **D** with excess BuLi at -78°C in THF afforded molecules **E** and **F** in nearly quantitative yields. This is the first report of a single nucleophile initiated cascading cyclization. Extension to longer molecules is in progress.

Q6:

<u>Subtask 4.2 Photoactive Organic Materials</u> (Gorman)

Scheme 2. Successful, *n*-BuLi mediated cyclization of model oligomers

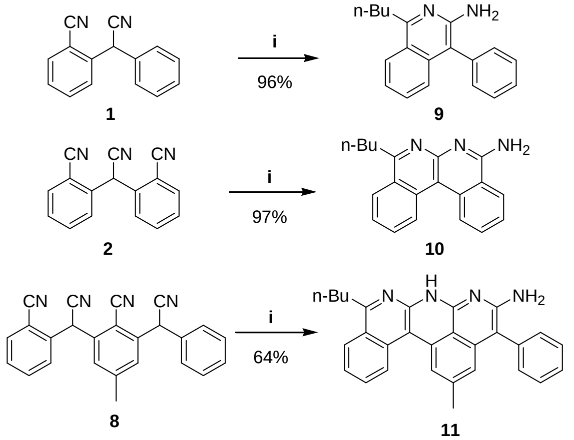

Conditions and Reagents: (**i**) *n*-BuLi, THF, -78°C, 2 h, 25°C, 20 m

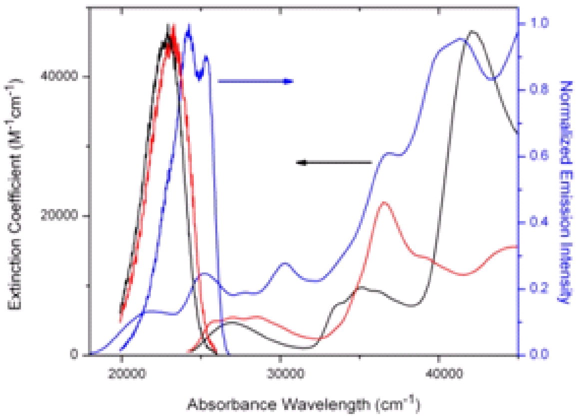

Figure 78. Absorbance and emission spectra of 9 (black), 10 (red) and 11 (blue) taken in CH_3CN solvent.

By adapting a previously reported cyclization to produce amino pyridines, cyclic oligomers containing two to five fused rings could be prepared. The reaction of molecules **1, 2** and **8**, with *n*-BuLi (Scheme 2) afforded cyclized derivatives **9-11** in acceptable to excellent yields. In each case the benzylic hydrogens tautomerized to nitrogen to form a completely aromatic heterocycle. To our knowledge, this is the first example of a cascading cyclization reaction to form fused, completely aromatic molecules. Note that only the terminal cyano group is attacked by the nucleophile. Products of the attack at internal cyano groups were not observed. Furthermore, only one regioisomer was observed in each case where the starting oligomer was not symmetric. All of these molecules have been characterized completely by NMR, Mass Spectrometry and X-ray crystallographic analysis. We have yet to attempt the cyclization of molecule **3** to determine whether the analogous system with seven fused rings can be prepared.

The absorbance and emission of cyclized oligomers **9-11** are shown in Figure 78. Molecules **9** and **10** have similar absorption spectra indicating that a fused and pendant phenyl group have a similar electronic effect here. This trend has been observed in other types of fused and conjugated systems. As

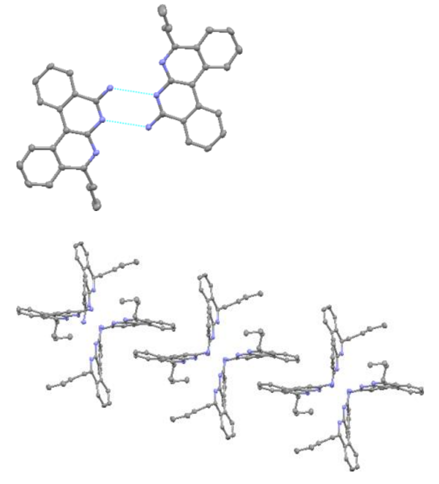

Figure 79. Hydrogen bonding interactions (top) and packing (bottom) of molecule 10.

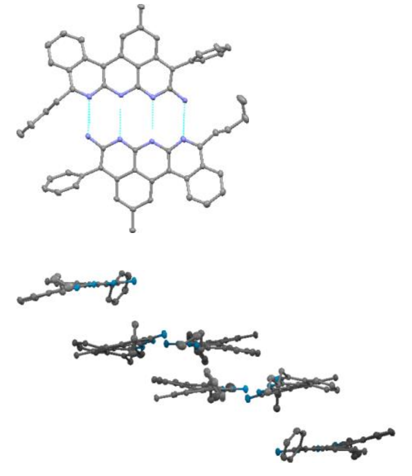

Figure 80. Hydrogen bonding interactions (top) and packing (bottom) of molecule 11.

expected molecule **11** shows a characteristic red-shift due to extended conjugation as compared to **9** and **10**. All molecules fluoresce with quantum yields ($\O_F$) of 0.63, 0.16 and 0.58 for molecules **9, 10** and **11** respectively. Note that the pendant phenyl group has a large effect on the quantum yield of these molecules. This behavior is observed when the quantum yields of anthracene and phenyl anthracene are compared. In that case, the pendant phenyl group effects the relative energies of the first excited singlet and triplet states, reducing the rate of intersystem crossing substantially and thus increasing the quantum yield for fluorescence. A similar mechanism may be operative here.

Packing, inter-molecular distance, and self-assembly are extremely important properties in organic conducting materials and can be determined through the crystal structures. Analysis of the crystal structures for molecules (Figure 79) and (Figure 80) indicates two structural features in these molecules that influence organization. First, all form multi-point hydrogen bonding interactions via the intermolecular interaction of the nitrogen as hydrogen bond acceptor and N-H as the hydrogen bond donor. This type of organizational motif has been illustrated previously. Molecule **10** has two non-bonded N-N distances of 3.05 Å and molecule **2c** has an average N-N distance of 3.04 Å. These values are comparable to those found for N-N distances in nucleic acids.

Second, molecule **11** forms tubular 2D close packed layers uncharacteristic of most tetracene derivatives. Here, hydrogen bonding appears to dominate over the face-to-face packing found in hydrocarbons. Thus, at most two molecules stack face-to-face (with an average of 4.0 ± 0.1 Å distance between them. The longer molecule **11** forms relatively flat, although slipped, 2-D close stacked layers with an average 3.8 ± 0.2 Å distance between molecules in the stacking direction. The slipped, 2D packing motif is typical of substituted pentacenes, and is the packing motif that offers the highest performance in thin film devices. It is intuitive that longer, fused, aromatic molecules should face-to-face stack more readily. This nicely illustrates the minimum size at which this packing motif is found in this series of molecules.

Q7:

Subtask 4.2 Photoactive Organic Materials (Gorman)

Scheme 3. Proposed route to an aromatic ladder polymer.

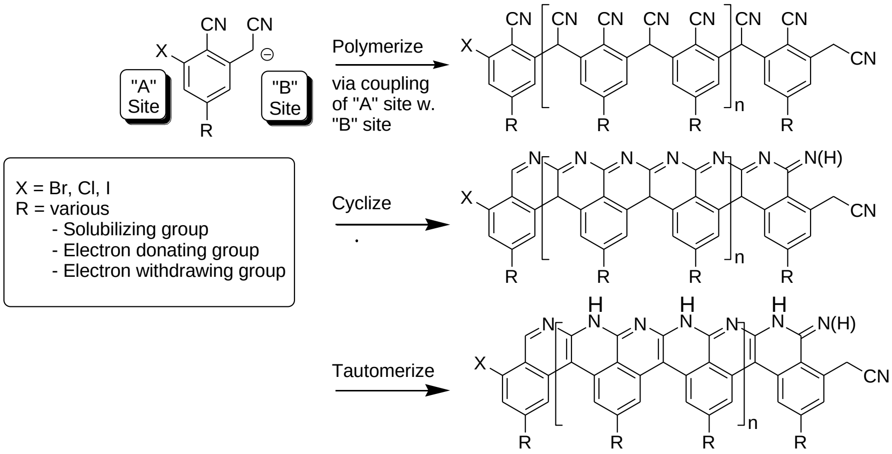

In this subtask, we have continue to work on our approach to new precursor polymers for direct writing as shown in Scheme 3. This route involves cyclization of benzylic nitriles – as we have shown on model oligomers, aromatization takes place via tautomerization. To determine how efficiently a coupling could occur to form a precursor polymer, a model reaction was devised (Table). The choice of solvent, base and ligand were varied. The data shown in Table represent only the last variation, but they illustrate that the yield of this coupling is sensitive to conditions but that the coupling is efficient under appropriate conditions.

Table 5. Variation of Supporting Ligand in a model coupling

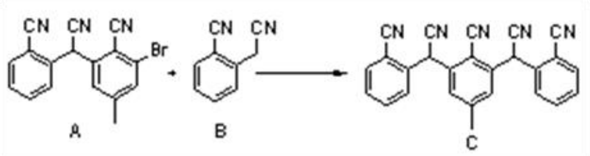

Conditions: THF/NMP 90/10 solvent, 3.2 eq. K-O*t*Bu, 0.1 eq. Pd(OAc)$_2$, 0.2 eq. ligand, 130°C, microwave at 100W, 5 m. Values were obtained from HPLC against a 3,5-dimethylanisole internal standard with an estimated error of ± 5%. [a]dppf = bis(diphenyl phosphino ferrocene), dppb = bis(diphenylphosphino butane), dppe = bis(diphenylphosphino ethane), tBu = *tert*-butyl, Cy = cyclohexyl, Ph = phenyl, [b]0.1 eq 18-crown-6 added.

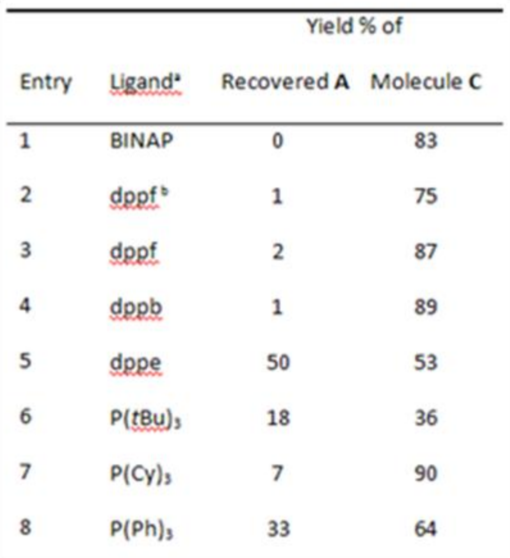

Entry	Ligand[a]	Yield % of Recovered **A**	Yield % of Molecule **C**
1	BINAP	0	83
2	dppf[b]	1	75
3	dppf	2	87
4	dppb	1	89
5	dppe	50	53
6	P(*t*Bu)$_3$	18	36
7	P(Cy)$_3$	7	90
8	P(Ph)$_3$	33	64

Q8:

Subtask 4.2 Photoactive Organic Materials *(Gorman)*

Scheme 4. Competition between C-Arylation and N-arylation in the synthesis of the precursor polymer.

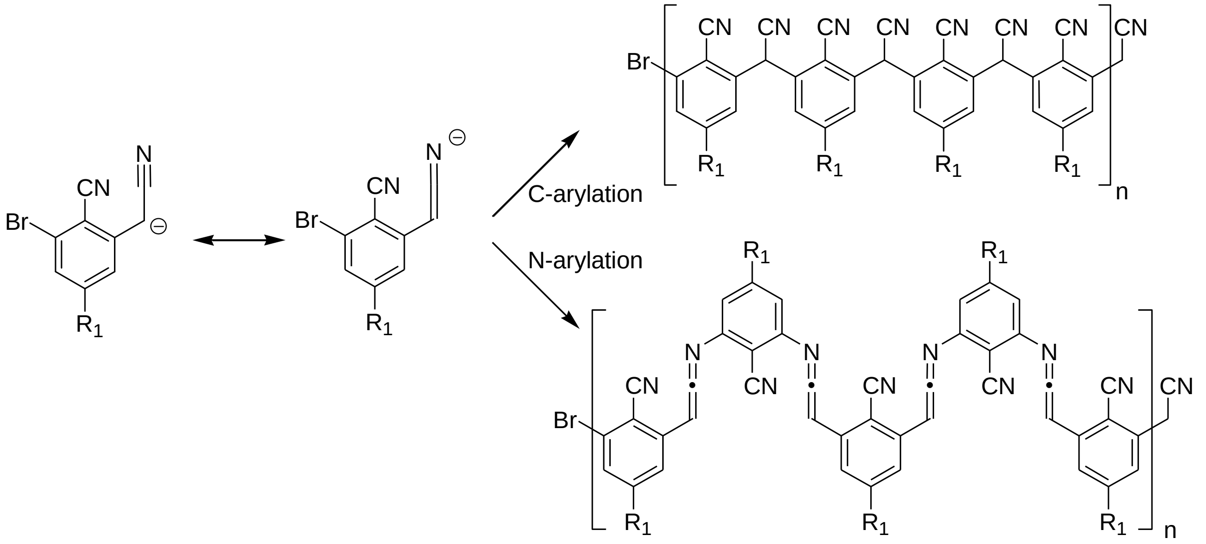

Scheme 5. Alternate approach to the precursor polymer using a fluoride-induced removal of a trimethyl silyl (TMS) group

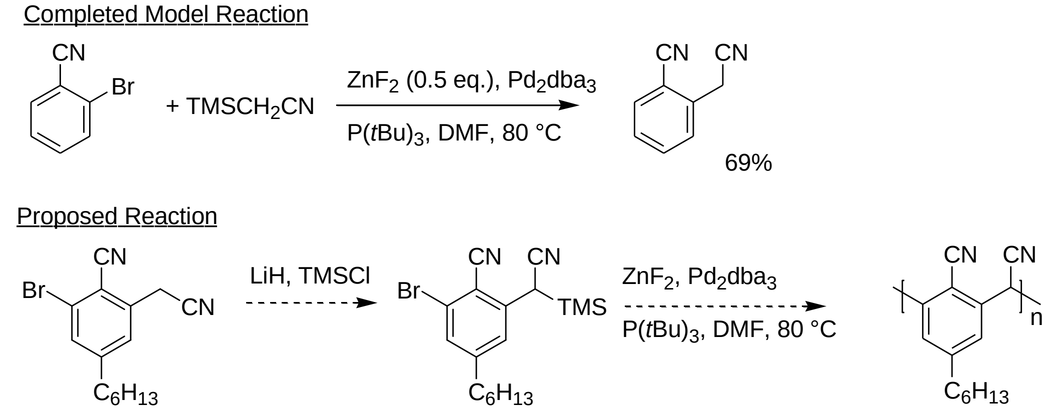

Scheme 6. Alternate approach to the precursor polymer using an *in* situ generated organozinc species.

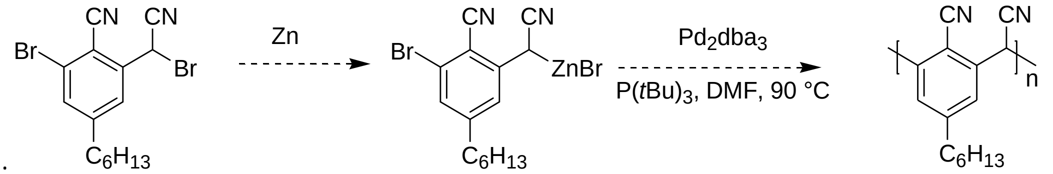

We have determined that the polymerization conditions for our precursor polymer do not give the desired polymer shows our working hypothesis as to what is happening. Specifically, undesirable N-Arylation is competing with C-Arylation. This becomes a frustrating problem for the materials scientist, but an important and intriguing problem for the synthetic materials chemist. Use of nitrile-based cascade cyclizations has a lot of promise for the synthesis of advanced, photovoltaic materials. However, this type of problem is going to be prevalent.

To avoid this problem, we have implemented a new approach and to avoid the naked benzyl cyano anion. Currently we preparing the organo-zinc and trimethyl silyl (TMS) functionalized monomers with the expectation that one or both of these routes will be effective for the preparation of the fully C-arylated precursor polymer.

Cyclization/Aromatization: To make the process of cyclization and aromatization more amenable to mild processing conditions, we have been exploring how mild of a base/nucleophile is required. To this end, we have backed off from the very harsh nucleophile *n*-butyl lithium to lithium piperide and potassium *tert*-butoxide. In both cases, cyclized products have been isolated. They continue to be the result of a "zip" synthesis in which multiple rings are closed simultaneously. We are currently working to improve the yield of these molecules.

Scheme 7. Cyclization/aromatization reactions.

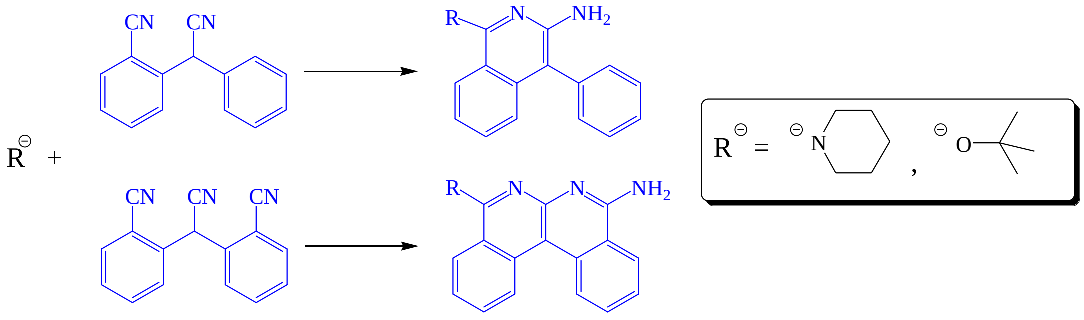

Q9:

<u>Subtask 4.2 Photoactive Organic Materials</u> (Gorman)

In this subtask we have previously reported on our approach to the development of new precursor polymers for direct writing by cyclization of benzylic nitriles and have shown that on model oligomers, aromatization takes place via tautomerization. A slightly modified approach for forming the precursor polymer has been developed. Based on the work of Wu and Hartwig (Wu, L. et al., *J. Am. Chem. Soc.* 2005), we have devised a route for coupling that does not require base. A new "modified monomer" with an organozinc nucleophile should bind readily to the catalyst, allowing for less formation of alternative products than the original monomer experienced (complexed to Li, K ions in excess base). Assuming appropriate interaction with the palladium catalyst, we expect results similar to those found for our model coupling of an aryl halide and benzyl nitrile derivative (92% yield of coupled product), with efficient C-C bond formation and high molecular weight polymers. Initial trials using this new approach and modified monomer appear to have successfully formed the desired C-C bond. Characterization by nuclear magnetic resonance spectroscopy (NMR), infrared spectroscopy (IR), and gel permeation chromatography (GPC), consistently suggest that "precursor oligomers" (3 or 4 coupled monomer units) were synthesized. These results are extremely encouraging for several reasons. Not only is it the first time that we have been able to succinctly form the desired bonds, but the reaction requires minimal catalyst loading (<5%), and can be accomplished at room temperature. This is opposed to the optimized model reaction where 10% palladium/phosphine ligand and microwave heating at 130°C were required for efficient conversions. Reaction conditions will be modified from here to increase the molecular weight and coupling efficiency.

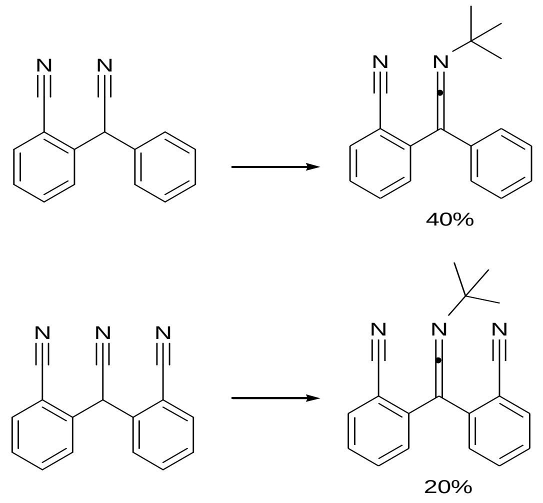

Figure 81. Conversion of model oligomers to N-tert-butyl ketene imines. Conditions: $AlCl_3$, *t*-buCl -30°C, then Et_3N -78°C

We are also exploring the conversion of several cyano oligomers to N-*tert*-butyl ketene imine derivatives. Formation of ketene imines from alkyl/aryl cyanides are well known and are typically used to activate or facilitate nucleophilic attack at the ketene carbon by increasing the electrophilicity. This should allow for the use of weaker nucleophiles to induce a cascading cyclization to form the final fused ring oligomers. The first two cyano oligomers have been successfully converted to the ketene imine derivatives (Figure 81). The products were recovered in low yields due to decomposition during purification, however, cyclization without further purification is currently being explored. If conversion of the cyano oligomers to the ketene imines is successful then the reaction will be applied to the purposed precursor polymer.

Q10:

Subtask 4.2 Photoactive Organic Materials (Gorman)

Our research has previously shown relatively low molecular weights during the polymerization of our precursor monomer. In this past quarter, we believe we have solved the problem with our polymerization to achieve high molecular weight materials. Namely, our monomer becomes deactivated when it is

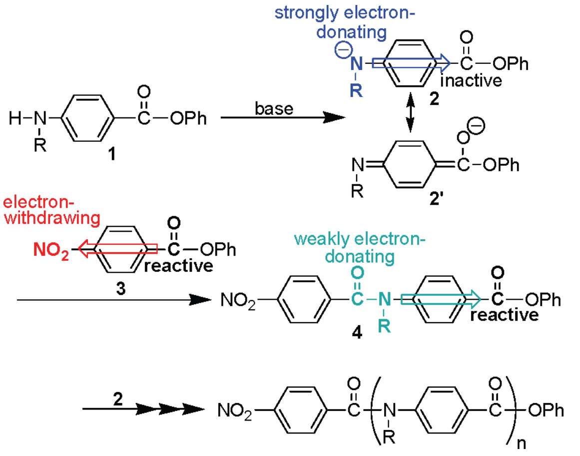

Figure 82. Mechanism for polymerization.

deprotonated. This effect was first observed in the synthesis of aromatic poly(amides). Deprotonation of the amine deactivates the carboxylic acid ester on the monomer. The solution we have developed to overcome this issue is the addition of an ‘initiator’ that can react with the amide anion (Figure 82). The resulting amide linkage does not deactivate the ester towards further reaction with another amide anion.

Our problem is similar in some respects. As oxidative addition produces an 'anionic' ligand, electron rich ligands are more reluctant to undergo this process. As our bifunctional monomer can be deprotonated, it thus is a reluctant ligand to undergo oxidative addition (Figure 83(a)). However, if a molecule that excludes the benzylic anion is introduced, it can undergo facile oxidative addition and act as an 'initiator' for the polymerization (Figure 83(b)). After transmetallation with the benzylic anion and reductive elimination, we have a dimer which can undergo deprotonation. This is a concern, however, it doesn’t ultimately cause a problem.

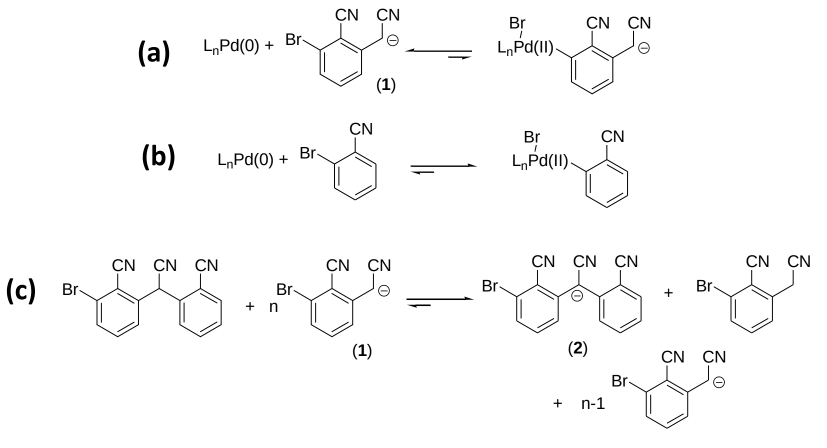

Figure 83. Monomer reaction preference (a)with and (b) without benzylic anion for initiator formation. (c) polymerization mechanism.

Given the experimental results, anion (**1,** from Figure 83) appears poorly reactive, but anion (**2**) has an acceptable reactivity. Moreover, anion (**2**) is the 'dimer' in our model dimer + monomer coupling. Our rationale is that anion (**2**) (and longer polymer chains with a chain end that is isoelectronic with anion (**2**) is at delocalized over two rings, and this extra delocalization (compared to anion (**1**)) ameliorates the problem where anion (**1**) is too electron rich to undergo facile, oxidative addition. This mechanism is elucidated in Figure 83(c).

Using 10 mol% of *ortho*-bromo benzonitrile, we now have produced the polymer with molecular weights in excess of 10 kDa (our target molecular weight). Current efforts are to purify the monomer so lower catalyst loadings are possible and to determine what maximum molecular weight can be obtained. These polymers should now be long enough that they are amenable to spin-coating, so experiments to make films will be attempted shortly.

Q11:

Subtask 4.2 Photoactive Organic Materials (Gorman)

In the last update, we described a synthetic problem with the precursor to our aromatic ladder polymer and our solution. We have further simplified our polymerization, using the much more easily prepared di-halide**1** and cyanoacetate salt **2** as co-monomers, as shown in Scheme 8. To date, we have made the target polymer in 46 % yield with a Mn of 3600 through palladium-catalyzed decarboxylative cross coupling reactions.

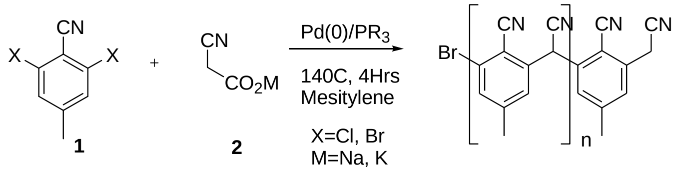

Scheme 8.

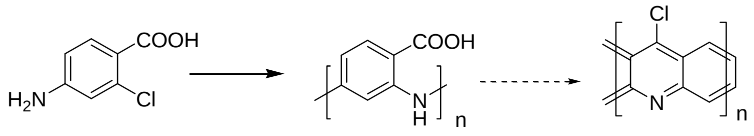

Scheme 9.

We have also begun a new route into poly(acridines) as a route to aromatic ladder polymers , shown in Scheme 9. To date, we have prepared the monomer shown below and have successfully polymerized it, albeit in low yield. We plan to optimize this polymerization and then explore the $POCl_3$-mediated cyclization/ aroma-tization shown below.

Q12:

Subtask 4.2 Photoactive Organic Materials (Gorman)

In the last update, we described a simpler, alternative method to synthesizing our precursor polymer using decarboxylative cross-coupling methods, but have since noted the limitations with this method, as the chain is contaminated with N-arylated coupling products (as opposed to the desired C-arylated product). We have thus returned to the initiator-assisted approach (outlined in the Q10 Report on May 31st, 2011) and with the addition of a solubilizing hexyl chain on the monomer (Scheme 10), we have managed to precisely control the molecular weights while maintaining polydispersities below 1.5. This work, focusing on the unique methods involved, is currently being compiled for publication.

We have also continued to optimize our synthesis of poly(acridines) as another route to aromatic ladder polymers. The Ullmann condensation reaction was first employed to synthesize the prepolymer. The yield was as low as 7%. To improve the yield, we studied the model reactions with varying concentrations, reaction times and amounts of catalyst. Microwave heating and thermal heating were both studied. The results (about 60% yield) are non-optimal. We plan to utilize the Buchwald-Hartwig reaction as another synthesis route. Different Palladium catalysts and phosphorus ligands are being explored.

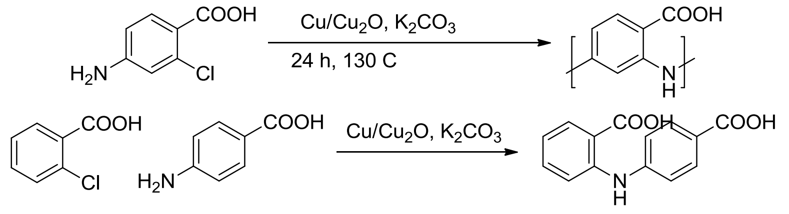

Scheme 10

Q13-15:

<u>Subtask 4.2 Photoactive Organic Materials</u> (Gorman)

In the last update, we described a simpler, alternative method to synthesizing our precursor polymer using decarboxylative cross-coupling methods, but have since noted the limitations with this method, as the chain is contaminated with N-arylated coupling products (as opposed to the desired C-arylated product). We have thus returned to the initiator-assisted approach (outlined in the 2011 1st quarter update) and with the addition of a solubilizing hexyl chain on the monomer, we have managed to precisely control the molecular weights while maintaining polydispersities below 1.5. This work, focusing on the unique methods involved, is currently being compiled for publication.

We have also continued to optimize our synthesis of poly(acridines) as another route to aromatic ladder polymers. The Ullmann condensation reaction was first employed to synthesize the prepolymer. The yield was as low as 7%. To improve the yield, we studied the model reactions with varying concentrations, reaction times and amounts of catalyst. Microwave heating and thermal heating were both studied. The results (about 60% yield) are non-optimal. We plan to utilize the Buchwald-Hartwig reaction as another synthesis route. Different Palladium catalysts and phosphorus ligands are being explored.

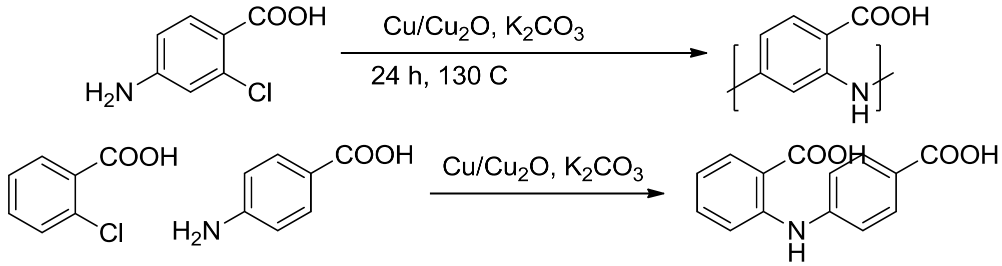

Figure 84. Comparison of Model Coupling and Polymerization

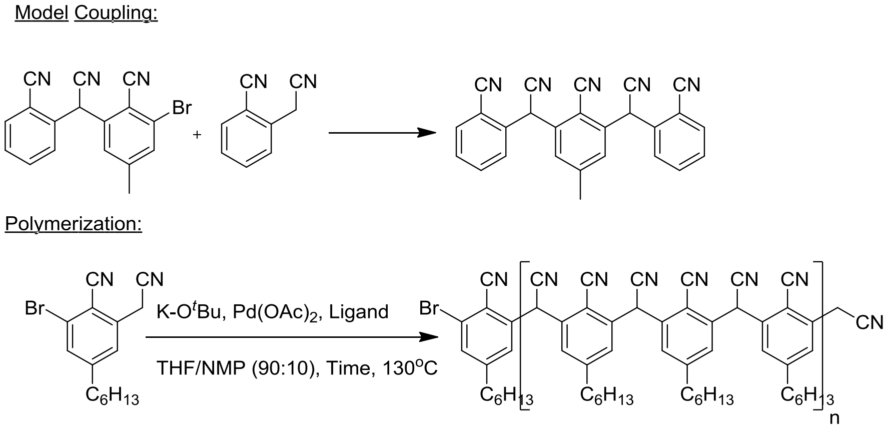

Figure 85. Comparison of Model Coupling and Polymerization

Invention Disclosures

1. "Stabilization of Chromophores on High Surface Area Metal Oxide Semiconductor Surfaces by Atomic Layer Deposition" (NCSU Ref. 13-159).

Articles in Preparation

1. S. C. Desai, Q. Wang, Y. Liu, J. Genzer, X. Zhao, M. D. Dickey, “Hierarchical Topography via Thermal and Electromechanical Thin Film Instabilities.” In preparation.
2. B. Kalanyan, M. D. Losego, G. N. Parsons, “Considerations for reproducible benchtop fabrication of high-performance silicon photocathodes for solar water splitting.” In preparation.
3. D. H. Kim, P. Lemaire, L. Alibabaei, S. E. Atanasov, G. N. Parsons, “PEDOT-ITO particles for dye-sensitized solar cells using PEDOT o-MLD.” In preparation.
4. D. H. Kim, M. D. Losego, K. Hanson, L. Alibabaei, K. Lee, T. J. Meyer, G. N. Parsons, “Stabilizing chromophores for dye-sensitized solar cells using multicomponent, sub-nanometer atomic layer deposition.” In preparation.
5. D. H. Kim and G. N. Parsons, “Atomic layer deposition for dye-sensitized solar cells.” In Preparation.
6. Ying Liu, Russell Mailen, Yong Zhu, Michael D. Dickey, “Strain Relaxation and Shrinkage Modeling of Pre-Stressed Polymer Sheets by Thermal Actuation for Self-Folding.” In preparation.
7. Ying Liu, Matthew Miskiewicz, Michael J. Escuti, Jan Genzer, Michael D. Dickey, “3-D Folding of Pre-Strained Polymer Sheets via Laser Light.” In preparation.

Publications (Q1-20)

1. K. Hanson, M. D. Losego, B. Kalanyan, G. N. Parsons, T. J. Meyer, “Stabilizing small molecules on metal oxide surfaces using atomic layer deposition.” Nano Letters, In Press (2013).
2. M.D. Casper, Arif O. Gozen, M.D. Dickey, J. Genzer, and J.P. Maria, “Surface wrinkling by chemical modification of Sylgard-184 poly(dimethylsiloxane) (PDMS) during sputtering” Soft Matter 2013, **9**, 7797-7803. DOI: 10.1039/C3SM50966D
3. K. Hanson, M. D. Losego, B. Kalanyan, H. Luo, D. L. Ashford, G. N. Parsons, and T. J. Meyer, “Stabilization of [Ru(Bpy)2(4,4’-(PO3H2)bpy)]2+ on TiO2 with Atomic Layer Deposition of Al2O3” Chem. Mater. 25 3 (2013).
4. D. H. Kim, M. Woodroof, K. Lee, G. N. Parsons, “Atomic layer deposition of high performance ultra-thin (< 10 nm) TiO2 blocking layers for dye-sensitized solar cells”, ChemSusChem, 6 (6), 1014, (2013). [featured on front cover].
5. H.-J. Koo and O. D. Velev, Scientific Reports (Nature), 3, article number: 2357. Regenerable Photovoltaic Devices with Hydrogel-Embedded Microvascular Network. DOI: 10.1038/srep02357
6. H.-J. Koo and O. D. Velev, J. Mater. Chem. A, 2013, 1, 11106. Biomimetic Photocatalytic Reactor with a Hydrogel-Embedded Microfluidic Network.
7. H.-J. Koo and O. D. Velev, Biomicrofluidics, 7, 031501, 1-10 (2013). Ionic Current Devices – Recent Progress in the Merging of Electronic, Microfluidic and Biomimetic Structures.

8. B. Gong, J. C. Spagnola and G. N. Parsons “Hydrophilic Mechanical Buffer Layers and Stable Hydrophilic Finishes on Polydimethylsiloxane using Combined Sequential Vapor Infiltration and Atomic/Molecular Layer Deposition” J. Vac. Sci. and Techn. A 30**,** 01A156 (2012).
9. D. H. Kim, H. J. Koo, J. S. Jur, M. Woodroof, B. Kalanyan, K. Lee, C. K. Devine, and G. N. Parsons, “Stable anatase TiO2 coating on quartz fibers by atomic layer deposition for photoactive light-scattering in dye-sensitized solar cells.” Nanoscale. 4 4731 (2012).
10. Y. Liu, J. Boyles, J. Genzer, and M.D. Dickey. “Self-folding of Polymer Thin Sheets Using Local Light Absorption,” Soft Matter, 2012. 8 (6), 1764-1769.
11. Y. Liu, J. Genzer, and M. D. Dickey. “Light converts 2D shapes into 3D shapes,” SPIE, 2012.
12. Q. Peng, J. S. Lewis, P. G. Hoertz, J. T. Glass and G. N. Parsons “Atomic Layer Deposition for Electrochemical Energy Generation and Storage Systems” J. Vac. Sci. and Techn. A 30, 010803 (2012).
13. J-.H. So, H-.J. Koo, M.D. Dickey, and O. Velev. “Ionic Current Rectification in Soft Matter Diodes with Liquid Metal Electrodes,” Advanced Functional Materials, 2012. 22(3), 625-631.
14. M.C. Brannock, W.J. Behof, G. Morrison, C.B. Gorman. “Overcoming challenges in the palladiumcatalyzed synthesis of electron deficient ortho-substituted aryl acetonitriles.” Org. Biomol. Chem., 2011, 9, 2661.
15. B. Kalanyan and G. N. Parsons “Atomic Layer Deposited Oxides for Passivation of Silicon Photoanodes for Solar Photoelectrochemical Cells” ECS Proceedings (2011).
16. H.-J. Koo, S. T. Chang, J. M. Slocik, R. R. Naik and O. D. Velev, *J. Mater. Chem.*, 21, 72-79 (2011). Aqueous soft matter based photovoltaic devices.
17. H-.J. Koo, J-.H. So, M. D. Dickey, and O. Velev. “Towards All-Soft Matter Circuits: Prototypes of Quasi-Liquid Devices with Memristor Characteristics,” Advanced Materials, 2011. 23(31): p. 3559-3564.
18. W. J. Behof, D. Wang, W. Niu, C. B. Gorman “Cascade cyclization to produce a series of fused, aromatic molecules” Org. Lett., 2010, 12 (9), 2146–2148 (Selected as SynFact of the month: Synfacts 2010, 7, 0763-0763). (DOI: 10.1021/ol100656d).
19. Hyde, G. K.; Scarel, G.; Spagnola, J. C.; Peng, Q.; Lee, K.; Gong, B.; Roberts, K. G.; Roth, K. M.; Hanson, C. A.; Devine, C. K.; Stewart, S. M.; Hojo, D.; Na, J.-S.; Jur, J. S.; Parsons, G. N., Atomic Layer Deposition and Abrupt Wetting Transitions on Nonwoven Polypropylene and Woven Cotton Fabrics. *Langmuir,* **26** 4 (2010).
20. Jur, J.S.; Spagnola, J.C.; Lee, K.; Gong, B. ; Peng, Q.; and Parsons, G.N., Temperature-Dependent Sub-Surface Growth during Atomic Layer Deposition on Polypropylene and Cellulose Fibers. *Langmuir* 2010**,** Jun 1;26(11):8239-44. doi: 10.1021/la904604z.
21. H.-J. Koo, S.-T. Chang and O. D. Velev, Small, 6, 1393-1397 (2010). Ion-current diode with aqueous Gel/SiO2 nanofilm interfaces.
22. S. Sarkar, J. H. Culp, J. T. Whyland, M. Garvan, and V. Misra, Organic Electronics, 11 1896-1900 (2010). Encapsulation of organic solar cells with ultrathin barrier layers deposited by ozone-based atomic layer deposition.

23. J. C. Spagnola, B. Gong, S. A. Arvidson, J.S. Jur, Saad Khan, and G. N. Parsons "Surface and Sub-Surface Reactions during Low Temperature Aluminum Oxide Atomic Layer Deposition on Fiberforming Polymers" J. Mater. Chem., 20, 4213-4222 (2010).

Presentations (Q1-20)

1. Actuating polymer sheets that self-fold in response to light, ACS National Meeting, Indianapolis, September 8, 2013. (talk to be given by M. D. Dickey)
2. D. H. Kim, M. D. Losego, K. Hanson, L. Alibabaei, K. Lee, T. J. Meyer, and G. N. Parsons, "Stabilizing Chromophores in Dye-Sensitized Solar Cells (DSSCs) Using Atomic Layer Deposition", 13th International Conference on Atomic Layer Deposition, San Diego, CA (July 2013).
3. M. D. Losego, "Atomic Layer Deposition to Improve the Attachment of Molecular Chromophores and Catalysts to Mesoporous Inorganic Photoelectrodes for Solar Fuels Production." nanoGe International Conference on New Advances in Materials Research for Solar Fuels Production, June 2013; Granada, Spain (researcher in G. N. Parsons' research group).
4. Soft Materials for Stretchable Electronics and Macroscopic Self-Folding Sheets, Naval Research Labs, May 14, 2013. (invited talk by M. D. Dickey)
5. Orlin D. Velev, Advances in Microfluidics & Nanofluidics 2013, University of Notre Dame, IN, May 2013 (Keynote talk: Ionic Circuits and Devices Combining Electronic, Microfluidic and Biomimetic Structures).
6. Self-folding of Polymer Sheets Responding to Light: Applications and Mechanistic Study, APS National Meeting, Baltimore, MD, March 27, 2013 (talk given by a student, Ying Liu, in M. D. Dickey's research group).
7. Soft Materials for Stretchable Electronics and Macroscopic Self-Folding Sheets, University of North Carolina MRS Seminar, February 28, 2013. (invited talk by M. D. Dickey)
8. D. H. Kim, M. D. Losego, K. Lee, and G. N. Parsons, "Ultra-thin TiO2 Blocking and Passivation Layers by Atomic Layer Deposition for Dye-Sensitized Solar Cells", Southeastern Regional Meeting of the American Chemical Society, Raleigh, NC (November 2012).
9. Origami Folding of Light Responsive Polymer Sheets, SERMACS, Raleigh, NC, November 2012. (talk given by a student, Ying Liu, in M. D. Dickey's research group).
10. M. D. Losego, "Dimensional Effects on the Performance of Mesostructured Silicon Photocathodes for Solar Water Splitting." South East Regional Meeting of the ACS, Raleigh, NC; November 2012 (researcher in G. N. Parsons' research group).
11. D. H. Kim, M. Woodroof, G. N. Parsons, "Ultra-thin TiO2 Blocking Layer by Atomic Layer Deposition for Dye-Sensitized Solar Cells", AVS 59th International Symposium and Exhibition, Tampa, FL (October/November 2012).
12. Orlin D. Velev, 3rd Unilever-RSC International Symposium on Functional Materials Science, Nanjing, China, September 2012. (Invited talk: Replicating the functionality of live tissue: from hydrogel based electronic devices to biomimetic soft robotics).
13. Self-Folding Polymer Sheets Using Local Light Absorption, Polymer Network Group Conference, Jackson Hole, WY, August 14, 2012. (invited talk by M. D. Dickey)

14. Self-Folding of Polymer Sheets Using Local Light Absorption, Soft Matter Symposium, NCSU, May 14, 2012 (poster given by a student, Ying Liu, in M. D. Dickey's research group).
15. Trends in University Nanotechnology Research (panel talk), Nanotech Commercialization Conference, Durham, NC April 5, 2012. (invited talk by M. D. Dickey)
16. H.-J. Koo, S. T. Chang, J. M. Slocik, R. R. Naik, O. D. Velev, MRS National Spring Meeting; San Francisco, CA, April 2012 (A New Class of Photovoltaic Devices with Ionically Conductive Hydrogel Matrix).
17. New Approaches for Soft, Stretchable, and Biomimetic Electronics, Georgia Tech, March 26, 2012. (invited talk by M. D. Dickey)
18. Self-Folding of Pre-Stressed Polymer Sheets, Schoenborn Symposium, January 23, 2012, Raleigh, NC (presentation given by a student, Ying Liu, in M. D. Dickey's research group).)
19. Self-Folding of Polymer Sheets Using Local Light Absorption, MRS National Meeting, November 2011, Boston, MA. (talk given by a student, Ying Liu, in M. D. Dickey's research group).
20. H.-J. Koo, S. T. Chang, J. M. Slocik, R. R. Naik, O. D. Velev, "A New Class of Aqueous Soft Matter Based Photovoltaic Devices", MRS Spring Meeting, San Francisco, CA, 2011.
21. D. H. Kim, G. N. Parsons, "Functionalized Quartz Fibers and Blocking Layer by Atomic Layer Deposition for Dye-Sensitized Solar Cells", AVS 58th International Symposium and Exhibition, Nashville, TN (October/November 2011).
22. D. H. Kim, G. N. Parsons, "High Performance Dye-Sensitized Photovoltaic Cells and Micro-Fiber Based Photoanodes Using TiO2 ALD", 220th ECS Meeting and Electrochemical Energy Summit, Boston, MA (October 2011).
23. Self-Folding of Polymer Sheets Using Local Light Absorption, IGRTG Workshop, October 2011, New Bern, NC. (talk given by a student, Ying Liu, in M. D. Dickey's research group).
24. Self-Folding of Polymer Sheets Using Local Light Absorption, Soft Matter Symposium, UNC, August 22, 2011. (poster given by a student, Ying Liu, in M. D. Dickey's research group).
25. D. H. Kim, M. Woodroof, G. N. Parsons, "Dye-Sensitized Solar Cells Incorporating Micro-Fibers with Conformal TiO2 Coating by Atomic Layer Deposition", 11th International Conference on ALD, Cambridge, MA (June 2011).
26. Enhanced Light Harvesting in Organic Photovoltaics, Sustainable Solar Energy Workshop, NCSU, May 3, 2011. (invited talk by M. D. Dickey)
27. J. S. Jur, North Carolina Nanotechnology Commercialization Conference, Moderator of Session entitled "Coatings, Composites, and Commercial Potential" (Oral), February 2011. (researcher in G. N. Parsons' research group)
28. J. S. Jur, Seminar at Sandia National Laboratory- CINT, "Vapor Phase Deposition Methods for the Nanoscale Inorganic Modification of Polymer Fiber Templates" (Oral), February 2011. (researcher in G. N. Parsons' research group)
29. G. N. Parsons, Presentation at UNC Solar Energy Research Conference, Chapel Hill NC (January 14, 2011). Solar Fuels Materials and Devices using Atomic Layer Deposition.
30. Gorman Group, ACS National Meeting in Boston, MA "Investigating the reactivity of benzylic nitriles in palladiumcatalyzed cross coupling reactions." (Oral), August 2010.

31. J. S. Jur and G. N. Parsons, “ALD at Atmospheric Pressure in a Gas Flow Tube: Process Results Between 1 and 760 Torr” Presentation at the 10th International Conference on Atomic Layer Deposition in Seoul, South Korea, June 2010.
32. C. J. Oldham, B. Gong, J. C. Spagnola, J. S. Jur, K. J. Senecal, T. A. Godfrey, and G. N. Parsons, “Molecular Layer Deposition for Chemical Encapsulation and Passivation of Electrospun Nylon Nanofibers” Poster at the 10th International Conference on Atomic Layer Deposition in Seoul, South Korea, June 2010.
33. J.C. Spagnola, B. Gong, J. S. Jur, and G. N. Parsons, “Surface and Sub-Surface Reactions During Aluminum Oxide ALD on Fiber Forming-Polymers” Presentation at the 10th International Conference on Atomic Layer Deposition in Seoul, South Korea, June 2010.
34. H.-J. Koo, J.-H. So, M. D. Dickey and O. D. Velev, "Towards Soft Matter Circuits: Quasi-liquid Diodes and Memristors", Triangle Soft Matter Workshop, Duke University, Durham, NC, May 2010.
35. Y. Liu and M. Dickey, "Light Harvesting for Organic Photovoltaics", Triangle Soft Matter Workshop, Duke University, Durham, NC, May 2010.
36. Jesse S. Jur, presentation and panel discussion “Nanotech is everywhere, but what is it and why should you care?” North Carolina Nanotechnology Commercialization Conference, Greensboro, NC, March 31 and April 1, 2010.
37. Efficient Light Harvesting by Organic Photovoltaics, Soft Matter Symposium, Duke University, May 12, 2010. (poster given by Ying Liu and Sharvil Desai, students in M. D. Dickey’s research group)
38. Efficient Light Harvesting by Organic Photovoltaics, National Academy of Engineering; Grand Summit Challenge, March 4, 2010, Raleigh, NC. (poster given by Ying Liu, student in M. D. Dickey’s research group).
39. Orlin D. Velev, "Colloidal electronics: Electrically active structures from water-based particles and gels" Invited seminar, Department of Chemical Engineering, University of New Mexico, NM, February 2010.
40. Poster presentation at a University of North Carolina System’s Core Lab Facilities Symposium, Office of Translational Technologies within the NC TraCS Institute held on January 26th, 2010.
41. Poster presentation on Nanotechnology Energy Laboratory and related project research at a conference, “Solar Fuels and Energy Storage: The Unmet Needs," held at the University of North Carolina on January 14-15, 2010.
42. Gorman Group, ACS National Meeting in Washington, D.C. “Optimization of palladium-catalyzed coupling reactions in the synthesis of electron deficient diaryl cyanomethanes.” (Oral), August 2009.
43. Jeong-Seok Na, Giovanna Scarel and Gregory N. Parsons “Correlation in Charge Transfer and Mass Uptake during Atomic Layer Deposition of Zinc Oxide and Aluminum-doped Zinc Oxide” 2009 International Atomic Layer Deposition Conference, Monterey CA, July 2009.
44. G.N. Parsons “Nanotechnology Research at NC State”, North Carolina Nanotechnology Commercialization Conference, North Carolina Department of Commerce, Raleigh NC, March 26, 2009.

Other Activities (Q1-20)

NC State-Sponsored Events

- Organization of a Solar Energy Meeting on October 14th, 2009 at NC State University. The goals of this meeting were to 1) to inform the NC State research community regarding current activities and plans in solar energy research; 2) to make researchers aware of research tools, facilities and expertise in this field available on campus; and 3) identify possible areas where NC State researchers could contribute to solar energy research.
- Led a technology sharing workshop on July 15th, 2009 at NC State University between Agilent Technologies and faculty at NC State (including Drs. Parsons, Jur, Dickey, and Misra) for the purpose of forming collaborative networks with NC State and Agilent Technologies in research fields related to renewable energy.
- Assisted in a NC State-sponsored Energy Fair open to the public on April 22nd, 2009.
- Established a bi-monthly meeting schedule for students and PIs to engage research results and education topics related to renewable energy.

Other Local and Statewide Events

- Poster presentation at a University of North Carolina System's Core Lab Facilities Symposium, Office of Translational Technologies within the NC TraCS Institute held on January 26th, 2010.
- Attendance by Dr. Jur at North Carolina Center of Innovation for Nanotechnology (COIN) open house in Durham, NC, March 2011.
- Representation by Dr. Jur at the North Carolina Nano Trade Association forum, focused on environmentally responsible development of nanotechnology in the North Carolina research community. At this meeting, a document was unveiled entitled: "2009 Environmental Health Summit: Environmentally Responsible Development of Nanotechnology; Recommendations from the Research Triangle Environmental Health Collaborative." This document was formed as a result of a Summit held in late 2009. The document can be found here: http://environmentalhealthcollaborative.org/images/Nano_Summit_White_Paper_Final.pdf
- Provide a poster display and information at a vendor booth during the annual North Carolina Technology Commercialization Conferences.

Nanotechnology Energy Laboratory Tours

- Laboratory visit by technology representatives from Liquidia, Research Triangle Park, NC to examine the use of the electrospun nanofibers for energy storage applications on October 13th, 2009.
- Laboratory visit by technology representatives from Amprius Inc, Menlo Park, CA to examine the use of the electrospun nanofibers for energy storage applications on July 14th, 2009.
- Laboratory visit by Ms. Kara Weishaar (Energy LA for US Sen. Richard Burr) on April 15th, 2009.
- Laboratory visit by Mr. Zach Pfister (LA with US Rep. Larry Kissell's) and Mr. James Hunter (LA with US Rep. David Price) on April 13th, 2009.

K-12 Outreach

- Conducted tours of Nanotechnology Energy Laboratory for several hundred middle and high school students every year (2009-2012) during NanoDays outreach events organized by NC State. Most recently, at the 2012 event Dr. Mark Losego and Berc Kalanyan (in Dr. Parsons' research group) offered presentations on solar water splitting to K-12 students, parents, and teachers.
- Conducted tours of Nanotechnology Energy Laboratory during NC State College of Engineering open house on March 14th, 2009.
- M. D. Dickey - Outreach 'module' on self-folding used by NC State's Engineering Place and:
    - Presented by M. D. Dickey and Y. Liu at Workshop at College of Design (April 16, 2013)
    - Presented by M.D. Dickey and colleagues at Meredith College (Feb 6, 2013) for the Pascal Scholars program.
    - National Science and Engineering Expo April 27, 2012 (150,000 attendees – estimated 5,000 visited demo)
    - Middle School Engineering camp in Hickory NC (Summer 2012)
    - Elementary camps in Raleigh (Summer 2012)
    - Presented by M. D. Dickey and colleagues at MRSEC NC Science Festival April 17, 2012.
    - Presented by M. D. Dickey and grad student to Middle School Engineering Camp (Summer 2011)
    - Presented by M. D. Engineering Place to Middle School Engineering Camp (Summer 2012, 2013)
    - Presented by M. D. Dickey and students at Nano Days (Spring 2013)
    - Presented by M. D. Dickey and colleagues at Elon University (Summer 2013)

In the Media

- The NC State Nanotechnology Energy laboratory was featured on a NC State sustainability promotional video that was filmed on April 7th 2010.
- Dr. Velev's work related to subtask 4.1 is highlighted in the October 4, 2010 issue of Chemical and Engineering News: http://pubs.acs.org/isubscribe/journals/cen/88/i40/html/8840scic7.html
- This project was adopted by the NC State Nanotechnology Initiative (www.ncsu.edu/nano). The Initiative has sponsored several information seminars on photovoltaic device operation and organic semiconductors. The seminars were geared to introduce students to concepts critical to the development of organic-based photovoltaic devices. These seminars have served as a communication bridge between students from the various groups involved in the project (Chemistry, Electrical Engineering, and Chemical and Biomolecular Engineering).
- A website was established for the "Nano Energy Lab": http://ncsu.edu/nano/centers/NANONCSTATENANOENERGYLAB.php
- Press Release (11/18/08) "NC State Secures Grant to Make Solar Energy Less Expensive": http://news.ncsu.edu/releases/nc-state-secures-grant-to-make-solar-energy-less-expensive/

BIOMICROFLUIDICS **7**, 031501 (2013)

Ionic current devices—Recent progress in the merging of electronic, microfluidic, and biomimetic structures

Hyung-Jun Koo[a] and Orlin D. Velev[b]
Department of Chemical and Biomolecular Engineering, North Carolina State University, Raleigh, North Carolina 27695-7905, USA

(Received 11 February 2013; accepted 17 April 2013; published online 9 May 2013)

We review the recent progress in the emerging area of devices and circuits operating on the basis of ionic currents. These devices operate at the intersection of electrochemistry, electronics, and microfluidics, and their potential applications are inspired by essential biological processes such as neural transmission. Ionic current rectification has been demonstrated in diode-like devices containing electrolyte solutions, hydrogel, or hydrated nanofilms. More complex functions have been realized in ionic current based transistors, solar cells, and switching memory devices. Microfluidic channels and networks—an intrinsic component of the ionic devices—could play the role of wires and circuits in conventional electronics. *© 2013 AIP Publishing LLC*. [http://dx.doi.org/10.1063/1.4804249]

I. INTRODUCTION

The ubiquitous electronic devices that make modern life possible predominantly operate by electron transport though metallic or semiconducting circuit components. Even these devices, however, include a few components, notably batteries and electrolytic capacitors, which rely on ionic charge generation and transport. The situation is drastically different in the biological domain, where many processes, ranging from photosynthesis to the functioning of the neurons and the brain, involve ionic migration and ionic currents. Ionic currents on the microscale and nanoscale can underlie the operation of future generations of man-made devices, which can interface and be intrinsically compatible with biological tissues. The micro- or nanoscale confinement of the liquid or semi-liquid medium, in which the ion transport takes place, naturally brings these devices into the microfluidic domain. We provide here a review and perspective on the recent developments of such ionic current devices.

The operation of the ionic current devices is dependent on the ion transport near charged surfaces in water medium. Due to the overall charge neutrality and local electrostatic attraction, each charged surface in water medium is surrounded by a highly concentrated layer of mobile counter-ions. The role of the mobile ions as a current carrier becomes more pronounced when the counter-ionic layers overlap in nanoscale proximity. One of the most intriguing ways to modulate the ionic current is to confine the electrostatic interactions with wall surface charges to the nanoscale.[1,2] The electric potential away from the charged surface, Ψ, decays approximately exponentially as described by the equation, $\Psi(x) \approx \Psi_s \exp(-\frac{x}{1/\kappa})$, where Ψ_s is the potential difference between the surface and the bulk, x is the distance away from the surface, and $1/\kappa$ is the characteristic decay distance known as the Debye length.[3] Since the Debye length of aqueous solutions is usually less than 100 nm, nanofluidic channels with charged walls could control ionic flows through the surface charge of the channel walls.[4] Charged nanochannels with diameter smaller than the Debye length enable selective transport of only one type of ions by electrostatic gating. Instead of confinement, the ionic current can be controlled by system asymmetry.

---

[a] Present address: Department of Materials Science and Engineering, University of Illinois at Urbana-Champaign, Urbana, Illinois 61801-2325, USA.
[b] Author to whom correspondence should be addressed. Electronic mail: odvelev@ncsu.edu. Tel.: 919-513-4318.

Interfacing of two electrolyte or polyelectrolyte media, with ionic carriers of opposite charge, allows rectification and making of nonlinear devices, broadly analogous to the opposite electronic carriers in p or n type semiconductors. Nonlinear conductivity and redox reaction of insulating oxide films can also control the directional ionic flow. The means used to control ionic currents with examples from literature sources are summarized in Table I.

Due to their ability to operate in aqueous phase, ionic current devices could find a range of bio-related applications, such as sensing, separation and manipulation of biomolecules. Nonlinear ionic current are also generated in a number of essential processes in the human body. For example, adenosine triphosphate (ATP), the energy source in the body, can be synthesized by selective transport of protons through a biological channel called ATP synthase. A neural signal is transmitted by propagation of action potential induced by preferential diffusion of Na^+ ions through the neural membrane.

In this perspective, we first review the results on rectification of ionic currents, corresponding to the function of the basic electronic diodes. We then discuss the emergence of more complicated functions by modulating ionic current in recent studies of ionic transistors, memristors, and solar cells. Sections IV and V focus on a discussion how microfluidics can be used as

TABLE I. Representative means of controlling ionic currents and the corresponding phenomena and applications.

Means	Schematics	Phenomena/applications
1. Electric field	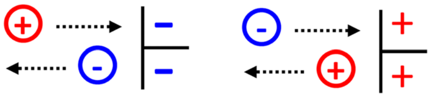	Electrophoresis, electric double layer on charged surfaces
2. Geometry of ion-channels	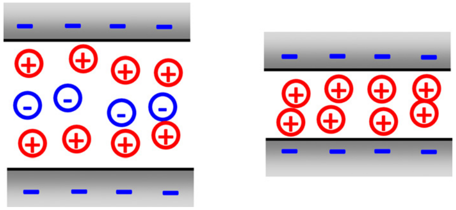 Micro-channels Nano-channels	Selective ion transport due to overlapping of electrical double layers
	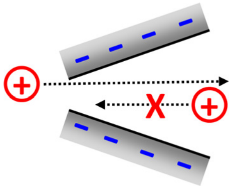 Asymmetrically shaped channels	Rectification by selective ion transport
3. Immobilization of ions	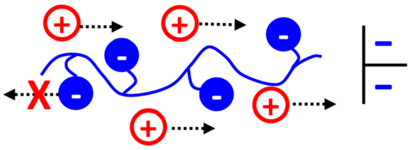	Using the two types of oppositely charged mobile ions as local charge carriers, analogous to electrons/holes in semiconductors
4. Electro-chemical reactions	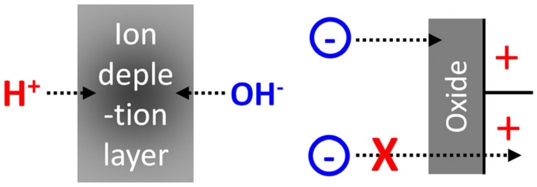 	Formation or removal of ion-depletion layer or non-conducting film (e.g., oxide)

means of fabricating the host matrix and wiring the ionic devices into early prototypes of electric and biomimetic circuits.

II. IONIC DIODES

A diode is a basic electronic component exhibiting current rectification by readily conducting electric current in one direction and inhibiting the reverse current. The making of rectifying ionic devices has been achieved by numerous means, which are exemplified schematically in Figure 1 and reviewed below.

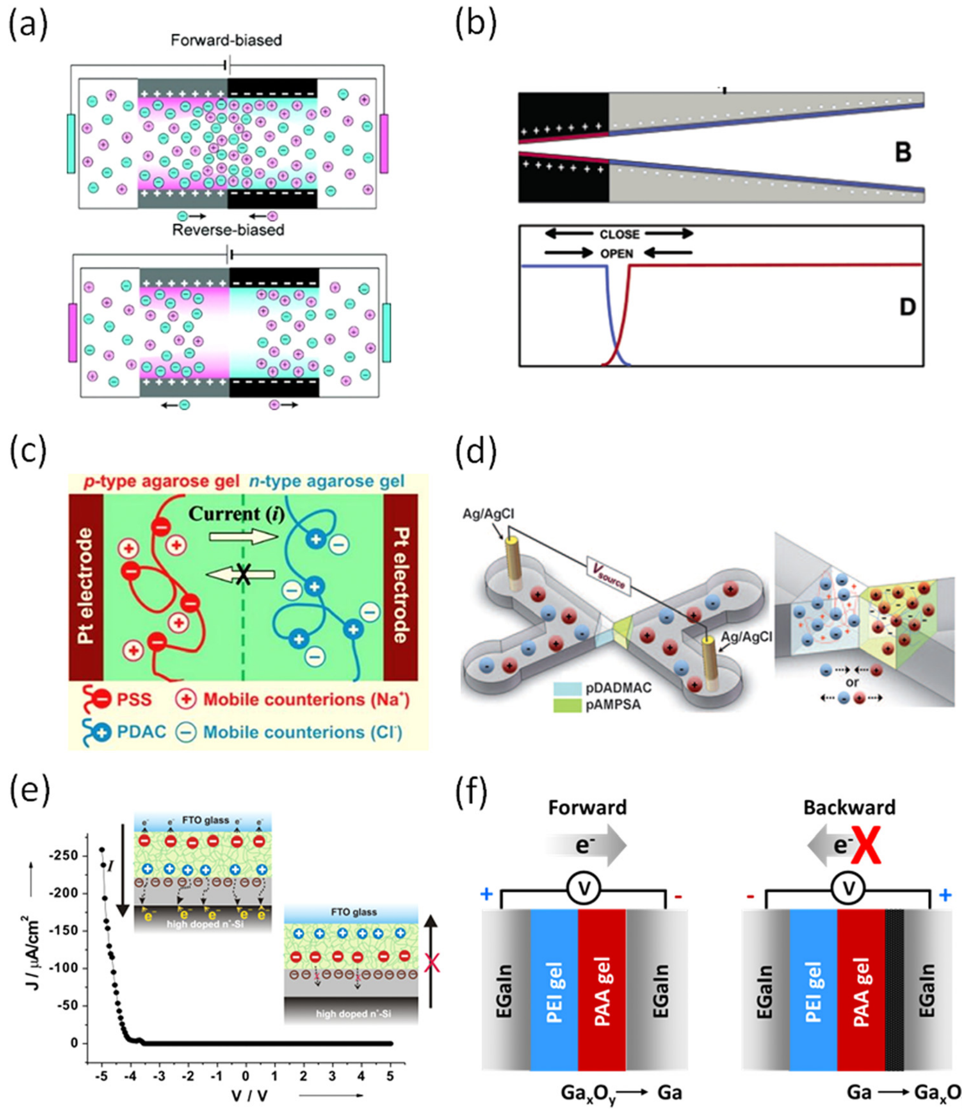

FIG. 1. Examples of ionic current rectifying systems. (a) Ionic current rectification in a nanochannel with asymmetric charge distribution. Reproduced with permission from Daiguji *et al.*, Nano Lett. **5**, 2274 (2005). Copyright 2005 ACS Publications. (b) A cone-shaped nanotube with asymmetric charge distribution. Reproduced with permission from Vlassiouk and Siwy, Nano Lett. **7**, 552 (2007). Copyright 2007 ACS Publications. (c) A polyelectrolyte diode with oppositely charged counter ion carriers. Reproduced with permission from Cayre *et al.*, J. Am. Chem. Soc. **129**, 10801 (2007). Copyright 2007 ACS publications. (d) A polyelectrolyte diode on a microchip. Reproduced with permission from Han *et al.*, Angew. Chem., Int. Ed. **48**, 3830 (2009). Copyright 2009 John Wiley & Sons, Ltd. (e) Selective ion transport in a device with the interface of hydrogel/SiO_2 nanofilm. Reproduced with permission from Koo *et al.*, Small **6**, 1393 (2010). Copyright 2010 John Wiley & Sons, Ltd. (f) Ionic current rectification in an entirely soft device composed of hydrogels and liquid metal. Reproduced with permission from So *et al.*, Adv. Funct. Mater. **22**, 625 (2012). Copyright 2012 John Wiley & Sons, Ltd.

An asymmetric distribution of the surface charge on the nanochannel walls could allow ionic current rectification. Daiguji *et al.* theoretically proved that a nanofluidic diode can be realized when the surface of either half of the channel is oppositely charged as shown in Figure 1(a).[5] Karnik *et al.* demonstrated nanofluidic diodes with asymmetric charge distribution by modifying one half of the neutral surface of biotin-adsorbed channel with positively charged avidin.[6] Gracheva *et al.* proposed a design of an electrically tunable rectifying membrane consisting of p-n semiconductor layers.[7]

The use of asymmetrically shaped nanochannels with charged walls also enables ionic current rectification. Siwy and coworkers performed both theoretical and experimental studies on selectivity and rectification of ionic current in cone-shaped nanochannels (Figure 1(b)).[1,8–10] Extensive study on inversion of the ionic current rectification depending on the surface charge density of the cone-shaped channels was conducted by Yu *et al.*[11] Cone-shaped nanopores with grafted DNA layers have been proposed as artificial ion channels where ionic current is rectified via electromechanical action of the bio-polyanions.[12] The negatively charged, flexible, DNA chains attached on the asymmetric nanopores move into and out of the small opening depending on the bias polarity, thereby gating the ionic current. Yossifon *et al.* reported a nonlinear ion flux resulting from instability of space-charge layer at only one of the asymmetric entrances of nanoslot arrays.[13,14] A pH-tunable nanofluidic diode with a cone-shaped amphoteric nanopore has also been constructed.[15] Similarly, ionic current rectification has been measured in nanopipettes with tapered openings.[16,17] Such nanochannel based devices could provide a precise control of small volume of an ionic flow with well-defined nanostructures. The ionic current flows in a nanoscale can be conveniently interpreted by electrokinetic phenomena in a laminar regime. The magnitude of the current in these devices lies in the nanoampere range, which could be a hurdle to interfacing conventional systems, but may open applications in ultralow current devices.

On a large scale, the formation of an ion depletion region at an interface of electrolytes was used for ionic current rectification. Intensive research on the ionic current rectification at a junction of acidic and basic electrolytes has been conducted.[22–26] The rectifying junction of these electrolyte diodes is formed in the hydrogel bridge which connects two electrolyte reservoirs. During reverse bias, where positive potential is applied to the electrode in the acid solution, H^+ and OH^- ions migrating from the electrolytes form water at the interface, where the ion concentration is drastically reduced. This junction has high impedance and acts as a depletion layer in a p-n junction diode. The formation of a more practical and stable device with nonlinear current response at the interface of two polyelectrolyte hydrogel layers was reported by Cayre *et al.* Figure 1(c).[18] The device is formed by interfacing two hydrogel layers doped with oppositely charged polyelectrolytes. The charged mobile counterions from the gels act as oppositely charged carriers and form a rectifying junction at the interface. The hydrogel matrix provides an excellent conductive medium for stable encapsulation of the liquid solution and polyelectrolytes. Conroy *et al.* performed in-depth theoretical and experimental research on a hysteretic current response under reverse bias in a bipolar hydrogel membrane.[27] Han *et al.* demonstrated a prototype logic circuit device by integrating similar polyelectrolyte diodes on a microchip Figure 1(d).[19]

Ionic current diodes can also be constructed on the basis of a the nonlinear electrical conductivity of hydrated SiO_2 layer between electrolyte and Si substrate.[28] We have demonstrated a highly efficient ionic current diode formed by bringing the SiO_2 nanolayer into contact with agarose gel Figure 1(e).[20] Optimum agarose concentration of 0.5 wt. % and doping with negatively charged polyelectrolyte and salt increases the ionic conductivity of the hydrogel, drastically improving the rectification performance. We also presented an ionic current diode composed entirely of soft matter: hydrogels, and liquid metal Figure 1(f).[21] Two polyelectrolyte hydrogel layers provide different pH environment on liquid metal (eutectic gallium indium, EGaIn) electrode surfaces, affecting the stability of the insulating oxide skin on the liquid metal. One liquid metal electrode interfacing a hydrogel layer with embedded polyethyleneimine (PEI) forms oxide-free surface due to high pH medium and is always conductive regardless of bias polarity. The thickness of the oxide layer at the other interface between the hydrogel with embedded poly(acrylic acid) (PAA) and the EGaIn changes depending on bias polarity, where the forward bias leads to oxide reduction and high charge transport. Thus, different formation and dissolution rates of the oxide skin at each hydrogel/liquid metal interface under electric bias enable ionic current rectification.

The rectification ratio, obtained by dividing the forward current direction by the reverse current, is one of the important parameters to evaluate a diode performance. The rectification ratios of ionic current diodes reported in the literature are summarized in Table II. The rectification ratios of the ionic current devices are generally low and not comparable with the conventional inorganic diode operated by electronic current. The low ratios possibly result from inefficient suppression of backward ionic current. For example, Vlassiouk and Siwy[10] and Cheng and Guo[30] reported relatively high rectification ratios of 217 and 321 with 2–20 nm channel diameter, which is more than one order of magnitude smaller than dimensions of other channels. Smaller channel diameter enhances the selectivity of ions by electrostatic interaction from the charged inner surface of the channels. Our device with SiO_2/hydrogel interface achieved extremely high rectification ratio of 38 000,[20] possibly as a result of the highly proton-selective current in the insulating oxide film that efficiently blocks the ionic current during reverse biasing.

III. IONIC TRANSISTORS, MEMRISTORS, AND SOLAR CELLS

The recent developments of more complex means of ionic current control enabled the construction of more sophisticated devices. Karnik *et al.* and Fan *et al.* reported an ionic current transistor with silica nanochannels on which gate electrodes were placed (Figure 2(a)).[33,34] The voltage applied to the gate controls the proton ion concentration in the silica channels, thereby modulating the ion conductivity through the channels, similar to the operation mechanism of field-effect transistors (FETs). Kalman *et al.* demonstrated ionic current bipolar junction transistors (BJTs) with double-conical nanopore, where the pore wall was separated by three different charge regions (positive-negative-positive).[35] The on/off switching of ionic current was performed chemically by changing the pH and concentration of electrolyte. Theoretical study of ion transport in nanofluidic devices also proved that an ionic current flow in nanofluidic channels with three different charged regions on the wall can be modulated depending on the charge density on the "gate" wall.[5]

Intense research has been conducted on photoelectrochemical cells with liquid medium,[36] where ionic current in electrolyte solution is involved in the regeneration processes of light-harvesting molecules. We reported recently an alternative design of a water-based photovoltaic system using gel matrices photogenerating an ionic current (Figure 2(b)).[37] Two photoactive dye ions embedded in a hydrogel matrix generate electrical current when photoexcited. A provisional

TABLE II. Comparison of the rectification ratios of ionic current diodes reported in the literature.

Rectification principles	Underlying mechanisms from Table I	Authors and publication year	Rectification ratios (sweep bias)
Acid-base electrolyte junctions	1, 4	Hegedüs *et al.* 1999[23]	∼40 (±5 V)
Conical nanochannels with asymmetrically charged inner walls	1, 2	Vlassiouk *et al.* 2007[10]	217 (±5 V)
Polyelectrolyte junction with oppositely charged backbones	1, 3, 4	Cayre *et al.* 2007[18]	∼40 (±5 V)
Conical nanochannels with charged polymer brushes	1, 2	Yameen *et al.* 2009[29]	22 (±2 V)
Nanochannels with asymmetrically charged inner walls	1, 2	Cheng *et al.* 2009[30]	321 (±1 V)
Nanochannels with asymmetric geometries and concentration polarization	1, 2	Jung *et al.* 2009[31]	∼2 (±3 V)
Polyelectrolyte junctions with oppositely charged backbones	1, 3, 4	Han *et al.* 2009[19]	∼ 100 (±1 V)
Nanochannels with asymmetrically charged inner walls	1, 2	Yan *et al.* 2009[32]	∼5 (±5 V)
Nonlinear conductivity of a SiO_2 nanofilm/agarose gel interface	1, 2, 3	Koo *et al.* 2010[20]	38 000 (±5 V)
Electric bias- and pH-dependent formation of insulating oxide layer	1, 4	So *et al.* 2012[21]	∼14 (±5 V)

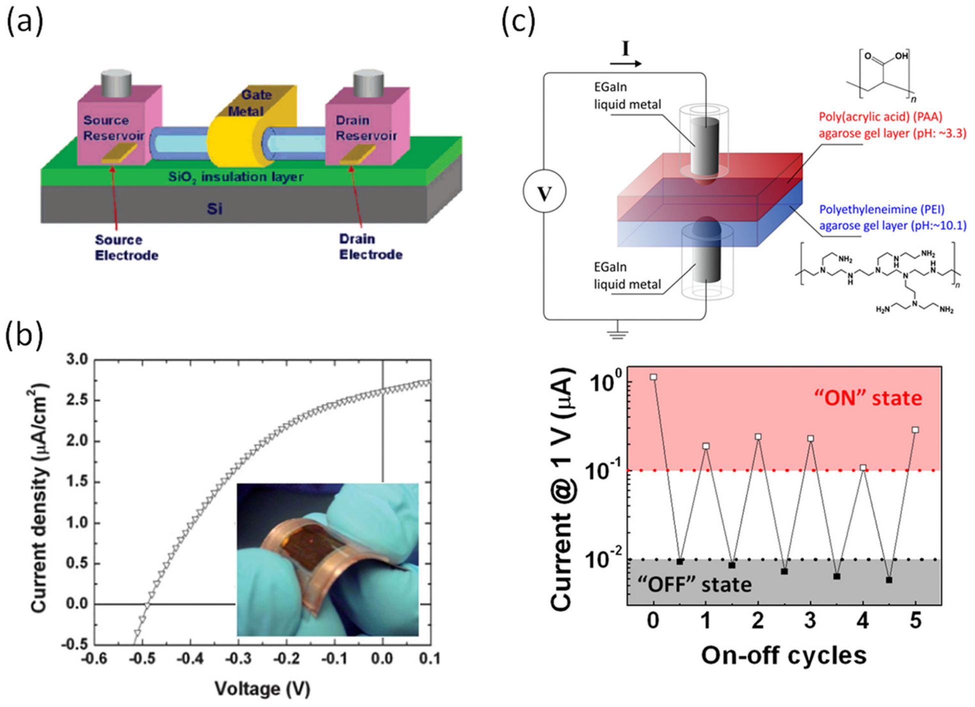

FIG. 2. Examples of ionic current devices with more complex functionalities. (a) A nanofluidic transistor. Reproduced with permission from Karnik *et al.*, Nano Lett. **5**, 943 (2005). Copyright 2005 ACS Publications. (b) A hydrogel based photovoltaic cell. Reproduced with permission from Koo *et al.*, J. Mater. Chem. **21**, 72 (2011). Copyright 2011 the RSC. (c) A soft memristor composed of hydrogels and liquid metal. The graph at the bottom illustrates the resistive switching characteristic of the device. Reproduced with permission from Koo *et al.*, Adv. Mater. **23**, 3559 (2011). Copyright 2011 John Wiley & Sons, Ltd.

mechanism of the device operation based on a synergistic effect of the two dye ions and ionic characteristic of photocurrent suggested that two dye ions work cooperatively in the gel, by facilitating electron transport and regenerating oxidized dye molecules. A flexible prototype of a photovoltaic device was constructed on the basis of the soft hydrogel matrix and plastic film conducting electrodes. Biologically derived molecules, such as Chlorophyll and Photosystem II, could be used as photoactive components in the aqueous gel media of such devices.

Another class of nonlinear elements that our group demonstrated recently is quasi-liquid resistive switching memory devices composed of hydrogels and liquid metal (Figure 2(c)).[38] Asymmetric pH environments provided by two polyelectrolyte gel layers caused different formation rates of the oxide skin on two liquid metal electrodes. The device has two discrete states of ion conductivity, depending on the polarity of the pre-bias voltage. Formation and reduction of the insulating oxide skin by electric bias determined the resistance state of the whole stack. The switchable formation of a permanent oxide skin enabled the device to exhibit memristive characteristics. Such devices composed of soft biomimetic matter could find applications in future neuromorphic systems.

IV. MICROFLUIDICS OUTLOOK—FUNCTIONAL MICROFLUIDIC MATERIALS

The ionic devices are generally made of liquid and hydrated soft matter, which are commonly hosted in microfluidic networks. To place this intrinsic relation in perspective, we overview briefly the recent research on functional materials with microfluidic networks, first from a general perspective, and then as promising structures for ionic device integration. Soft materials with embedded microvascular networks can serve as a flexible and reconfigurable matrix for constructing 2-D or 3-D architectures with fluidic or electronic functionality. Depending on the physical, chemical, and electrical properties of the fluid in the channels, the resulting microvascular materials can achieve a wide variety of functionalities, a few of which are illustrated in Figure 3.

Chang *et al.* reported a shape-memory elastomer with microvascular networks (Figure 3(a)).[39] When the liquid photocurable polymer in the channels is solidified by UV illumination, it retains the user-defined shapes. Siegel *et al.* reported a technique called microsolidics by injecting liquid solder into microfluidic channels and solidifying by cooling.[40] The technique has offered a facile way to construct a complex metallic structures. So *et al.*[41] and Kubo *et al.*[42] described a technique for fabricating a flexible and stretchable microfluidic antenna, where the channels were filled with a highly conductive liquid metal alloy (Figure 3(b)). A simple stretchable radio frequency electronic device was also demonstrated with a liquid alloy-filled microfluidic antenna.[43] Toohey *et al.* reported a 3-D microvascular network-embedded material with a self-healing function, inspired by the blood vessels protecting human skin (Figure 3(c)).[44] The microvascular channels rapidly and efficiently supplied a liquid healing agent, which enabled repetitive healing of the cracked surface of the materials. Transparent soft elastomers with microfluidic channels can be used as a smart windows or robot-camouflage materials, changing their color, contrast, or luminescence depending on filling solution

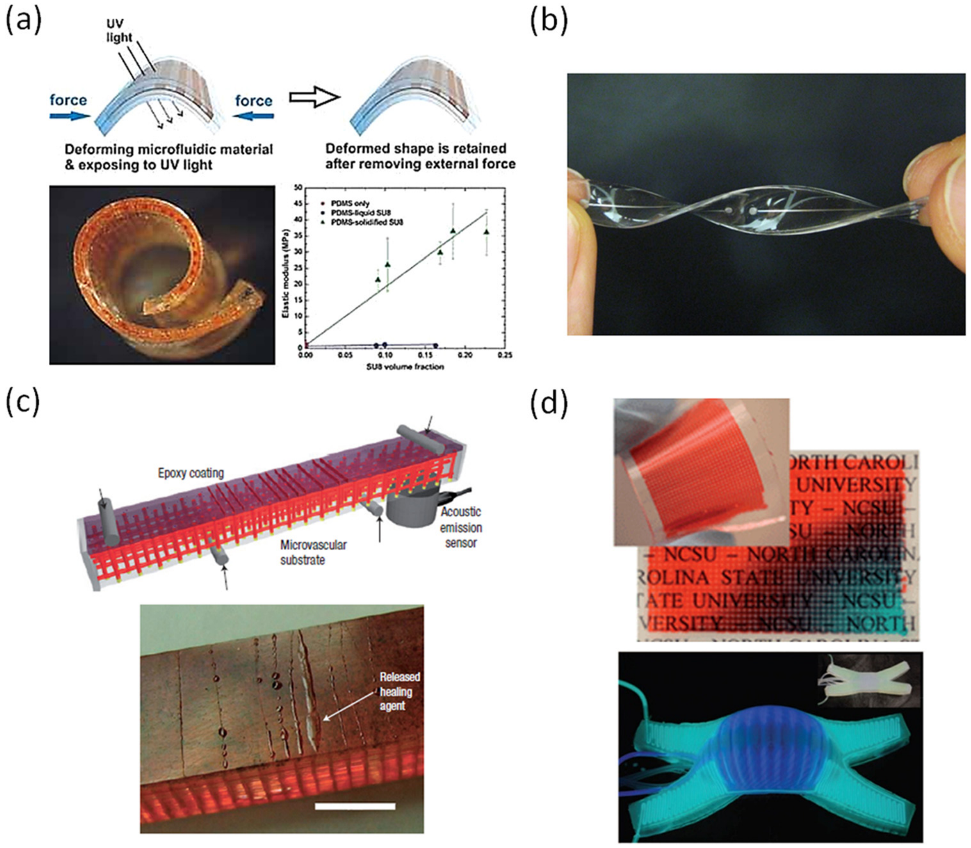

FIG. 3. Examples of functional microfluidic materials. (a) Soft materials of controlled shape and stiffness. Microvascular networks filled with a photocurable polymer allow retaining a pre-defined shape after UV illumination. Reproduced with permission from Chang *et al.*, Adv. Mater. **21**, 2803 (2009). Copyright 2009 John Wiley & Sons, Ltd. (b) Reversibly deformable microfluidic antenna filled with conducting liquid alloy. Reproduced with permission from So *et al.*, Adv. Funct. Mater. **19**, 3632 (2009). Copyright 2009 John Wiley & Sons, Ltd. (c) Schematic and optical image of a self-healing microfluidic material filled with a polymerizable healing agent. The healed cracks are visible in the image. Reproduced with permission from Toohey *et al.*, Nature Mater. **6**, 581 (2007). Copyright 2007 Nature Publishing Group. (d) Color changing soft materials with microfluidic networks. (Top) A microfluidic elastomer sheet demonstrating a color change from red to blue. Reproduced with permission from Uçar and Velev, Soft Matter **8**, 11232 (2012). Copyright 2012 the RSC. (Bottom) A soft robot with microfluidic channels filled with chemiluminescent solution. Reproduced with permission from Morin *et al.*, Science **337**, 828 (2012). Copyright 2007 AAAS.

(Figure 3(d)).[45,46] As opposed to microfluidic devices made of conventional materials, highly porous gel-based microfluidic devices could utilize the mass transport through the channel walls for efficient supply or exchange of solute molecules. Stroock and coworkers reported microfluidic scaffolds based on alginate hydrogel for tissue engineering.[47,48] They have investigated the convective and diffusive transport mechanisms in microfluidic hydrogel matrices with various channel structures as means to control the distribution and supply of solutes in a bio-scaffold.

V. MICROFLUIDIC STRATEGIES FOR DESIGN OF IMPROVED IONIC CURRENT DEVICES

Compared to normal electronic devices, the ionic current based devices have the potential to be more readily interfaced with biosystems where the ionic current is the dominant signal carrier. Since ions are intrinsically slower than electrons, however, the operational speed of the ionic current based devices could be an obstacle to practical applications. One can compensate for the disadvantage of the ionic system by miniaturizing the conductive paths or operating parallel circuits. 2D- or 3D-microfluidic networks could provide a feasible template for wiring the ionic device component. Microfluidic channels can also serve as a means for efficient supply and replenishment of active ions, which allows repeated regeneration of ionic devices.

Materials with microfluidic networks similar to the ones mentioned in Sec. IV represent a promising platform for parallel device integration. Recently, a series of wiring techniques and integrated circuits based on microfluidic channels have been demonstrated. The channels can be simply filled with a highly conducting fluid, such as liquid metal.[49] We demonstrated how a small array of hydrogel memristors can be integrated in the first prototype of an ionic current based memory circuit, by wiring them though channels filled with liquid EGaIn (Figure 4(a)).[38] The microchannel design of this multiple-element device has crossbar array structure, where each intersection is a single memristive node.

The fluidic or gel environment in ionic current devices allows for the ions participating in device operation to be replenished and replaced,[50] a regeneration capability that can hardly be achieved in conventional electronics composed of stationary solid phase materials. This enables

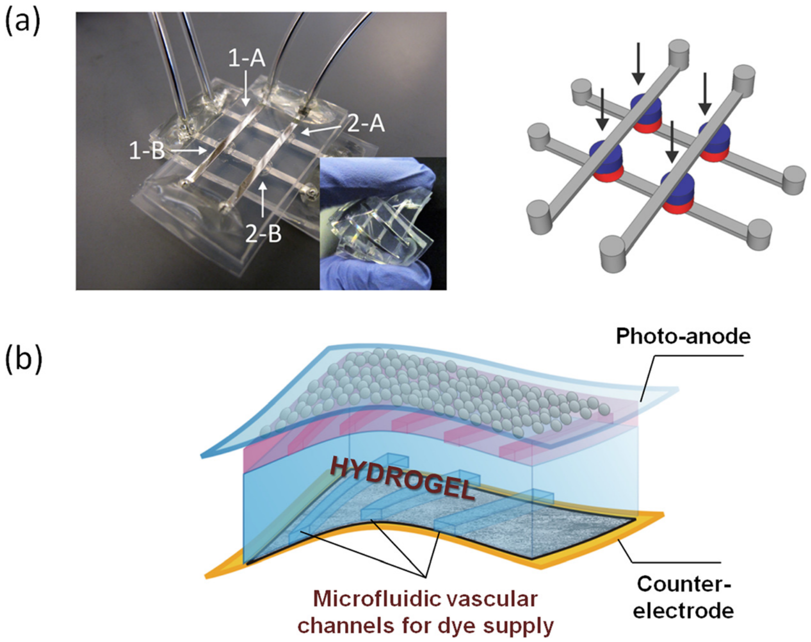

FIG. 4. Ionic current devices hosted by microfluidic networks. (a) Integration of memristor elements in a soft matrix by using microfluidic channels. Each intersection of the crossbar array channels acts as one memory node, as shown in the bottom image. Reproduced with permission from Koo *et al.*, Adv. Mater. **23**, 3559 (2011). Copyright 2011 John Wiley & Sons, Ltd. (b) A schematic of a new photovoltaic concept with biomimetic regeneration functionality.[51] The embedded microfluidic network allows uniform and efficient replacement of photoactive molecules or electrolyte ions.

the repeated regeneration of ionic current devices after photodegradation or electrochemical damage of active ionic species. Microfluidic networks offer the means for efficient supply or replenishment of the active molecules similar to the continuous operation of the photosystems in a natural leaf. The concept of a microfluidic hydrogel solar cell with biomimetic regeneration functionality is schematically shown in Figure 4(b).[51] Photovoltaic reagents, dyes, and redox electrolytes can be uniformly delivered via microfluidic networks embedded in porous media, such as a hydrogel.[47,48,52,53] Such photovoltaic cells with embedded microfluidic networks show the way to biomimetic regenerative ionic-microfluidic devices.

VI. CONCLUDING REMARKS

Ionic current devices are emerging as a potential bridge between artificial and biological circuit and sensing systems. Intensive research has led to various means of ionic current rectification by using charged nanostructures, forming ion depletion barriers, and manipulating insulating oxide layers. Ionic current devices with functionalities beyond basic rectification, such as transistors, photovoltaic cells, and memristors are presently emerging as the next research frontier. As the operation speeds of the ionic devices are much slower than that of the electronic ones, it is likely that the ionic electronics will first penetrate areas that are unfeasible for conventional electronics—such as devices that interface liquid medium, biological systems, and live organisms. Microfluidic networks could serve as a platform for this forthcoming multilevel environmental and biological integration. Moreover, the use of microfluidic channels can enable an additional biomimetic functionality that complements the electrical ionic transport, such as mechanical actuation, sensing, and self-regeneration.[50,51,54–58] As an example, the functionality imitating the regeneration procedure of photoactive biomolecules in a natural leaf can be realized on the basis of dynamic replacement of active ions via the microfluidic networks in ionic devices. Thus, the combination of microfluidics with ionic electronics could in the future lead to exciting new generations of biomimetic/electronic devices.

ACKNOWLEDGMENTS

The authors gratefully acknowledge the support from the NSF Triangle MRSEC for Programmable Soft Matter (DMR-1121107), the NSF-ASSIST Nanosystems Engineering Research Center (EEC-1160483), and DOE (08NT0001925).

[1] Z. Siwy, E. Heins, C. C. Harrell, P. Kohli, and C. R. Martin, J. Am. Chem. Soc. **126**, 10850 (2004).
[2] Z. S. Siwy and S. Howorka, Chem. Soc. Rev. **39**, 1115 (2010).
[3] J. N. Israelachvili, *Intermolecular and Surface Forces* (Academic Press, San Diego, 1992).
[4] H. Daiguji, Chem. Soc. Rev. **39**, 901 (2010).
[5] H. Daiguji, Y. Oka, and K. Shirono, Nano Lett. **5**, 2274 (2005).
[6] R. Karnik, C. Duan, K. Castelino, H. Daiguji, and A. Majumdar, Nano Lett. **7**, 547 (2007).
[7] M. E. Gracheva, J. Vidal, and J.-P. Leburton, Nano Lett. **7**, 1717 (2007).
[8] I. Vlassiouk, S. Smirnov, and Z. Siwy, Nano Lett. **8**, 1978 (2008).
[9] Z. S. Siwy, Adv. Funct. Mater. **16**, 735 (2006).
[10] I. Vlassiouk and Z. S. Siwy, Nano Lett. **7**, 552 (2007).
[11] Y. Yan, L. Wang, J. Xue, and H.-C. Chang, J. Chem. Phys. **138**, 044706 (2013).
[12] C. C. Harrell, P. Kohli, Z. Siwy, and C. R. Martin, J. Am. Chem. Soc. **126**, 15646 (2004).
[13] G. Yossifon, Y.-C. Chang, and H.-C. Chang, Phys. Rev. Lett. **103**, 154502 (2009).
[14] H.-C. Chang, G. Yossifon, and E. A. Demekhin, Annu. Rev. Fluid. Mech. **44**, 401 (2012).
[15] M. Ali, P. Ramirez, S. Mafeé, R. Neumann, and W. Ensinger, ACS Nano **3**, 603 (2009).
[16] C. Wei, A. J. Bard, and S. W. Feldberg, Anal. Chem. **69**, 4627 (1997).
[17] S. Umehara, N. Pourmand, C. D. Webb, R. W. Davis, K. Yasuda, and M. Karhanek, Nano Lett. **6**, 2486 (2006).
[18] O. J. Cayre, S. T. Chang, and O. D. Velev, J. Am. Chem. Soc. **129**, 10801 (2007).
[19] J.-H. Han, K. B. Kim, H. C. Kim, and T. D. Chung, Angew. Chem., Int. Ed. **48**, 3830 (2009).
[20] H.-J. Koo, S. T. Chang, and O. D. Velev, Small **6**, 1393 (2010).
[21] J.-H. So, H.-J. Koo, M. D. Dickey, and O. D. Velev, Adv. Funct. Mater. **22**, 625 (2012).
[22] L. Hegedüs, M. Wittmann, N. Kirschner, and Z. Noszticzius, "Reaction, diffusion, electric conduction and determination of fixed ions in a hydrogel," in *Gels* (Springer, 1996), Vol. 102, p. 101.
[23] L. Hegedüs, N. Kirschner, M. Wittmann, P. Simon, Z. Noszticzius, T. Amemiya, T. Ohmori, and T. Yamaguchi, Chaos **9**, 283 (1999).
[24] B. Lovrecek, A. Despic, and J. O. M. Bockris, J. Phys. Chem. **63**, 750 (1959).
[25] J. Lindner, D. Snita, and M. Marek, Phys. Chem. Chem. Phys. **4**, 1348 (2002).

[26] K. Iván, M. Wittmann, P. L. Simon, Z. Noszticzius, and J. Vollmer, Phys. Rev. E **70**, 061402 (2004).
[27] D. T. Conroy, R. V. Craster, O. K. Matar, L. J. Cheng, and H. C. Chang, Phys. Rev. E **86**, 056104 (2012).
[28] Y. Zhang, T. C. Gamble, A. Neumann, G. P. Lopez, S. R. J. Brueck, and D. N. Petsev, Lab Chip **8**, 1671 (2008).
[29] B. Yameen, M. Ali, R. Neumann, W. Ensinger, W. Knoll, and O. Azzaroni, J. Am. Chem. Soc. **131**, 2070 (2009).
[30] L.-J. Cheng and L. J. Guo, ACS Nano **3**, 575 (2009).
[31] J.-Y. Jung, P. Joshi, L. Petrossian, T. J. Thornton, and J. D. Posner, Anal. Chem. **81**, 3128 (2009).
[32] R. Yan, W. Liang, R. Fan, and P. Yang, Nano Lett. **9**, 3820 (2009).
[33] R. Karnik, R. Fan, M. Yue, D. Li, P. Yang, and A. Majumdar, Nano Lett. **5**, 943 (2005).
[34] R. Fan, S. Huh, R. Yan, J. Arnold, and P. Yang, Nature Mater. **7**, 303 (2008).
[35] E. B. Kalman, I. Vlassiouk, and Z. S. Siwy, Adv. Mater. **20**, 293 (2008).
[36] M. Gratzel, Nature **414**, 338 (2001).
[37] H.-J. Koo, S. T. Chang, J. M. Slocik, R. R. Naik, and O. D. Velev, J. Mater. Chem. **21**, 72 (2011).
[38] H.-J. Koo, J.-H. So, M. D. Dickey, and O. D. Velev, Adv. Mater. **23**, 3559 (2011).
[39] S. T. Chang, A. B. Uçar, G. R. Swindlehurst, R. O. Bradley, F. J. Renk, and O. D. Velev, Adv. Mater. **21**, 2803 (2009).
[40] A. C. Siegel, D. A. Bruzewicz, D. B. Weibel, and G. M. Whitesides, Adv. Mater. **19**, 727 (2007).
[41] J.-H. So, J. Thelen, A. Qusba, G. J. Hayes, G. Lazzi, and M. D. Dickey, Adv. Funct. Mater. **19**, 3632 (2009).
[42] M. Kubo, X. Li, C. Kim, M. Hashimoto, B. J. Wiley, D. Ham, and G. M. Whitesides, Adv. Mater. **22**, 2749 (2010).
[43] S. Cheng and Z. Wu, Lab Chip **10**, 3227 (2010).
[44] K. S. Toohey, N. R. Sottos, J. A. Lewis, J. S. Moore, and S. R. White, Nature Mater. **6**, 581 (2007).
[45] A. B. Uçar and O. D. Velev, Soft Matter **8**, 11232 (2012).
[46] S. A. Morin, R. F. Shepherd, S. W. Kwok, A. A. Stokes, A. Nemiroski, and G. M. Whitesides, Science **337**, 828 (2012).
[47] N. W. Choi, M. Cabodi, B. Held, J. P. Gleghorn, L. J. Bonassar, and A. D. Stroock, Nature Mater. **6**, 908 (2007).
[48] M. Cabodi, N. W. Choi, J. P. Gleghorn, C. S. D. Lee, L. J. Bonassar, and A. D. Stroock, J. Am. Chem. Soc. **127**, 13788 (2005).
[49] S. Cheng and Z. Wu, Lab Chip **12**, 2782 (2012).
[50] M.-H. Ham, J. H. Choi, A. A. Boghossian, E. S. Jeng, R. A. Graff, D. A. Heller, A. C. Chang, A. Mattis, T. H. Bayburt, Y. V. Grinkova, A. S. Zeiger, K. J. Van Vliet, E. K. Hobbie, S. G. Sligar, C. A. Wraight, and M. S. Strano, Nat. Chem. **2**, 929 (2010).
[51] H.-J. Koo and O. D. Velev (unpublished).
[52] H.-J. Koo and O. D. Velev (unpublished).
[53] Y. Ling, J. Rubin, Y. Deng, C. Huang, U. Demirci, J. M. Karp, and A. Khademhosseini, Lab Chip **7**, 756 (2007).
[54] R. F. Shepherd, F. Ilievski, W. Choi, S. A. Morin, A. A. Stokes, A. D. Mazzeo, X. Chen, M. Wang, and G. M. Whitesides, Proc. Natl. Acad. Sci. U.S.A. **108**(51), 20400-20403 (2011).
[55] F. Ilievski, A. D. Mazzeo, R. F. Shepherd, X. Chen, and G. M. Whitesides, Angew. Chem., Int. Ed. **50**, 1890 (2011).
[56] L. Y. Yeo, H.-C. Chang, P. P. Y. Chan, and J. R. Friend, Small **7**, 12 (2011).
[57] S. Senapati, A. R. Mahon, J. Gordon, C. Nowak, S. Sengupta, T. H. Q. Powell, J. Feder, D. M. Lodge, and H.-C. Chang, Biomicrofluidics **3**, 022407 (2009).
[58] J. S. Lee, S. H. Lee, J. H. Kim, and C. B. Park, Lab Chip **11**, 2309 (2011).